Università degli Studi di Cagliari

PHD DEGREE

INDUSTRIAL ENGINEERING

Cycle XXX

MODELING AND ANALYSIS OF THE CO_2 POST-COMBUSTION CAPTURE PROCESS WITH MEA

Scientific Disciplinary Sectors

ING-IND/26 - ING-IND/25

PhD Student:	Claudio Madeddu
Coordinator of the PhD Programme:	Prof. Francesco Aymerich
Supervisor:	Prof. Roberto Baratti
Co-Supervisor:	Prof. Massimiliano Errico

Final exam. Academic Year 2016 – 2017
Thesis defence: February-March 2018 Session

Modeling and Analysis of the CO_2 Post-Combustion Capture Process with MEA

Claudio Madeddu

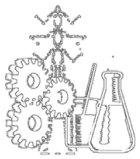

Dottorato di Ricerca in Ingegneria Industriale
Università degli Studi di Cagliari
XXX Ciclo


Modeling and Analysis of the CO_2 Post-Combustion Capture Process with MEA

Claudio Madeddu

Supervisors:

Prof. Roberto Baratti

Prof. Massimiliano Errico

Dottorato di Ricerca in Ingegneria Industriale
Università degli Studi di Cagliari
XXX Ciclo

Acknowledgements

I gratefully acknowledge Sardinia Regional Government for the financial support of my PhD scolarship (P.O.R. Sardegna F.S.E. Operational Programme of the Autonomous Region of Sardinia, European Social Fund 2007-2013 - Axis IV Human Resources, Objective 1.3, Line of Activity 1.3.1.)

I want to be thankful to my supervisor, Prof. Roberto Baratti, for giving me the opportunity to work with him and for sharing his knowledge with me.
A big thank you goes to my "Danish" supervisor, Prof. Massimiliano Errico, for his helpfulness and for his useful suggestions and observations.
An immense thank you goes to all the colleagues I was lucky to meet and share this great PhD experience with, both in Cagliari and Odense. Thank you very much guys!
Finally, a giant thank you goes to my parents, for their love and support.

Contents

List of Figures

List of Tables

Abstract

Carbon dioxide capture by means of reactive absorption-stripping using MEA is a very extensively studied process and its modeling represents an open issue in the specialized literature.
In this thesis a rigorous rate-based model is developed in Aspen Plus® environment. A new approach to the modeling based on the analysis of the system fluid dynamics is adopted. In this way, it is possibile to find the correct numerical solution of the system of equations derived from the material and energy balances. As part of the model development, the kinetic parameters of the reaction between CO_2 and MEA are calibrated to minimize the standard error between the model results and the experimental data. The model is validated for both the absorber and the stripper considering several pilot-plant facilities with different sizes and operating conditions. Moreover, in the case of the stripper it is found that a correct model of the process leads to a significant improvement in the estimation of the reboiler duty.
Subsequent to the model validation, the analysis of the design of an industrial-scale plant is taken into account for different values of the lean solvent loading. In particular, a two-step procedure that consists in the evaluation of the minimum solvent flow rate with an infinite packing height and the subsequent evaluation of the effective solvent flow rate and packing height is used for the absorption column. Moreover, the operating conditions to avoid isothermal zones in the absorber are determined. When the stripper is considered, it is highlighted that the reboiler duty is needed to reverse the absorption reactions only. For this reason, an alternative plant configuration that reduces the energy consumption is adopted and a new criterion for the determination of the packing height is proposed for the stripping column. In the end, in order to obtain the minimum reboiler duty, it is found that the rich solvent, i.e., the stripper feed, must be sent at the highest possible temperature, which is limited by the minimum temperature approach in the cross heat-exchanger.

Chapter 1

Introduction

In this first chapter, after an introduction about the problem of the CO_2 emissions and the carbon capture and storage technologies, the motivations of the thesis are presented. Then, a brief summary of the different chapters is reported. In the end, the contributions to the literature derived from this work are listed.

1.1 The problem of carbon dioxide emissions

The reduction of the carbon dioxide emissions in the atmosphere is nowadays one of the most actual problems in the field of environmental pollution. It is a fact that from 1958, when Charles D. Keating started measuring the carbon dioxide concentration in the atmosphere of Mauna Loa Island (Hawaii), as reported in Figure 1.1, this value has risen from 317 ppm to the actual value of 400 ppm. It was evaluated that keeping this growing trend, the value of 450 ppm could be reached in 2040. The threshold of 400 ppm is more than a psychological value considering that the last time the Earth reached this number was three to five million years ago [1].

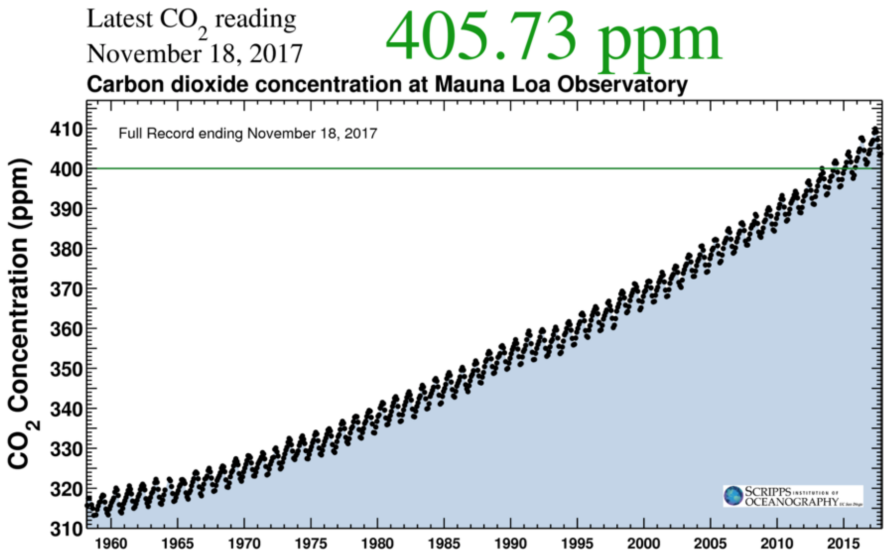

Figure 1.1: Measurement of the CO_2 concentration in the atmosphere of Mauna Loa Island

Nowadays the dualism carbon dioxide emission - climate change is a topic able to influence and to drive agreements between nations, to set global targets to be achieved, to define local regulations and also single plant sustainable programs [2]. According to Climate Change 2014: Mitigation of Climate Change, carbon dioxide contributes for 76% of the total greenhouse gases emitted and the energy production and transportation are the main responsible sectors [3]. The high impact of the topic to the public eye, together with the strict emission limits imposed by the Governments, influences also the industrial production for both retrofit of existing plants or design of new ones.

1.2 Carbon Capture and Storage Technologies

Carbon dioxide is produced in any process which involves a combustion reaction. With the advent of the industrialization, the amount of CO_2 produced by human activity has been growing continuously, raising the problem of the global warming. Among the different industrial processes, power plants fed by fossil fuels still represent one of the main contributors to satisfy the global energy demand, although in the last years the utilization of renewable energy sources has had a constant positive trend. Since it was not economically sustainable to substitute the power plants production with the renewable sources technologies, it was necessary to find a solution that was able to at least mitigate the emissions of carbon dioxide in the atmosphere. For this reason, Carbon Capture and Storage (CCS) technologies were born with the purpose of continuing the energy production by means of fossil fuels, while at the same time limiting the emissions of carbon dioxide. Of course this discussion is not limited to power plants only, but it is extended to all the industries which involve combustion processes and consequent large amount of CO_2 produced. Carbon Capture and Storage was defined in the IPCC 2005 report [4]:

> Carbon dioxide capture and storage is a process consisting of the separation of CO_2 from industrial and energy-related sources, transport to a storage location and long-term isolation from the atmosphere [...]. The CO_2 would be compressed and transported for storage in geological formations, in the ocean, in mineral carbonates, or for use in industrial processes.

CCS technologies can be divided into three main categories:

- Pre-Combustion Capture: in this case the CO_2 is captured before the combustion process by means of reforming and gasification processes, obtaining the so-called *syngas*, which is a gas mixture of essentially H_2 and CO. Together with the CO_2 capture, the object of this process is to produce a gas stream with a high hydrogen content which can be used in IGCC (Integrated Gasification Combined Cycle) processes. Due to the high costs, this technology is not diffused;

- Oxy-Combustion: in this process the combustion is conducted with pure oxygen instead of air. The final product is an exhaust gas highly concentrated in CO_2 which can be immediately captured and stored. The main problem related to this technology is the necessity of a continuous oxygen supply, which leads to high costs.

- Post-Combustion Capture: CO_2 is captured from the exhaust gas generated from the combustion of fuel. In general, carbon dioxide is diluted in the exhaust gas, leading to the necessity to use specific processes for its removal. Different separation alternatives are available such as adsorption, physical absorption, cryogenic separation, membrane absorption, chemical absorption or algal system [5]. Among them, chemical absorption is undoubtedly the most used method. The main advantage of this technology relies in the fact that it can be easily integrated in existing plants compared to the other two options [6].

In this thesis, the CO_2 post-combustion capture by means of chemical absorption was chosen as target process, since it is considered the most mature and promising technology for industrial development [5].

1.3 CO_2 post-combustion capture by chemical absorption review

Many research works about the CO_2 post-combustion capture by means of chemical absorption can be found in the literature and they can be grouped in four different categories:

1. identification of the best solvent for the carbon dioxide absorption;
2. kinetic studies;
3. synthesis of new process configurations;
4. process modeling.

In the first group, solvents are compared for their efficiency in carbon dioxide absorption, foam tendency, degradation, corrosion properties, regeneration easiness and many other physical properties [7,8]. The proposal of a reaction mechanism and the evaluation of the kinetic parameters characterizes the scope of the second group [9, 10]. In the third group, different process configurations are proposed in order to decrease the energy consumption of the plant. Absorber intercooling, stripper interheating, split of the stripper feed are some of the possible alternatives discussed and compared in the work of Jung et al. [11].
The last group concerning the process modeling can be divided into two further categories, steady-state and dynamic modeling. Steady-state models have been mainly used for comparative assessment of different power plant technologies and to study how the CO_2 removal section affects the overall performance of a defined power plant flowsheet [12, 13]. Moreover,

steady-state models are applied in the optimization of key process operating parameters, to predict the composition and temperature profiles, data validation and to optimize the energy consumption [14–18]. Dynamic models are mainly used to study different transient operational scenarios [19–21] or to optimize operating conditions to minimize for example the power plant lost work [22].
The present thesis belongs to the fourth group, i.e., it deals with the process modeling.

1.4 Motivations of the thesis

This thesis, as reported in the title, deals with the modeling and analysis of the CO_2 post-combustion capture by means of reactive absorption-stripping using monoethanolamine (MEA) as solvent. In particular, the work can be divided into two main parts:

1. model validation;

2. analysis of the design of an industrial plant.

In the first part, a model based on the state of art among the different models for reactive absorption-stripping, the rate-based model, is developed and applied for validation purposes using different experimental data sets. This thesis brings a correct solution method to the process modeling. In fact, a new approach, based on the analysis of the system fluid dynamics, is applied in this work. In general, reactive absorption-stripping processes have been modeled, from a fluid dynamic point of view, as ideal plug-flow. This assumption has always been overlooked up to now in the open literature and deserved a thorough examination. Mathematically speaking, the ideal plug-flow assumption leads to a system of differential-algebraic equations and for its solution it rises the problem of the determination of a proper number of segments for the discretization of the axial domain. This procedure leads to obtain a model which is numerically correct and allows to focus the attention on the model parameters to improve the agreement between the model and the experimental data. In fact, another part in the model development is dedicated to the calibration of the kinetic parameters with the purpose of minimizing the standard error between the model results and the experimental data. The model is validated both for the absorption and the stripping section considering different facilities and operating conditions.
After the validation, the model developed is used to design an industrial-scale plant. In particular, for what concerns the absorption section, great attention is given to the investigation of the operating conditions which lead

to columns that work correctly without isothermal zones and contemporarily respecting the performance target. In this perspective, it is highlighted the importance of the internal profiles analysis, that are normally neglected when the process design is considered. On the other hand, when the stripping section is considered, it is proposed an alternative configuration without reflux with the aim of avoiding an unnecessary energy consumption. Then, since the classic procedure based on the minimum stripping agent is not possible in the examined process, it is proposed a new approach for the determination of the stripper packing height by means of the temperature profiles analysis. In the end, the conditions that lead to the minimum energy consumption in the reboiler, which is considered the main obstacle for the industrial development of the process, are evaluated and reported.

1.5 Thesis Overview

The content of this section is a brief summary of each chapter, where the main contribution of the thesis are reported in italics.

- **Chapter 2**. The state of art concerning the reactive absorption-stripping of carbon dioxide with MEA is reported. *The theory regarding the approach based on the analysis of the system fluid dynamics is also presented. In particular, the Peclet number and the number of segments analyses are described in detail.*

- **Chapter 3**. The development of the model in Aspen Plus® using the rate-based approach is described in detail.

- **Chapter 4**. *The procedure proposed in Chapter 2 and the model developed in Chapter 3 are applied to the absorption section. As part of the model development, the kinetic parameters are calibrated with the purpose of minimizing the standard error between the model results and the experimental data. The model is validated for all the case studies.* Two pilot-plant facilities are considered with different operating conditions and the possibility of different positions of the typical temperature bulge.

- **Chapter 5**. The model is validated for the stripping section using again two pilot-plant facilities. *Two different sets of degrees of freedom are defined in order to investigate the effect of the proposed procedure on the system profiles and the reboiler duty evaluation.*

- **Chapter 6**. The analyis of the design of an industrial-scale absorber by means of the proposed model is considered. A two-step procedure

consisting in the evaluation of the minimum solvent flow rate with an infinite packing height followed by the determination of the effective solvent flow rate and the column dimensions is applied. *The operating conditions leading to a column without isothermal zones are defined by means of the temperature profiles analysis.*

- **Chapter 7**. The results from the design of the absorber are used as starting point for the analysis of the design of an industrial-scale stripper, *for which it is highlighted that the reboiler duty is needed only to reverse the absorption reactions. For this reason an alternative configuration without reflux is adopted and a new approach for the determination of the packing height is proposed. The conditions leading to the minimum reboiler duty are determined. In particular it is found that the most crucial parameter to minimize the energy consumption is the rich solvent temperature, which must be sent at the highest possible value, limited by the minimum temperature approach in the cross heat-exchanger.*

1.6 Contributions

Some of the topics treated in this thesis were used for the following contributions in terms of papers on international journals and participations to national and international conferences.

- Chapter 2, Chapter 3, Chapter 4
  - M. Errico, **C. Madeddu**, D. Pinna, R. Baratti, "Model calibration for the carbon dioxide-amine absorption system", *Appl. Energy*, vol. 183, p. 958, 2016;
  - **C. Madeddu**, M. Errico, R. Baratti, "Modeling of a CO_2-MEA absorption system - A new view in the steady-state analysis", *GRICU MEETING 2016*, September 12-14, 2016, Anacapri (NA), Italy
- Chapter 5
  - **C. Madeddu**, M. Errico, R. Baratti, "Proper estimation of the energy consumption in a carbon dioxide-amine stripper", Poster presented at the "IEA CLEAN COAL CENTRE - The eight international conference on Clean Coal Technologies", Cagliari (CA), Italy, May 8-12, 2017;

  - **C. Madeddu**, M. Errico, R. Baratti, "Rigorous modeling of a CO_2-MEA stripping system", *Chem. Eng. Trans.*, vol. 57, p. 451, 2017

- Chapter 6, Chapter 7

  - **C. Madeddu**, M. Errico, R. Baratti, "Process analysis for the carbon dioxide chemical absorption-regeneration system", *Appl. Energy*, vol. 215, p. 532, 2018;

Part I

Process Modeling

Chapter 2

Modeling the CO_2 post-combustion capture process with MEA

The state of art regarding the modeling of the CO_2 post-combustion capture by reactive absorption-stripping with MEA is reported in this chapter. In particular, the rate-based approach, considered mandatory for this kind of process, is extensively described. The last part of the chapter is dedicated to the examination of the system fluid dynamics by means of the evaluation of the Peclet number and the number of segments analysis, which represent one of the main contribution of this thesis to the reactive absorption-stripping process modeling.

2.1 Process description

The CO_2 post-combustion capture using amine aqueous solutions consists in an absorption-solvent regeneration process. The plant is divided into two main sections: the absorption, where the CO_2 is transferred from the vapor/gas phase to the liquid one, and the stripping, where the solvent is regenerated. The two sections are interconnected by means of a cross heat-exchanger. A simplified flowsheet of the system is reported in Figure 2.1.

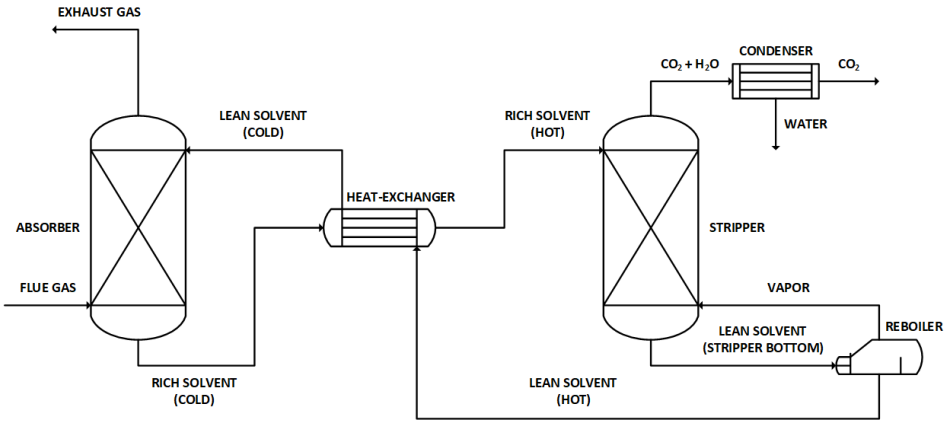

Figure 2.1: Simplified flowsheet of a CO_2 post-combustion capture by absorption/stripping plant

The CO_2-rich flue gas enters the bottom of the absorber where it flows countercurrent with the liquid solvent. From the top of the column, the exhaust vapor/gas exits and is sent to the stack. On the other hand, the CO_2-rich solvent exits the bottom of the absorber and, after being heated in the heat-exchanger, is sent to the top of the stripper, where it flows countercurrent with a vapor stream generated by the reboiler. A mixture containing mainly CO_2 and H_2O exits from the top of the column and is sent to the partial condenser where the CO_2 is concentrated in the gas phase while the water is recovered in the liquid phase. In this thesis, different plant configurations were considered for what concerns the stripper with particular attention to the water flow rate from the condenser (Chapters 5-7). For this reason, in this section no further information is given on the water recovered in the condenser. The regenerated solvent exiting the bottom of the stripper is firstly sent to the reboiler, where it is partially vaporized, and then to the heat-exchanger, where it supplies its sensible heat to the rich solvent. After the heat-exchanger, the lean solvent is recycled back to the top of the absorber. The two columns are typically packed columns, chosen over

the plate ones because the packing is able to provide a higher contact area between the gaseous and the liquid phase and ensures less pressure drop.
From the process point of view, the CO_2 post-combustion capture with MEA is a reactive absorption-stripping. In particular, in the absorber the CO_2 is transferred from the vapor/gas to the liquid phase, where then it reacts with the MEA to enhance the absorption process. On the other hand, in the stripper the CO_2 is detached from the amine, then it is transferred from the liquid phase to the vapor/gas phase. Different phenomena are involved in the process:

- non-ideal thermodynamics (Section 2.2);
- chemical equilibrium and kinetic reactions (Section 2.3);
- simultaneous material and energy transfer (Section 2.4);
- vapor-liquid and gas-liquid equilibria (Section 2.4);
- distribution of the components between the liquid and the gaseous phase (Section 2.4).

Then, due to the complex nature of the process, in order to obtain a correct mathematical description of the system a model that is able to take contemporarily into account all of these phenomena is needed. In the next sections the modeling of each item in the aforementioned list is analyzed.

2.2 Thermodynamics

The CO_2-MEA-H_2O system is an electrolyte system characterized by a non-ideal behavior due to the presence of ions [23,24]. For this reason, the thermodynamic model for the liquid phase must be able to describe the interactions between electrolytes. In particular, the correct evaluation of the components activity coefficients is crucial, since these parameters are involved in the calculation of the vapor-liquid and gas-liquid equilibria, the equilibrium and kinetic reactions and the calculation of the driving force for the interphase material transfer.
Different models with varying level of detail have been used in the literature for the computation of the liquid phase thermodynamic properties. For example, the simple Kent-Eisenberg model, which fixes all the activities to unity (ideal behavior) was used by several authors [25–29]. In the early '80s, Deshmukh & Mather [30] and Chen & Evans [31], proposed two different models based on rigorous thermodynamic principles [32]. The first model, used by various authors [32–34], involves the Guggenheim equation [35] to compute the activity coefficients, while the latter, which can be

found in a significant number of works [2, 14, 17, 19, 22–24, 36–47], is known as Electrolyte-NRTL model, and applies the Pitzer-Debye-Hückel theory together with the Electrolyte-NRTL equation for the evaluation of the activity coefficients. More recently, Hoff et al. [48] developed a model, used by different authors [16, 49, 50] that includes the non-idealities of the liquid phase by means of the salting-out correlation proposed by Van Krevelen et al. [51], obtaining results which are very similar to the Electrolyte-NRTL model.
The CO_2 post-combustion capture process is operated at low pressures (1 bar for the absorption and 1.5-2 bar for the stripper). For this reason, as reported by Freguia [52], no relevant non-idealities are present for what concerns the thermodynamics of the vapor/gas phase in this system. Nevertheless, different equations of state (EoS) have been used in the literature for the evaluation of the fugacity coefficients of the components, such as the Peng-Robinson EoS [27,33,34,53], the Redlich-Kwong Eos [2,23,36,42,46,54] and the Soave-Redlich-Kwong EoS [24, 43, 52].
Furthermore, as carbon dioxide is a gas, the solubility of CO_2 in the amine aqueous solution is typically modeled by means of the Henry's law.
In this thesis, as it is going to be reported in Chapter 3, the Electrolyte-NRTL model and the Redlich-Kwong EoS were used for the description of the thermodynamics of the liquid phase and the vapor/gas phase, respectively.

2.3 Chemical reactions

2.3.1 Reactions set

The definition of the reaction scheme is essential for the correct description of the CO_2-MEA-H_2O system, where the chemical reactions are limited to the liquid phase only. A significant number of reactions sets have been proposed in the literature. Some authors have proposed a purely equilibrium reactions set [19, 23, 33, 36, 55], reported in Eqs. 2.1-2.5:

$$2H_2O \rightleftarrows H_3O^+ + OH^- \tag{2.1}$$

$$CO_2 + 2H_2O \rightleftarrows H_3O^+ + HCO_3^- \tag{2.2}$$

$$HCO_3^- + H_2O \rightleftarrows H_3O^+ + CO_3^{2-} \tag{2.3}$$

$$MEA^+ + H_2O \rightleftarrows H_3O^+ + MEA \tag{2.4}$$

$$MEACOO^- + H_2O \rightleftarrows HCO_3^- + MEA \tag{2.5}$$

while others have considered only one kinetic reaction between CO_2 and MEA [20, 56–58], or two kinetic reactions involving CO_2 and MEA and OH^-

ions [37,39]. With regards to the reaction between CO_2 and MEA, different forms have been proposed in the literature, depending on which equilibrium reactions are considered for their derivation [52]. Table 2.1 resumes some of the most-used expressions from the literature.

Reactions	**References**
$CO_2 + MEA + H_2O \rightleftarrows MEACOO^- + H_3O^+$	[2, 27, 39, 43, 46, 52, 59]
$CO_2 + 2MEA \rightleftarrows MEACOO^- + MEA^+$	[16, 20, 22, 37, 38, 57, 58]
$CO_2 + MEA + H_2O \rightleftarrows HCO_3^- + MEA^+$	[22, 38, 57]

Table 2.1: Different reactions involving CO_2 and MEA

While the reaction between CO_2 and the OH^- ions is described by [60, 61]:

$$CO_2 + OH^- \rightleftarrows HCO_3^- \tag{2.6}$$

However, the most used approach is to consider a hybrid set that takes into account both equilibrium and kinetic reactions [2, 16, 17, 27, 38, 42–44, 46, 53, 59, 61–63]. This approach appears to be the most correct for two main reasons:

- it has been demonstrated [60, 64–66] that the reactions involving CO_2 have kinetic limitations, therefore they cannot be described rigorously by a pure chemical equilibrium approach;
- the presence of MEA and carbonate in water generates ions. Consequently, ionic equilibrium reactions are needed to describe the reactions involving electrolytes.

The reaction scheme chosen in this work is going to be discussed in detail in Chapter 3.

2.3.2 Equilibrium constant and reaction rate expressions

In order to include the reactions in the model, an expression for the equilibrium constant for what concerns the equilibrium reactions and a reaction rate equation for the kinetic reactions must be considered.
The equilibrium constant is a function of the temperature and can be evaluated rigorously by means of the standard Gibbs free-energy change or a

parameter-based correlation. In the first case, the equilibrium constant has the following expression (Eq. 2.7):

$$K_{eq} = \exp\left(-\frac{\Delta G^0}{RT^L}\right) \tag{2.7}$$

In the latter case, the expression of the equilibrium constant has the following form (Eq. 2.8):

$$\ln K_{eq} = A + \frac{B}{T^L} + C\ \ln T^L + D\ T^L \tag{2.8}$$

where the coefficients A, B, C, D can be found in different sources [23,67]. For what concerns the expression of the equilibrium constant as function of the components concentration, typically the activities are used as concentration basis (Eq. 2.9):

$$K_{eq} = \frac{\prod_{i=1}^{n_c^f} a_i^{\nu_i}}{\prod_{i=1}^{n_c^r} a_i^{\nu_i}} = \frac{\prod_{i=1}^{n_c^f} (\gamma_i x_i)^{\nu_i}}{\prod_{i=1}^{n_c^r} (\gamma_i x_i)^{\nu_i}} \tag{2.9}$$

With regards to the reversible kinetic reactions, the typical expression for the reaction rate is the classic power law:

$$r = r_f - r_r = k_f \prod_{i=1}^{n_c^f} \left(C_i^L\right)^{\nu_i} - k_r \prod_{i=1}^{n_c^r} \left(C_i^L\right)^{\nu_i} \tag{2.10}$$

The kinetic constants for the forward and reverse reactions are expressed by means of the Arrhenius law:

$$k = k^0 \exp\left(-\frac{E_a}{RT^L}\right) \tag{2.11}$$

2.4 Material and energy transfer

At the end of Section 2.1, it was highlighted the complex nature of the process that involves several different phenomena. Then, in order to obtain a correct mathematical description of the system, a model that is able to describe contemporarily the non-ideal thermodynamics, the chemical reactions, the interphase transfer, the component transport in the two phases and the fluid dynamics is needed. The first two phenomena, which are common to every modeling approach, were described in Section 2.2 and 2.3, respectively. This section deals with the modeling of the interphase transfer and

the components transport in the two phases. In the literature, two different approaches are reported: the equilibrium stage model (Subsection 2.4.1) and the rate-based model (Subsection 2.4.2). In both cases, the column height is discretized into a certain number of parts, which are referred to as *stages* for the first model and as *segments* for the latter. In the following Subsections, the material and energy balances for the two models, together with the correlations associated with them, are reported and analyzed.

2.4.1 Equilibrium Stage Model

The equilibrium stage model represents the simplest way to model simultaneous material and energy transfer processes [68, 69]. In particular, in the case of intimate contact between the phases and sufficient residence time, it can be assumed that the streams exiting each stage reach the thermodynamic equilibrium. To write the material and energy balances for the equilibrium stage model it is made reference to the graphical representation of one stage reported in Figure 2.2. In Eqs. 2.12- 2.17, index i indicates the components, while index j indicates the stage.

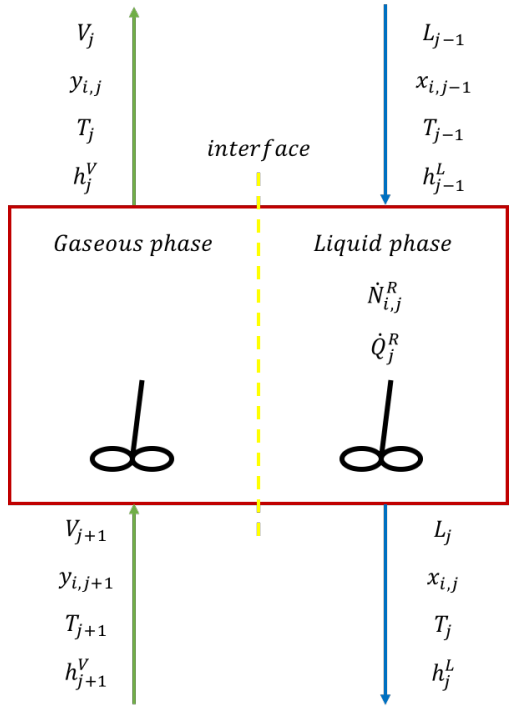

Figure 2.2: Equilibrium stage representation

- Component material balance

$$\frac{dM_{i,j}}{dt} = L_{j-1}\ x_{i,j-1} + V_{j+1}\ y_{i,j+1} - L_j\ x_{i,j} - V_j\ y_{i,j} + \dot{N}^R_{i,j} \quad (2.12)$$

- Energy balance

$$\frac{dU_j}{dt} = L_{j-1}\ h^L_{j-1} + V_{j+1}\ h^V_{j+1} - L_j\ h^L_j - V_j\ h^V_j + \dot{Q}^R_j \quad (2.13)$$

- Vapor-liquid equilibrium

$$P\ \phi_{i,j}\ y^*_{i,j} = P^{sat}_{i,j}\ \gamma_{i,j}\ x_{i,j} \quad (2.14)$$

- Gas-liquid equilibrium

$$P\ \phi_{i,j}\ y^*_{i,j} = He_{i,j}\ \gamma_{i,j}\ x_{i,j} \quad (2.15)$$

- Summation equations

$$\sum_{i=1}^{n^L_c} x_{i,j} \quad (2.16)$$

$$\sum_{i=1}^{n^V_c} y_{i,j} \quad (2.17)$$

- Material and energy hold-up

$$M_{i,j} = \epsilon\ S\ dz\ (\psi^L_j\ C^L_j\ x_{i,j} + \psi^V_j\ C^V_j\ y_{i,j}) \quad (2.18)$$

$$U_{i,j} = \epsilon\ S\ dz\ (\psi^L_j\ C^L_j\ h^L_j + \psi^V_j\ C^V_j\ h^V_j) \quad (2.19)$$

In the case of CO_2 absorption-stripping with MEA the phase equilibrium assumption is inadequate, due to the contemporary presence of material transfer and chemical reactions. Nevertheless, this model can still be used introducing an efficiency that takes into account the deviation from equilibrium [68]. The most used expression for the efficiency is the one proposed by Murphree [70]:

$$\eta_{i,j} = \frac{y_{i,j} - y_{i,j+1}}{y^*_{i,j} - y_{i,j+1}} \quad (2.20)$$

Values of the Murphree efficiency are typically very low when CO_2 reactive absorption is considered. For example, Walter & Sherwood [71] found an efficiency range between 0.65-4.2% using a glycerine aqueous solution as solvent in a plate column, while Afkhamipour & Mofarahi [72] used a range

of efficiencies between 0.1 and 0.4 with a AMP solution as absorbent in a packed column. Using MEA as solvent, Øi [25, 73] defined a Murphree efficiency of 0.25 for a packed column.
The equilibrium stage model combined with the Murphree efficiency was applied in several works [25, 26, 36, 73].

2.4.2 Rate-Based Model

The efficiency values reported at the end of Subsection 2.4.1 give a clear indication on how the CO_2 absorption process is far from the ideal equilibrium. For this reason, a more rigorous non-equilibrium model is necessary. In particular, this model must be able to take into account the material transfer limitations due to the presence of chemical reaction. For this purpose, a so-called *rate-based* model was developed, which accounts for interfacial material and energy transfer between the gaseous and the liquid phases, the reaction kinetics and the electrolytic interactions.
The main assumption of this approach is that phase equilibrium occurs at the vapor/gas-liquid interface only and that material and energy transport in the two phases are described separately. Furthermore, the first implication of this assumption is the fact that two distinct balances must be written for the two phases. For what concerns the material and energy balances for the rate-based model, reference is made to the rate-based segment representation reported in Figure 2.3.
In general, two different approaches can be used to write the balances:

- a differential form, which leads to an ideal Plug-Flow reactor model without axial dispersion;
- a discrete form, which leads to a Plug-Flow reactor modeled as a series of n-CSTR reactors.

Both the forms are reported below.

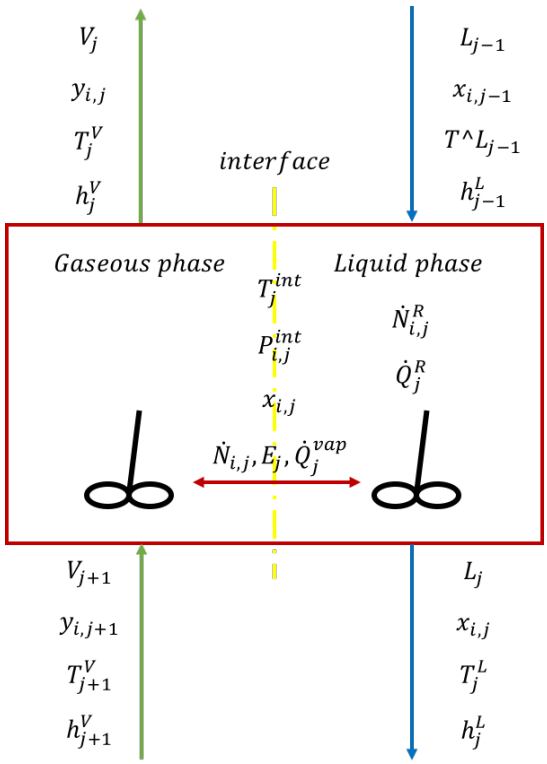

Figure 2.3: Rate-based segment representation

Ideal Plug-Flow reactor without axial dispersion

- Component material balance in the liquid phase

$$\frac{\partial M_i^L}{\partial t} = \frac{\partial (L x_i)}{\partial z} + \frac{\dot{N}_i^L}{dz} + \frac{\dot{N}_i^R}{dz} \tag{2.21}$$

$$\begin{cases} x_i = x_i^{SS} \\ L = L^{SS} \end{cases} \quad @ \quad t = 0 \quad , \quad \forall\ z$$

$$\begin{cases} x_i = x_i^{IN} \\ L = L^{IN} \end{cases} \quad @ \quad z = 0 \quad , \quad \forall\ t$$

- Component material balance in the gaseous phase

$$\frac{\partial M_i^V}{\partial t} = \frac{\partial (V y_i)}{\partial z} - \frac{\dot{N}_i^V}{dz} \tag{2.22}$$

$$\begin{cases} y_i = y_i^{SS} \\ V = V^{SS} \end{cases} \quad @ \quad t = 0 \quad , \quad \forall\ z$$

$$\begin{cases} y_i = y_i^{IN} \\ V = V^{IN} \end{cases} \quad @ \quad z = H \quad , \quad \forall\, t$$

- Energy balance in the liquid phase

$$\frac{\partial U_j^L}{\partial t} = \frac{\partial (L h^L)}{\partial z} + \frac{\dot{E}^L}{dz} + \frac{\dot{Q}^R}{dz} + \frac{\dot{Q}^{L_{vap}}}{dz} \tag{2.23}$$

$$\begin{cases} T^L = T^{L,SS} & @ \quad t = 0 \quad , \quad \forall\, z \\ T^L = T^{L,IN} & @ \quad z = 0 \quad , \quad \forall\, t \end{cases}$$

- Energy balance in the gaseous phase

$$\frac{\partial U_j^V}{\partial t} = \frac{\partial (V h^V)}{\partial z} - \frac{\dot{E}^V}{dz} - \frac{\dot{Q}^{V_{vap}}}{dz} \tag{2.24}$$

$$\begin{cases} T^V = T^{V,SS} & @ \quad t = 0 \quad , \quad \forall\, z \\ T^V = T^{V,IN} & @ \quad z = H \quad , \quad \forall\, t \end{cases}$$

Plug-Flow reactor as a series of n-CSTR reactors

- Component material balance in the liquid phase

$$\frac{dM_{i,j}^L}{dt} = L_{j-1}\ x_{i,j-1} - L_j\ x_{i,j} + \dot{N}_{i,j}^L + \dot{N}_{i,j}^R \tag{2.25}$$

$$\begin{cases} x_i = x_i^{SS} \\ L = L^{SS} \end{cases} \quad @ \quad t = 0$$

- Component material balance in the gaseous phase

$$\frac{dM_{i,j}^V}{dt} = V_{j+1}\ y_{i,j+1} - V_j\ y_{i,j} - \dot{N}_{i,j}^V \tag{2.26}$$

$$\begin{cases} y_i = y_i^{SS} \\ V = V^{SS} \end{cases} \quad @ \quad t = 0 \quad , \quad \forall\, z$$

- Energy balance in the liquid phase

$$\frac{dU_j^L}{dt} = L_{j-1}\ h_{i,j-1}^L - L_j\ h_{i,j}^L + \dot{E}_j^L + \dot{Q}_j^R + \dot{Q}_j^{L_{vap}} \tag{2.27}$$

$$T^L = T^{L,SS} \quad @ \quad t = 0$$

- Energy balance in the gaseous phase

$$\frac{dU_j^V}{dt} = V_{j+1}\ h_{i,j+1}^V - V_j\ h_{i,j}^V - \dot{E}_j^V - \dot{Q}_j^{Vvap} \tag{2.28}$$

$$T^V = T^{V,SS} \quad @ \quad t = 0$$

Common equations

- Material and energy fluxes equality at the interface

$$\dot{N}_i^{L,int} = \dot{N}_i^{V,int} \tag{2.29}$$

$$\dot{E}^{L,int} = \dot{E}^{V,int} \tag{2.30}$$

- Vapor-liquid equilibrium

$$P\ \phi_{i,j}\ y_{i,j}^{int} = P_{i,j}^{sat}\ \gamma_{i,j}\ x_{i,j}^{int} \tag{2.31}$$

- Gas-liquid equilibrium

$$P\ \phi_{i,j}\ y_{i,j}^{int} = He_{i,j}\ \gamma_{i,j}\ x_{i,j}^{int} \tag{2.32}$$

- Summation equations

$$\sum_{i=1}^{n_c^L} x_{i,j} \tag{2.33}$$

$$\sum_{i=1}^{n_c^V} y_{i,j} \tag{2.34}$$

- Material and energy hold-up

$$M_{i,j}^L = \epsilon\ S\ dz\ \phi_j^L\ C_j^L\ x_{i,j} \tag{2.35}$$

$$M_{i,j}^V = \epsilon\ S\ dz\ \phi_j^V\ C_j^V\ y_{i,j} \tag{2.36}$$

$$U_{i,j}^L = \epsilon\ S\ dz\ \phi_j^L\ C_j^L\ h_j^L \tag{2.37}$$

$$U_{i,j}^V = \epsilon\ S\ dz\ \phi_j^V\ C_j^V\ h_j^V \tag{2.38}$$

As it is possible to notice, the material and energy balances for the rate-based model are more detailed compared to equilibrium stage model, especially due to the separated description of what happens inside the two phases. At the same time, the rate-based model is more rigorous than the equilibrium stage one. The main innovation of the model relies in the addition of the interphase material and energy transfer terms, $\dot{N}_i$ and $\dot{E}$. These terms can be evaluated in different ways, as it is going to be discussed in Subsection 2.4.2.1.

2.4.2.1 Interphase material transfer equations

Three main theories have been proposed to describe the material transport across the gaseous-liquid interface:

- the two-film theory by Lewis & Whitman [74] → steady-state model;
- the penetration theory by Higbie [75] → unsteady-state model;
- the surface renewal model by Danckwerts [76] → unsteady-state model.

Although applications of the penetration theory and the surface renewal model can be find in the literature for CO_2 absorption [16, 64, 77], the two-film theory is by far the most used model in this field [2, 19–22, 36–39, 44, 46, 47, 50, 53, 57, 62, 63, 78–84], due to the fact that it is simple and a significant number of correlations for the parameters evaluation is present in the literature [85, 86].
A graphical representation of the two-film theory in the presence of chemical reaction in the liquid phase is reported in Figure 2.4, both for absorption (a) and stripping (b). The profiles are referred to the CO_2 molar fraction.

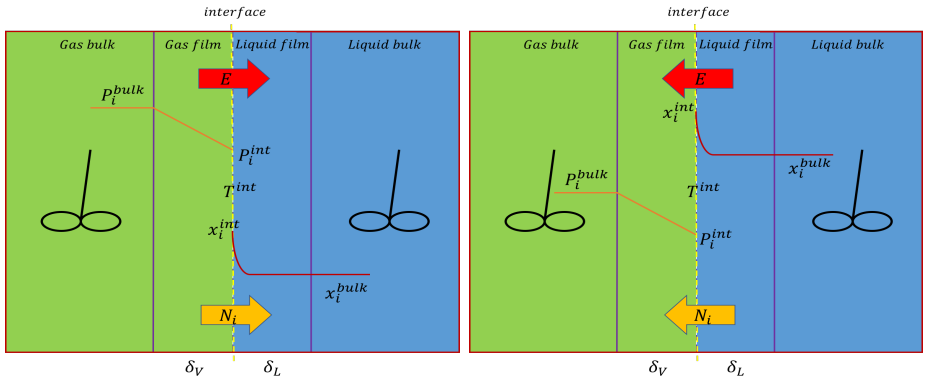

(a) Absorber (b) Stripper

Figure 2.4: Representation of the two-film theory

The model is based on the following assumption: close to the gaseous-liquid interface, where phase equilibrium exists, two thin films are present where all the resistance to material and energy transfer is concentrated. In particular, the spatial domain can be divided in four parts:

- gaseous bulk;
- gaseous film;
- liquid film;
- liquid bulk.

In the absorption process, the CO_2 is transferred from the gaseous bulk to the interface through the gaseous film. Since no reactions are present in the gaseous phase, the concentration profile is linear. Then CO_2 is absorbed in the liquid, where it reacts with the solvent. The presence of the reactions causes the profile to be strongly not linear. The remaining CO_2 dissolved in the liquid is finally transferred to the liquid bulk. When the stripping process is considered, the desorbed component follows the exact opposite way.
The main variable that is needed to be evaluated is the interphase molar flux N_i, which is related to the diffusive flux J_i by means of the following relations for the two phases:

$$N_i^L = J_i^L + \frac{x_i^{int} + x_i}{2} \sum_{i=1}^{n_c^L} N_i^L = J_i^L + x_i^{avg}\ N_t^L \tag{2.39}$$

$$N_i^V = J_i^V + \frac{y_i^{int} + y_i}{2} \sum_{i=1}^{n_c^V} N_i^V = J_i^V + y_i^{avg}\ N_t^V \tag{2.40}$$

where x_i^{avg} and y_i^{avg} are the mean molar fractions of component i in the liquid and gaseous phase, respectively, and N_t is the mixture molar flux. Then, to evaluate the interphase molar flux, it is necessary to evaluate the diffusive flux, J_i. Two rigorous approaches can be used in this case [87]:

- the Maxwell-Stefan diffusion equations for multicomponent systems;
- the generalized Fick's law.

The equations for the two approaches are reported below for both the gaseous and liquid film.

Maxwell-Stefan diffusion equations for multicomponent systems

For what concerns the gaseous film, the Maxwell-Stefan equation assumes the following form, where it can be noticed that the driving force is given by the chemical potential gradient:

$$\sum_{\substack{k=1 \\ k\neq i}}^{n_c^V} \frac{y_i^f J_k^V - y_k^f J_i^V}{C^V \mathfrak{D}_{i,k}^V} = \frac{y_i^f}{\delta^V R\ T^V}\ \frac{d\mu_i^V}{d\xi^V} \tag{2.41}$$

When the liquid film is considered, the complexity of the Maxwell-Stefan equation increases because the electrolytic interactions must be taken into account. For this reason, differently from Eq. 2.41, the driving force is represented by the chemical potential and the electrical potential gradients:

$$\sum_{\substack{k=1 \\ k\neq i}}^{n_c^L} \frac{x_i^f J_k^L - x_k^f J_i^L}{C^L \mathfrak{D}_{i,k}^L} = \frac{x_i^f}{\delta^L R\ T^L}\ \frac{d\mu_i^L}{d\xi^L} + \frac{x_i^f \hat{z}_i\ \mathfrak{F}}{\delta^L R\ T^L} \frac{d\Phi}{d\xi^L} \tag{2.42}$$

In the case of dilute electrolyte solutions Eq. 2.42 can be simplified obtaining the Nernst-Planck equation [79, 87]:

$$J_i^L = -\frac{C^L \mathfrak{D}_{i,n}^o}{\delta^L} \frac{dx_i^f}{d\xi^L} - \frac{C^L x_i^f \hat{z}_i\ \mathfrak{D}_{i,n}^o \mathfrak{F}}{\delta^L R\ T^L} \frac{d\Phi}{d\xi^L} \tag{2.43}$$

For both Eqs. 2.42 and 2.43, the expression for the electrical potential is given by Eq. 2.44 [87]:

$$\frac{d\Phi}{d\xi^L} = -\frac{R\ T^L}{\mathfrak{F}} \frac{\displaystyle\sum_{k=1}^{n_c^L-1} \hat{z}_k\ \mathfrak{D}_{i,n}^o \frac{dx_k^f}{d\xi^L}}{\displaystyle\sum_{k=1}^{n_c^L-1} \hat{z}_k^2\ \mathfrak{D}_{i,n}^o x_k^f} \tag{2.44}$$

Finally, in order to guarantee the electroneutrality of the solution, the electroneutrality condition must be coupled to Eqs. 2.42 and 2.43:

$$\sum_{i=1}^{n_c^L} \hat{z}_i\ x_i^f = 0 \tag{2.45}$$

Generalized Fick's law

An alternative approach to the Maxwell-Stefan equations is represented by the Fick's law for multicomponent systems. In this case the expression of

the diffusive flux J_i is the same for the gaseous and the liquid phase and reported in Eqs. 2.48 and 2.49, respectively.

$$J_i^V = -\frac{C^V}{\delta^V} \sum_{k=1}^{n_c^V - 1} \mathscr{D}_{i,k}^V \frac{dy_k^f}{d\xi^V} \tag{2.46}$$

$$J_i^L = -\frac{C^L}{\delta^L} \sum_{k=1}^{n_c^L - 1} \mathscr{D}_{i,k}^L \frac{dx_k^f}{d\xi^L} \tag{2.47}$$

Eqs. 2.48 and 2.49 can be written also in terms of material transfer coefficients:

$$J_i^V = C^V \sum_{k=1}^{n_c^V - 1} k_{M_{i,k}}^V \ (y_k - y_k^{int}) \tag{2.48}$$

$$J_i^L = C^L \sum_{k=1}^{n_c^L - 1} k_{M_{i,k}}^L \ (x_k^{int} - x_k) \tag{2.49}$$

where:

$$k_{M_{i,k}}^V = \frac{\mathscr{D}_{i,k}^V}{\delta^V} \quad ; \quad k_{M_{i,k}}^L = \frac{\mathscr{D}_{i,k}^L}{\delta^L} \tag{2.50}$$

2.4.2.2 Inclusion of the chemical reactions

In Subsection 2.4.2.1 the equations related to the interphase material transfer without reactions were reported. Since the CO_2-MEA-H_2O is a reactive system, chemical reactions must be included in the liquid film balances. This can be done in two different ways:

- Write a differential or discrete balance in the liquid film [79]:

$$\frac{1}{\delta^L} \frac{d\dot{N}_i^L}{d\xi^L} - \dot{N}_i^{R,f} = 0 \tag{2.51}$$

$$\dot{N}_i^{L,int} = \dot{N}_i^{V,int} \quad @ \quad \xi = 0$$
$$\dot{N}_i^{L,int} - \dot{N}_i^L - \dot{N}_i^{R,f} = 0 \tag{2.52}$$

- Substitute Eq. 2.39 with the following expression:

$$N_i^L = C^L \ EF_i \ k_{M_{i,mix}}^L \ (x_i^{int} - x_i) + x_i^{avg} \ N_t^L \tag{2.53}$$

  where EF_i represents the enhancement factor [88], which is defined as the ratio between material transfer in the presence of chemical reaction and pure diffusive material transfer [89]:

$$EF_i = \frac{N_i^L}{k_{M_{i,mix}}^L \ C^L \ (x_i^{int} - x_i)} \tag{2.54}$$

The first approach is certainly the most rigorous one, while the latter simplifies the system solution notably. There is no agreement in the literature on whether one approach is better than the other. For instance, Kucka et al. [79] recommend to use the rigorous differential balance approach since the enhancement factor based model predicts too high concentration values for what concerns the gaseous phase in an industrial case application analyzed. Different authors used the rigorous approach [2, 38, 39, 46, 90]. Nevertheless, a significant number of authors implemented their model using the enhancement factor [15, 16, 21, 49, 50, 62, 80, 84]. It can be said that the differential balance approach, though it is definitely preferable for a rigorous and correct process modeling as it offers greater insights on the phenomena happening in the liquid film, has the disadvantage to make the solution of the system more difficult. On the other hand, the enhancement factor is very simple but offers a less detailed description of what happens in the liquid film. Furthemore, it must be taken into account that there is no unanimously accepted expression for the enhancement factor in the literature.
In general, the rigorous approach is of easy use with commercial simulators such as Aspen Plus® where it is already implemented, while the enhancement factor is preferred in equation-oriented models, due to its simplicity.

2.4.2.3 Interphase energy transfer equations

As already stated in the previous sections, the process is characterized by simultaneous material and energy transfer. For what concerns the energy transfer, the two-film theory is applied following the approach by Taylor & Krishna [87]. In particular, the energy flux for both the phases is given by Eqs. 2.56-2.55:

$$E^L = q^L + \sum_{i=1}^{n_c^L} N_i^L (h_i^L + \lambda_i) \tag{2.55}$$

$$E^V = q^V + \sum_{i=1}^{n_c^V} N_i^V (h_i^V + \lambda_i) \tag{2.56}$$

where it can be noticed that, in analogy with Eqs. 2.39 and 2.40, the energy flux is the sum of a conductive flux, q, and a convective term, which contains the component enthalpy and its latent heat of vaporization/condensation. In particular, the conductive flux is evaluated by means of the Fourier's law:

$$q^V = -\frac{k_T^V}{\delta^V} \frac{dT^V}{d\xi^V} \tag{2.57}$$

$$q^L = -\frac{k_T^L}{\delta^L} \frac{dT^L}{d\xi^L} \tag{2.58}$$

which can be also expressed in terms of heat transfer coefficients:

$$q^V = h_T^V \left(T^V - T^{int}\right) \tag{2.59}$$

$$q^L = h_T^L \left(T^{int} - T^L\right) \tag{2.60}$$

Moreover, since the reactions generate (or produce) heat, a further (differential or discrete) balance to take account of the heat of reaction is needed:

$$\frac{1}{\delta^L}\frac{d\dot{E}^L}{d\xi^L} - \dot{Q}^{R,f} = 0 \tag{2.61}$$

$$\dot{E}^{L,int} = \dot{E}^{V,int} \quad @ \quad \xi = 0$$

$$\dot{E}^{L,int} - \dot{E}^L - \dot{Q}^{R,f} = 0 \tag{2.62}$$

2.4.3 Rate-Based model correlations

A further aspect that demonstrates the higher level of detail of the rate-based model compared to the equilibrium stage one is the need to evaluate the following parameters:

- wetted surface area;
- material transfer coefficients;
- heat transfer coefficients;
- fractional liquid hold-up.

Different correlations are available for the calculation of these parameters based on the packing type, i.e., random or structured packing. A brief literature review about these correlations is presented in the following Subections, while the specific correlations used in this work together with the equations are discussed in Chapter 3.

2.4.3.1 Wetted surface area

One characteristic parameter of the packing is the dry specific area, i.e., the packing surface available per cubic meter of packing. When the liquid irrigates the packing, it covers a fraction of this available surface, which is referred to as wetted surface area. This parameter indicates the contact surface between the gaseous and the liquid phase. Typically, it is a function of the liquid properties and the packing geometry and its expression is usually given with reference to the three dimensionless numbers of Reynolds, Freud and Weber.
Several correlations have been developed for the evaluation of the wetted surface area, depending on the packing type, as they can be used for:

- random packing only: Onda et al. (1968) [91];
- structured packing only: Bravo et al. (1985,1992) [92, 93], Henriques de Brito et al. (1994) [94], Tsai et al. (2008,2011) [95, 96];
- all kinds of packing: Billet & Schultes (1993) [97], Hanley & Chen (2012) [98].

Table 2.2 reports a selection of works with the used correlations divided by packing type.

References	**Packing**	**Correlation**
Random packing		
[39]	CMR#2	Onda et al. (1968) [91]
[19, 21, 36, 38, 50]	IMTP#40	Onda et al. (1968) [91]
[28]		Hanley & Chen (2012) [98]
[53]	IMTP#50	Hanley & Chen (2012) [98]
[2, 57, 83]	Ceramic Berl Saddles	Onda et al. (1968) [91]
Structured packing		
[46]	Mellapak 250Y	Bravo et al. (1985) [92]
[37]		Bravo et al. (1992) [93]
[16, 20, 49]		Henriques de Brito et al. (1994) [94]
[47]		Tsai (2011) [96]
[53]		Hanley & Chen (2012) [98]
[2]	Mellapak 2X	Bravo et al. (1985) [92]
[38]	Flexipac 1Y	Bravo et al. (1985) [92]
[37]		Tsai (2009) [95]
[57]	Gempak 4A	Bravo et al. (1985) [92]

Table 2.2: Literature review on the correlations used for the evaluation of the wetted surface area

2.4.3.2 Material transfer and heat transfer coefficients

For the description of the interphase material and energy transfer, material and energy transfer coefficients were introduced and defined as the ratio between the diffusion coefficient (material transfer) or the thermal conductivity (energy transfer) and the film thickness:

$$k_M^p = \frac{\mathscr{D}^p}{\delta^p} \quad ; \quad h_T^p = \frac{k_T^p}{\delta^p} \tag{2.63}$$

where p indicates the phase.
Since the estimation of the film thickness is difficult, these coefficients are

typically evaluated by means of empirical correlations [87]. The discussion is the same as the previous one on the wetted surface area. The coefficients are functions of the phase properties and the geometric features of the packing. Depending on the packing type the correlations for the estimation of the material transfer coefficients can be applied for:

- random packing only: Onda et al. (1968) [91];
- structured packing only: Bravo et al. (1985,1992) [92, 93], Rocha et al. (1996) [99];
- all kinds of packing: Billet & Schultes (1993) [97], Hanley & Chen (2012) [98].

Table 2.3 reports a selection of works with the used correlations and the corresponding packing type.

References	**Packing**	**Correlation**
Random packing		
[39]	CMR#2	Onda et al. (1968) [91]
[19, 21, 29, 36, 38, 50]	IMTP#40	Onda et al. (1968) [91]
[53]	IMTP#50	Hanley & Chen (2012) [98]
[2, 57, 83]	Ceramic Berl Saddles	Onda et al. (1968) [91]
Structured packing		
[22]	Mellapak 250Y	Onda et al. (1968) [91]
[46]		Bravo et al. (1985) [92]
[37]		Bravo et al. (1992) [93]
[47]		Billet & Schultes (1993) [97]
[16, 20, 49]		Rocha et al. (1996) [99]
[53]		Hanley & Chen (2012) [98]
[2]	Mellapak 2X	Bravo et al. (1985) [92]
[38]	Flexipac 1Y	Bravo et al. (1985) [92]
[37]		Bravo et al. (1992) [93]
[57]	Gempak 4A	Bravo et al. (1985) [92]

Table 2.3: Literature review on the correlations used for the evaluation of the material transfer coefficients

Once the computation of the material transfer coefficient is performed, the most used approach for the evaluation of the heat transfer coefficients is the Chilton-Colburn analogy [100]. According to the theory, the mechanisms through which material and heat transfer happen are identical. Then, once the transfer coefficient is known for one transfer type, the evaluation of the remaining transfer coefficient is straightforward.

2.4.3.3 Fractional liquid hold-up

Once the packing is placed in the column, the volume-free portion for the liquid and the gaseous phase is identified by the packing void fraction. When the column operates, a percentage of this volume is occupied by the liquid, while the gaseous phase occupies the remaining part. In order to properly evaluate the control volumes in which the balances must be written, it is necessary to evaluate the fractional liquid hold-up, i.e., the volume fraction occupied by the liquid. Once this parameter is known, the volume fraction occupied by the gas/vapor evaluation is immediate, since the sum of the two fractions must be equal to unity.
Even in this case, several relationships are present based on the packing type. Differently from the wetted surface area and the material transfer coefficients, no random packing only correlation are available. The fractional liquid hold-up can be evaluated for:

- structured packing only: Suess & Spiegel (1992) [101], Bravo et al. (1992) [93], Rocha et al. (1993) [102];
- all kinds of packing: Stichlmair et al. (1989) [103], Billet & Schultes (1993,1997,1999) [97, 104, 105].

Table 2.4 reports a selection of works with the used correlations and the corresponding packing type.

References	**Packing**	**Correlation**
Random packing		
[39]	CMR#2	Stichlmair et al. (1989) [103]
[38]	IMTP#40	Stichlmair et al. (1989) [103]
[28, 29, 58]		Billet & Schultes (1999) [105]
[2]	Ceramic Berl Saddles	Stichlmair et al. (1989) [103]
Structured packing		
[16, 22]	Mellapak 250Y	Suess & Spiegel (1992) [101]
[46]		Bravo et al. (1992) [93]
[47]		Billet & Schulter (1993) [97]
[20]		Rocha et al. (1993) [102]
[2]	Mellapak 2X	Bravo et al. (1992) [93]
[38]	Flexipac 1Y	Bravo et al. (1992) [93]

Table 2.4: Literature review on the correlations used for the evaluation of the fractional liquid hold-up

2.4.4 Fluid dynamics

Once the modeling of a single segment is defined, another fundamental aspect that must be taken into account is the one regarding the system fluid dynamics. As reported in Subsection 2.4.2, reactive absorption-stripping packed columns are typically modeled as PFRs without axial dispersion from the fluid dynamic point of view. The PFR model without axial dispersion, although it is by far the most used model to describe the fluid dynamics of the absorption-stripping columns, is an assumption which must be validated in order to be definitely acceptable. In particular, it must be verified that the columns have a fluid dynamic behavior that resembles that of an ideal plug-flow. In general, two factors can make the PFR assumption fall:

- the axial diffusion/dispersion (microscale phenomenon)
- the backmixing due to the countercurrent (macroscale phenomenon)

If only one of these factors had an important effect on the process, the PFR assumption would not be valid anymore. The methods to analyze the influence of the axial diffusion/dispersion and the backmixing due to the countercurrent are presented in Subsection 2.4.4.1 and Subsection 2.4.4.2. Then, the influence of the fluid dynamics on the mathematical solution of the resulting system of equation is discussed in Subsection 2.4.4.3.

2.4.4.1 Axial diffusion/dispersion: Peclet number definition

In order to analyze the possible effect of the axial diffusion/dispersion on the system fluid dynamics, it is worth to evaluate the Peclet number. This dimensionless group is defined as:

$$Pe = \frac{\text{rate of transport by convection}}{\text{rate of transport by diffusion/dispersion}} = \frac{F\ L_c}{\epsilon\ \psi\ S\ C\ \mathscr{D}}$$

where L_c represents the characteristic lenght.
In general, high values of the Peclet number indicate a column behavior close to that of an ideal plug-flow. On the other hand, if the value of the dimensionless group is small, the axial diffusion/dispersion has an effect on the process that could not be neglected.
The Peclet number can be defined for both the phases either for what concerns the material transport and the energy transport. Moreover, two characteristic lenghts can be considered, i.e., the column height and the packing equivalent diameter. The former provides information on the overall column behavior, while the latter considers the effect of the diffusion/dispersion at a local level, around the packing.
For what concerns the material transport, the Peclet number is defined for

all the components and the mixture and for both the phases, in Eq. 2.64 with reference to the packing height and in Eq. 2.65 with reference to the packing equivalent diameter:

$$Pe^V_{M,H_i} = \frac{V\ H}{\epsilon\ \psi^V\ S\ C^V\ \mathscr{D}^V_{i,mix}} \quad ; \quad Pe^L_{M,H_i} = \frac{L\ H}{\epsilon\ \psi^L\ S\ C^L\ \mathscr{D}^L_{i,mix}} \tag{2.64}$$

$$Pe^V_{M,d_{eq_i}} = \frac{V\ d_{eq}}{\epsilon\ \psi^V\ S\ C^V\ \mathscr{D}^V_{i,mix}} \quad ; \quad Pe^L_{M,d_{eq_i}} = \frac{L\ d_{eq}}{\epsilon\ \psi^L\ S\ C^L\ \mathscr{D}^L_{i,mix}} \tag{2.65}$$

Similarly, the thermal Peclet number is defined as following for both the phases and with reference to the packing height in Eq. 2.66 and in Eq. 2.67 with reference to packing equivalent diameter:

$$Pe^V_{T,H} = \frac{c^V_{P,mix}\ V\ H}{\epsilon\ \psi^V\ S\ k^V_T} \quad ; \quad Pe^L_{T,H} = \frac{c^L_{P,mix}\ L\ H}{\epsilon\ \psi^L\ S\ k^L_T} \tag{2.66}$$

$$Pe^V_{T,d_{eq}} = \frac{c^V_{P,mix}\ V\ d_{eq}}{\epsilon\ \psi^V\ S\ k^V_T} \quad ; \quad Pe^L_{T,d_{eq}} = \frac{c^L_{P,mix}\ L\ d_{eq}}{\epsilon\ \psi^L\ S\ k^L_T} \tag{2.67}$$

The expression of the Peclet number is obtained from the dimensionless form of the material and energy balances considering the diffusion/dispersion term. Therefore, to evaluate the dimensionless group, an appropriate reference condition is required. The easiest choice is to consider the feed conditions (top for the liquid phase and bottom for gaseous one) as reference for the physical properties, in order to make the Peclet number analysis independent from the system solution, since the results are known before performing any simulation.

2.4.4.2 Backmixing due to the countercurrent effect

The second factor which affects the ideal plug-flow assumption is represented by the backmixing due to the countercurrent. This macroscale phenomenon is not taken into account by the Peclet number, which contains the axial diffusion/dispersion, a microscale phenomenon. The backmixing is implicitly included in the material and energy balances because of the countercurrent streams arrangement and to investigate its possible effect on the process it is necessary to obtain the correct numerical solution of the resulting system of equation.

2.4.4.3 The number of segments analysis

The discussion on the modeling of the system fluid dynamics up to now dealt with the physics only, but it is strictly linked to a fundamental mathematical aspect which is the solution of the resulting system of equations obtained from the model development. It was outlined that two equivalent models can be used to write the material and energy balances:

- Ideal plug-flow reactor;
- Series of n-CSTRs.

In the first case, the balances describing the system at steady-state are Ordinary Differential Equations (ODEs). Since a set of algebraic equations is coupled with the differential balances, the resulting system is a Differential Algebraic Equations (DAEs) system. Due to the presence of the counter-current streams arrangement, the easiest way to solve the resulting ODEs system is by means of an implicit method (for example the Implicit Newton Method), and this leads to the resolution of a system of algebraic equations. In the latter case, since the equations describing a CSTR at steady-state are algebraic equations, again a system of algebraic equations must be solved to find the system profiles and outputs.
When dealing with a system of algebraic equations, a crucial step to find the solution is the correct definition of the number of points in the axial domain, i.e., the packing height, where this system is to be solved. In other words, it must be defined an appropriate number of segments for the discretization of the packing height. Very often this parameter has been too easily defined in the literature, and its influence on the model has not been appropriately discussed. For example, Mores et al. [27], Kucka et al. [79] and Mac Dowell et al. [83] focused their research on the mathematical modeling of the CO_2-MEA absorption system, validating their models using the experimental data reported in the work of Tontiwachwuthikul et al. [56]. They all considered the same absorber with a packing height of 6.55 m. The first research group discretized the packing height using 10 segments, the second one 15 and the third 25. The same discussion can be made with reference to several authors who validated their model using the experimental data from the work of Dugas [106], who made an experimental campaign using a pilot-plant facility at the University of Texas at Austin. Plaza et al. [37], Kvamsdal & Rochelle [39], Lawal et al. [36] and Zhang et al. [38] all used a different number of segments of discretization, although they all dealt with same exact column. To furtherly corroborate this fact, a list of some relevant works where the rate-based method was used to model the CO_2-MEA absorber is reported in Table 2.5.

Reference	Segments	Height [m]	Diameter [m]
Absorber			
[20]	39	3.89	0.15
[90]	20	4.25	0.125
[37]	12	6.10	0.427
[27]	10	6.55	0.100
[79]	15	6.55	0.100
[83]	25	6.55	0.100
[39]	30	6.10	0.427
[36]	15	6.10	0.427
[38]	20	6.10	0.427
[78]	15	8.00	1.680
[45]	24	12.00	0.150
[44]	40	17.00	1.100

Table 2.5: Literature review on the number of segments applied in the rate-based model for the CO_2-MEA absorption-stripping system

From the analysis of Table 2.5 it can be noticed that there is not correspondence between the number of segments and the column dimensions. Even when the same column height is considered, there is still a variation in the number of segment considered. This disagreement deserves to be explored in detail.
The definition of a correct number of segments for the discretization of the axial domain is strictly related to the possible influence that the axial dispersion and the backmixing due to the countercurrent have on the process. In particular:

- for large values of the Peclet number the axial dispersion effect can be neglected. In this case the system fluid dynamics resembles that of an ideal plug-flow and, consequently, a high number of segments would be needed to correctly describe the process;

- due to the countercurrent streams arrangement, even if the axial dispersion had no influence, the plug-flow assumption would fall if the backmixing generated by the countercurrent played an important role on the process. As already reported in Subsection 2.4.4.2, to investigate the possible effect of the backmixing, it is necessary to obtain the correct numerical solution of the resulting DAEs system. This means that the the number of segments must be increased until an asymptotic

behavior is reached [107–109], i.e., until the differences between two consecutive simulations with different number of segments are negligible. If the number of segments for the discretization of the axial domain necessary to obtain the correct solution is sufficiently high, it can be concluded that the backmixing due to the countercurrent has no important effect on the process.

The definition of a proper number of segments is of fundamental importance to obtain a robust and correct model from a numerical point of view. The application of this analysis was done in this thesis for both the absorber (Chapter 4) and the stripper (Chapter 5).

2.5 Chapter 2 Summary

In this chapter, a general review for what concerns the process modeling of the CO_2 Post-Combustion Capture by means of reactive absorption-stripping using amine aqueous solutions, with focus on MEA as solvent, was made. In particular, the necessity of a thermodynamic model such as the Electrolyte-NRTL model for the description of the non-ideal ionic liquid solution was highlighted. It was shown the importance of the chemical reactions, which in this case are of both equilibrium and kinetic nature, leading to a hybrid set of reactions. Then, two different approaches to write the material and energy balances were presented: the equilibrium stage model and the rate-based model. The high complexity of the process, which involves several different phenomena, leads inevitably to the necessity of using a rate-based approach for the correct mathematical description of the process itself. Two equivalent approaches were presented to write the material and energy balances in the bulk of the two phases, i.e., ideal PFR and plug-flow reactor as a series of n-CSTR. Successively the focus was concentrated on the description of the interphase material and energy transfer, showing that the approach based on the two-film theory is the most-used in the literature. In particular, two rigorous ways to describe the simultaneous material and energy transfer at the interphase, i.e., the Maxwell-Stefan model for multicomponent systems and the Fick's law for multicomponent systems were presented. To conclude the part regarding the description of the film, the chemical reactions were introduced in the system by means of a rigorous differential equation in the liquid film or a simple enhancement factor. Then, the correlations needed to estimate the several parameters included in the rate-based model were reported. For each parameter, after a brief introduction of the physical meaning, it was reported a review based on the different kinds of packing that can be found in the open literature. The end of the chapter was dedicated to the fluid dynamics of the system, pointing out the

main factors that influence the correctness of the ideal plug-flow assumption, represented by the axial diffusion/dispersion and the backmixing due to the countercurrent. Then, it was highlighted the connection between the fluid dynamics and the mathematical solution of the system introducing the number of segments analysis. In fact, since a system of algebraic equations must be solved, the choice of an appropriate number of segments is fundamental to correctly describe the process.
In the next chapter the focus is moved to the process modeling by means of the rate-based approach in Aspen Plus®, which is the software used in this work for all the simulations.

Chapter 3

Process modeling on Aspen Plus®

The implementation of the rate-based model included in the Aspen Plus® package is the object of this chapter. Components, thermodynamics and chemical reactions are taken into account in the first place. Then, the material and energy balances and a detailed description of the parameters to tune the model for the modeling of the bulk and the film are reported. The final chapter section is dedicated to the correlations used for the evaluation of the wetted surface area, the material and energy transfer coefficients and the fractional liquid hold-up.

3.1 Introduction

Aspen Plus® from AspenTech is one of the most used steady-state process modeling and simulation software in process engineering. It is widely used both at an academic and industrial level. It offers the possibility to model a broad spectrum of processes, from the classic distillation columns to different kinds of reactors, and includes also all the necessary equipment typical of a chemical plant, such as heat exchangers or pumps. The suite offers the possibility to link the modeling part with Aspen Properties®, which is the package from the same company that gives the possibility to access an extremely large database of physical properties.
As reported in Chapter 2, the CO_2 post-combustion capture by means of MEA consists in a reactive absorption-stripping process. In Aspen Plus® this kind of processes are typically modeled using the so-called *RadFrac*™ model [2,38,46], which permits to model absorbers and strippers with chemical reactions using either the equilibrium stage model (Subsection 2.4.1) and the rate-based model (Subsection 2.4.2). In this work, the rigorous rate-based model was used for both the absorber and the stripper, and from now on it is the only considered model. In the following sections, the model is described for what concerns:

- thermodynamics;
- chemical reactions;
- material and energy balances;
- fluid dynamics;
- interphase transfer.

3.2 The Aspen Plus® *RadFrac*™ model - Rate-Based mode

3.2.1 Components and system thermodynamics

The first step in building a model on Aspen Plus® was the definition of the components involved, followed by the definition of the system thermodynamics. It must be noted that for this part the software leans on the Aspen Properties® package.
In the case of the CO_2 post-combustion capture with MEA aqueous solutions the process involves two different phases, the vapor/gas and the liquid one, which are characterized by different components. In particular, while the gaseous phase contains only gases, with the exception of water vapor,

the liquid phase contains all the ions involved in the CO_2-MEA-H_2O system. Table 3.1 resumes the components for the two phases.

Gaseous phase		**Liquid phase**	
Component	*Name*	*Component*	*Name*
CO_2	Carbon dioxide	CO_2	Free carbon dioxide
H_2O	Water	CO_3^{2-}	Carbonate ion
MEA	Monoethanolamine	H_2O	Free water
N_2	Nitrogen	H_3O^+	Hydronium ion
O_2	Oxigen	HCO_3^-	Bicarbonate ion
		MEA	Free monoethanolamine
		MEA^+	Protonated monoethanolamine
		$MEACOO^-$	Carbamate ion
		OH^-	Hydroxide ion

Table 3.1: Model components

For what concerns the system thermodynamics, the Elec-NRTL model [31], discussed in Section 2.2, was used in this work for the evaluation of the activity coefficients of the non-ideal ionic liquid solution. Furthermore, the Elec-NRTL model was coupled with the Redlich-Kwong EoS for the computation of the fugacity coefficients for the gaseous phase components.

3.2.1.1 Apparent and actual composition

As reported in Table 3.1, the CO_2-MEA-H_2O system is characterized by the presence of ions, for a total of 9 components in the liquid phase. The ions are a convenient way to represent the process by means of a mathematical model, but from an experimental point of view, the evaluation of their actual composition is not advantageous. Typically, the composition measurements in the liquid phase are given in terms of apparent carbon dioxide, monoethanolamine and water concentrations. The apparent compositions are related to the actual ions compositions by means of the following relations in terms of molar fractions (Eq. 3.1-3.3):

$$x_{CO_2}^{app} = x_{CO_2} + x_{CO_3^{2-}} + x_{HCO_3^-} + x_{MEACOO^-} \tag{3.1}$$

$$x_{MEA}^{app} = x_{MEA} + x_{MEA^+} + x_{MEACOO^-} \tag{3.2}$$

$$x_{H_2O}^{app} = x_{H_2O} + x_{H_3O^+} + x_{HCO_3^-} + x_{OH^-} \tag{3.3}$$

Since, 9 compositions are to be computed for modeling purposes, there is the need for 6 more equations to square the system. These equations are represented by the ionic equilibrium relations and the summation equation (Eqs. 3.4-3.9):

$$2H_2O \rightleftarrows H_3O^+ + OH^-$$

$$K_{eq_1} = \frac{a_{H_3O^+}\ a_{OH^-}}{a^2_{H_2O}} \tag{3.4}$$

$$CO_2 + 2H_2O \rightleftarrows H_3O^+ + HCO_3^-$$

$$K_{eq_2} = \frac{a_{H_3O^+}\ a_{HCO_3^-}}{a_{CO_2}\ a^2_{H_2O}} \tag{3.5}$$

$$HCO_3^- + H_2O \rightleftarrows H_3O^+ + CO_3^{2-}$$

$$K_{eq_3} = \frac{a_{H_3O^+}\ a_{CO_3^{2-}}}{a_{HCO_3^-}\ a_{H_2O}} \tag{3.6}$$

$$MEA^+ + H_2O \rightleftarrows H_3O^+ + MEA$$

$$K_{eq_4} = \frac{a_{H_3O^+}\ a_{MEA}}{a_{MEA^+}\ a_{H_2O}} \tag{3.7}$$

$$MEACOO^- + H_2O \rightleftarrows HCO_3^- + MEA$$

$$K_{eq_5} = \frac{a_{HCO_3^-+}\ a_{MEA}}{a_{MEACOO^-}\ a_{H_2O}} \tag{3.8}$$

$$\sum_{i=1}^{N_C^L} x_i = 1 \tag{3.9}$$

These equations are used by Aspen Plus® in the simulations to characterize all the liquid streams composition. It must be noted that these reactions are not the same used to describe the reactions that happen inside the columns, which are discussed in the next section.

3.3 Chemical reactions

As extensively discussed in Section 2.3, to properly describe the chemical reactions that happen in the system, a reaction set composed by kinetic limited reactions involving CO_2 and equilibrium reactions must be used.
In this work, the hybrid scheme including three ionic equilibrium reactions from Eqs. 3.10-3.12 and the two kinetic reversible reactions 3.13 and Eq. 3.14 was considered [2, 46].

- *Self-ionization of water*

$$2H_2O \rightleftarrows H_3O^+ + OH^- \tag{3.10}$$

- *Dissociation of MEA*

$$MEA^+ + H_2O \rightleftarrows H_3O^+ + MEA \tag{3.11}$$

- *Dissociation of bicarbonate ion*

$$HCO_3^- + H_2O \rightleftarrows H_3O^+ + CO_3^{2-} \tag{3.12}$$

- *Formation of carbamate*

$$CO_2 + MEA + H_2O \rightleftarrows MEACOO^- + H_3O^+ \tag{3.13}$$

- *Formation of bicarbonate ion*

$$CO_2 + OH^- \rightleftarrows HCO_3^- \tag{3.14}$$

The equilibrium reactions 3.10-3.12 were considered instantaneous, while the last two reactions, which have kinetic limitations, were assumed to be reversible.
For the mathematical description of the equilibrium reactions, the equilibrium constant in terms of temperature were computed by means of the standard Gibbs free-energy change, while activities were used as concentration basis for the equilibrium constants in terms of concentrations (Eqs. 2.7-2.9). For what concerns the kinetic reversible reactions, the reaction rate was expressed by a second order power law expression, where the kinetic constant resulted from the Arrhenius equation and the concentration basis was expressed in terms of molarities:

- Formation of carbamate

$$r_1 = r_{1,f} - r_{1,r} = k_{1,f}\ C^L_{CO_2}\ C^L_{MEA} - k_{1,r}\ C^L_{MEACOO^-}\ C^L_{H_3O^+} \tag{3.15}$$

- Formation of bicarbonate ion

$$r_2 = r_{2,f} - r_{2,r} = k_{2,f}\ C^L_{CO_2}\ C^L_{OH^-} - k_{2,r}\ C^L_{HCO_3^-} \tag{3.16}$$

The kinetic parameters chosen in this work for reactions 3.13 and 3.14 are going to be discussed in Chapter 4.

3.4 Material and energy balances

Once the thermodynamics and the chemical reactions were defined, the next step was to describe what happens inside the column. The *RadFrac*^{TM} block contains the material and energy balances of the rate-based model, for which it is necessary to define a series of parameters for both the bulk and the film modeling. Furthermore, the column is divided into a user-specified number of segments where the balances are to be applied. The material and energy balances for the *RadFrac*^{TM} - Rate-Based mode are presented in the following subsections.

3.4.1 Modeling the bulk

3.4.1.1 Balances

The *RadFrac*^{TM} - Rate-Based mode, like all the Aspen Plus® blocks, is constituted by algebraic equations. For this reason, reactive columns are modeled as a series of n-CSTRs. Material and energy balances for the two phases bulk are reported in Eqs. 3.17-3.20, with reference to Figure 3.1 where index i indicates the component, while index j indicates the segment:

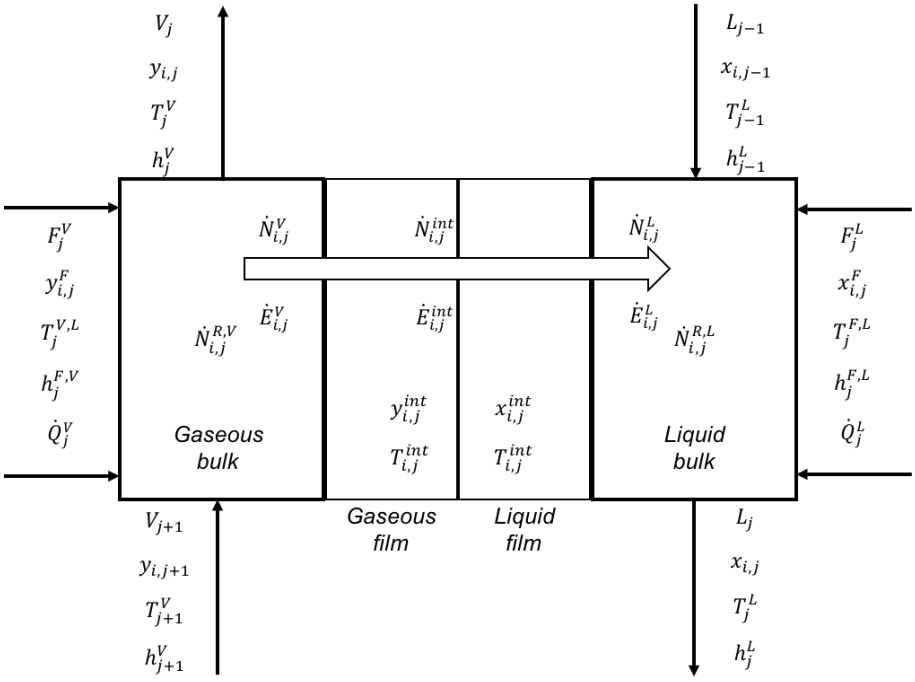

Figure 3.1: RadFrac^{TM} *- Rate-Based mode segment*

- Material balance in the liquid bulk

$$F_j^L \; x_{i,j}^F + L_{j-1} \; x_{i,j-1} + \dot{N}_{i,j}^L + \dot{N}_{i,j}^{R,L} - L_j \; x_{i,j} = 0 \tag{3.17}$$

- Material balance in the gaseous bulk

$$F_j^V \; y_{i,j}^F + V_{j-1} \; y_{i,j+1} - \dot{N}_{i,j}^V + \dot{N}_{i,j}^{R,V} - V_j \; y_{i,j} = 0 \tag{3.18}$$

- Energy balance in the liquid bulk

$$F_j^L \; h_j^{F,L} + L_{j-1} \; h_{j-1}^L + \dot{Q}_j^L + \dot{E}_j^L - L_j \; h_j^L = 0 \tag{3.19}$$

- Energy balance in the gaseous bulk

$$F_j^V \; h_j^{F,V} + V_{j+1} \; h_{j+1}^V + \dot{Q}_j^V - \dot{E}_j^V - V_j \; h_j^V = 0 \tag{3.20}$$

Also, the summation equations for both the phases are present in the system:

$$\sum_{i=1}^{n_c^L} x_{i,j} = 1 \tag{3.21}$$

$$\sum_{i=1}^{n_c^V} y_{i,j} = 1 \tag{3.22}$$

3.4.1.2 Flow models

For what concerns the evaluation of the bulk conditions in each segment, five different flow models are available in the *RadFrac*$^{\text{TM}}$ model. In particular, bulk properties can be assumed to be equal to the outlet conditions (Mixed flow), obtaining an ideal CSTR, or they can be computed as an average between the inlet and the outlet conditions (Countercurrent flow), or as a combination of average conditions for one phase and outlet conditions for the other one (VPlug flow, VPlugP flow and LPlug flow). Figure 3.2 resumes schematically the different flow models.

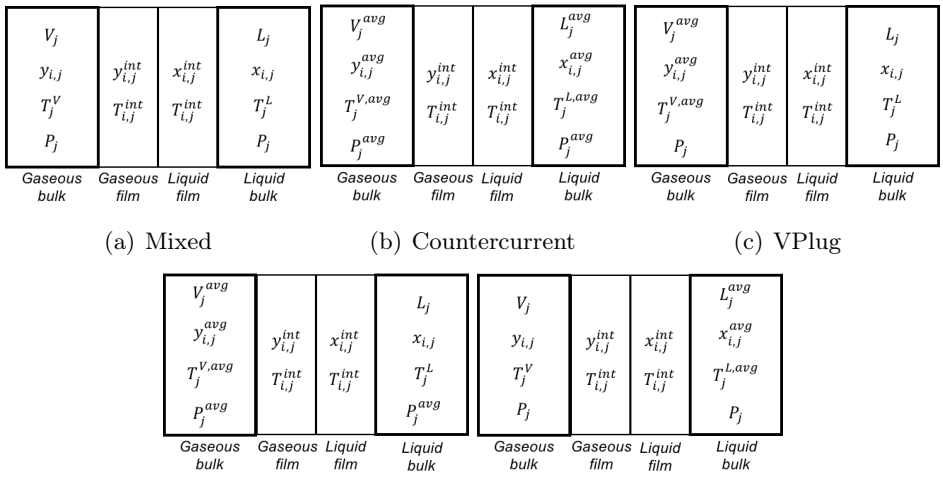

(a) Mixed (b) Countercurrent (c) VPlug

(d) VPlugP (e) LPlug

Figure 3.2: RadFrac^{TM} flow models

A comparison between the different flow models is going to be made in Subsection 4.5.1.5.

3.4.2 Modeling the film

3.4.2.1 Film resistances

To model the film, the *RadFrac*$^{\mathrm{TM}}$ model offers different options to establish which resistances are to be considered:

- *Nofilm*: there is no distinction between bulk and film, the entire phase is completely mixed and treated like an equilibrium stage;
- *Film*: only resistance to material diffusion is considered and no reactions are present;
- *Filmrxn*: both resistance to diffusion and reactions are present. The film is not discretized;
- *Discrxn*: both resistance to diffusion and reactions are present, but this time the film is discretized. This option is suggested whenever the reactions lead to significant changes in the concentration profiles in the film.

As the gaseous phase does not involve chemical reactions, the option *Film* was chosen for this phase in this work. For what concerns the liquid film, reactions involving CO_2 are typically very fast [2,38,46,79] and lead to steep

profiles close to the interface. For this reason the option *Discrxn* was chosen to model the liquid film.

3.4.2.2 Evaluation of the interphase fluxes

From the modeling point of view, the *RadFrac*$^{\text{TM}}$ model - Rate-Based mode applies the rigorous Maxwell-Stefan equations (Subsection 2.4.2.1) in an algebraic-matrix form for the evaluation of the interphase fluxes coupled with the algebraic balances in the film given by Eq. 2.52. The equations are listed below together with the balances in the film, where indexes i and k indicate the components, while index j indicates the segment.

- Material balance in the liquid film

$$\dot{N}_{i,j}^{int} - \dot{N}_{i,j}^{R_f,L} - \dot{N}_{i,j}^{L} = 0 \tag{3.23}$$

- Material flux for the liquid film

$$\underline{\underline{\Gamma}}_j^L \ \left(\underline{x}_j^{int} - \underline{x}_j\right) + \Delta\Phi_j^E \left(\underline{x}_j \ \hat{\underline{z}}_j\right) - \underline{\underline{R}}_j^L \ \left(\underline{\dot{N}}_j^L - \underline{\dot{N}}_t^L \ \underline{x}_j\right) = 0 \tag{3.24}$$

where matrix $\underline{\underline{\Gamma}}_j^L$ is called matrix of thermodynamic factors and is defined as [87]:

$$\Gamma_{i,j,k}^L = \delta_{i,k} + x_{i,j} \ \frac{\partial \ln \phi_{i,j}^L}{\partial x_{i,j}} \tag{3.25}$$

while matrix $\underline{\underline{R}}_j^L$ represents the inverse of the material transfer coefficients matrix [87]:

$$R_{i,i,j}^L = \frac{x_{i,j}}{C_j^L \ a_{w,j} \ k_{M_{i,n,j}}^L} + \sum_{\substack{m=1 \\ m \neq i}}^{n_c^L} \frac{x_{m,j}}{C_j^L \ a_{w,j} \ k_{M_{i,m,j}}^L} \quad i = 1, \ldots, n-1 \tag{3.26}$$

$$R_{i,k,j}^L = -x_{i,j} \left(\frac{1}{C_j^L \ a_{w,j} \ k_{M_{i,k,j}}^L} - \frac{1}{C_j^L \ a_{w,j} \ k_{M_{i,n,j}}^L} \right) \quad i = 1, \ldots, n-1 \ , \ i \neq k \tag{3.27}$$

- Energy balance in the liquid film

$$\dot{E}_j^{int} - \dot{E}_j^L = 0 \tag{3.28}$$

- Material balance in the gaseous film

$$\dot{N}_{i,j}^{int} - \dot{N}_{i,j}^{R_f,V} - \dot{N}_{i,j}^{V} = 0 \tag{3.29}$$

- Material flux for the gaseous film

$$\underline{\underline{\Gamma}}_j^V \left(\underline{y}_j^{int} - \underline{y}_j\right) + \underline{\underline{R}}_j^V \left(\underline{\dot{N}}_j^V - \underline{\dot{N}}_t^V \, \underline{y}_j\right) = 0 \tag{3.30}$$

  where the matrices $\underline{\underline{\Gamma}}_j^V$ and $\underline{\underline{R}}_j^L$ are defined like the same matrices for the liquid phase.

- Summation equations at the interface

$$\sum_{i=1}^{n_c^L} x_{i,j}^{int} = 1 \tag{3.31}$$

$$\sum_{i=1}^{n_c^V} y_{i,j}^{int} = 1 \tag{3.32}$$

- Energy balance in the gaseous film

$$\dot{E}_j^V - \dot{E}_j^{int} = 0 \tag{3.33}$$

3.4.2.3 Discretization of the liquid film

The choice of the *Discrxn* option implicates that the liquid film is discretized into a certain number of points and gives the possibility to choose how to arrange these points. Since the chemical reactions involving CO_2 are fast, the profiles in the liquid film are expected to be significantly steep close to the interface, until the variables reach their equilibrium value [38, 79]. For this reason, the discretization points must be concentrated close to the interface in order to describe these profiles correctly. To do so, the *geometric* discretization option was used in this work. In this way, the discretization points are non-equidistant. In the *RadFrac*$^{\text{TM}}$ model - Rate-Based mode three parameters must be defined to setup the film discretization:

- *Reaction Condition Factor* (RCF). This parameter weights the interface and bulk compositions and temperature in the computation of the reaction rates within the film. A large value of this parameter increases the influence of the bulk conditions on the computation of the film reaction rate. Considering the molar fraction for the i-th component in the liquid film, its relation with the RCF is evidenced in Eq. 3.34:

$$x_i^f = RCF \; x_i + (1 - RCF) \; x_i^{int} \tag{3.34}$$

  For the CO_2 capture with MEA process, the film reactions are very fast; consequently the bulk conditions must have a higher weight on the film modeling.

- *Number of discretization points in the film.* According to the work of Kucka et al. [79], 5 non-equidistant points are sufficient for a correct description of the film concentration profiles.

- *Film Discretization Ratio.* This parameter is related to the distance between the segments in the film. It is defined, according to Eq. 3.35, as the ratio between adjacent film segments moving in the direction of the interface:

$$FDR = \frac{\delta_k}{\delta_{k+1}} \tag{3.35}$$

  where δ_k is the thickness of the k-th segment.
  The film profiles are very steep close to the interface and they approach the equilibrium value close to the bulk. Therefore, it is preferable to use a small number of points placing most of them close to the interface, rather than use a high number of equidistant points [79]. However, there must be a compromise between the number of points and the film discretization ratio. Even if it is necessary to define a FDR higher than one in order to concentrate the internal points near the interface, a high value can lead to numerical problems due to the small discretization steps close to the interface.

The definition of the liquid film discretization parameters for the model developed in this work is going to be discussed in Subsection 4.5.1.1.

3.4.3 Rate-Based parameters evaluation

As already discussed in Subsection 2.4.3, the higher complexity of the rate-based model involves the evaluation of several parameters. In this section, the correlations used to evaluate the model parameters are reported. Since in this work both random and structured packings are considered, the equations are reported for both the kinds of packing.

3.4.3.1 Wetted surface area

- Random packing: Onda et al. [91]

$$\frac{a_{w,j}}{a_{dry}} = 1 - \exp\left[-1.45 \left(\frac{\sigma_C}{\sigma_j^L}\right)^{0.75} \left(Re_j^L\right)^{0.1} \left(Fr_j^L\right)^{-0.05} \left(We_j^L\right)^{0.2}\right] \tag{3.36}$$

  where the dimensionless Reynolds, Freud and Weber numbers are defined according to Eqs. 3.37-3.39:

$$Re_j^L = \frac{L_{s_j}^2}{a_{dry}\ \hat{\mu}_j^L} \tag{3.37}$$

$$Fr_j^L = \frac{L_{s_j}^2 \; a_{dry}}{{\rho_j^L}^2 \; g} \tag{3.38}$$

$$We_j^L = \frac{L_{s_j}^2}{\rho_j^L \; \sigma_j^L \; a_{dry}} \tag{3.39}$$

- Structured packing: Bravo et al. [92]

$$a_{w,j} = a_{dry} \tag{3.40}$$

3.4.3.2 Material transfer coefficients

- Random packing: Onda et al. [91]

$$k_{M_{i,j}}^L \left(\frac{\rho_j^L}{\hat{\mu}^L}\right)^{1/3} = 0.0051 \left(\frac{L_{s_j}}{a_{w,j} \; \hat{\mu}_j^L}\right)^{2/3} \left(\frac{\hat{\mu}_j^L}{\rho_j^L \; \mathscr{D}_{i,j}^L}\right)^{-1/2} (a_{dry} \; d_{eq})^{0.4} \tag{3.41}$$

$$\frac{k_{M_{i,j}}^V \; R \; T_j^V}{a_{dry} \; \mathscr{D}_{i,j}^V} = K_5 \left(\frac{V_{s_j}}{a_{dry} \; \hat{\mu}_j^L}\right)^{0.7} \left(\frac{\hat{\mu}_j^V}{\rho_j^V \; \mathscr{D}_{i,j}^V}\right)^{1/3} (a_{dry} \; d_{eq})^{-2} \tag{3.42}$$

- Structured packing: Bravo et al. [92]

$$k_{M_{i,j}}^L = 2 \sqrt{\frac{\mathscr{D}_{i,j}^L}{\pi \; t_j^L}} \tag{3.43}$$

where t_j^L is the residence time.

$$k_{M_{i,j}}^V = 0.0338 \; \frac{\mathscr{D}_{i,k}^V}{d_{eq}} \; {Re_j^V}^{0.8} \; {Sc_{i,j}^V}^{0.333} \tag{3.44}$$

where the dimensionless group of Reynolds and Schmidt are defined as following:

$$Re_j^V = \frac{d_{eq} \rho_j^V \; \left(u_{eff_j}^V + u_{eff,j}^L\right)}{\hat{\mu}_j^V} \tag{3.45}$$

where u_{eff} is the effective velocity through the channel.

$$Sc_{i,j}^V = \frac{\hat{\mu}_i^V}{\rho_j^V \; \mathscr{D}_{i,j}^V} \tag{3.46}$$

3.4.3.3 Heat transfer coefficients

Random & Structured packing: Chilton-Colbun analogy [100]

$$h_j^L = \bar{k}_{M_j}^L \; C_j^L \; c_{P_j}^L \left(\frac{k_{T_j}^L}{C_j^L \; c_{p_j}^L \; \bar{\mathscr{D}}_j^L} \right)^{2/3} \tag{3.47}$$

$$h_j^V = \bar{k}_{M_j}^V \; C_j^V \; c_{P_j}^V \left(\frac{k_{T_j}^V}{C_j^V \; c_{p_j}^V \; \bar{\mathscr{D}}_j^V} \right)^{2/3} \tag{3.48}$$

where $\bar{k}_j$ and $\bar{\mathscr{D}}_j$ are the average material transfer coefficient and average diffusivity, respectively, defined in Eqs. 3.49-3.50:

$$\bar{k}_{M_j} = \frac{\sum_{i=1}^{n_c-1} \sum_{k=i+1}^{n_c} (x_{i,j} + \delta^{CC})(x_{k,j} + \delta^{CC}) k_{M_{i,k,j}}}{\sum_{i=1}^{n_c-1} \sum_{k=i+1}^{n_c} (x_{i,j} + \delta^{CC})(x_{k,j} + \delta^{CC})} \tag{3.49}$$

$$\bar{\mathscr{D}}_j = \frac{\sum_{i=1}^{n_c-1} \sum_{k=i+1}^{n_c} (x_{i,j} + \delta^{CC})(x_{k,j} + \delta^{CC}) \mathscr{D}_{i,k,j}}{\sum_{i=1}^{n_c-1} \sum_{k=i+1}^{n_c} (x_{i,j} + \delta^{CC})(x_{k,j} + \delta^{CC})} \tag{3.50}$$

where δ^{CC} is the Chilton-Colburn averaging parameter.

3.4.3.4 Fractional Liquid Hold-up

- Random packing: Stichlmair et al. [103]

$$\psi_j^L = 0.555 \; {Fr_j^L}^{1/3} \left(1 + 20\Delta P^2\right) \tag{3.51}$$

  where ΔP is the pressure drop and the Freud number is defined as:

$$Fr_j^L = \frac{a_{dry} \; {u_j^L}^2}{g \; \epsilon^{4.65}} \tag{3.52}$$

  where u_j^L is the superficial velocity for the liquid.

- Structured packing: Bravo et al. [93]

$$\psi_j^L = \left(4 \; \frac{F_t}{S}\right)^{2/3} \left(\frac{3 \; \hat{\mu}_j^L \; u_j^L}{\rho_j^L \; g_{eff} \; \epsilon \sin\theta} \right)^{1/3} \tag{3.53}$$

3.5 Chapter 3 Summary

In this chapter, the main features of the *RadFrac*™ model - Rate-Based mode were described. In particular, it was shown how Aspen Plus® manages the modeling of the bulk and the film. For what concerns the bulk, different flow models are present for the evaluation of the compositions and temperature based on the outlet conditions only or a combination between the inlet and outlet conditions. For the description of the film, the software uses the rigorous Maxwell-Stefan approach in a matrix form with respect to the computation of the interphase fluxes. Moreover, since the profiles in the liquid film are very steep close to the interface due to the chemical reactions involving CO_2, a geometric discretization was adopted in this thesis for the liquid film. In this way, the points in the spatial film domain were concentrated close to the interface in order to describe correctly the high gradients in the liquid film.
The next chapter is dedicated to the validation of the model for the absorber using the *RadFrac*™ model - Rate-Based mode.

Part II

Model validation

Chapter 4

Model validation for the absorber

The model developed in Chapter 3 is applied in this chapter to the absorption section of two different pilot-plant facilities. The Peclet number is evaluated for all the cases examined, highlighting that the columns have a plug-flow like behavior. Then, with the purpose of investigating the possible effect of the backmixing due to the countercurrent, the number of segments analysis is performed, in order to obtain a correct model of the process. After the identification of a proper number of segments, the uncertainty of some model parameters is taken into account. In particular, the kinetic parameters of the reaction involving CO_2 and MEA are optimized with the purpose of minimizing the standard error between the model results and the experimental data. The proposed model describes correctly the experimental data and particularly the typical temperature bulge, independently on its location.

4.1 Absorption section case studies

The first part concerning the validation of the model proposed in Chapter 3 regarded the absorber. In particular, in this work two experimental pilot-plant facilities with different peculiarities were chosen. The first case considered was the laboratory-scale absorption plant designed by Tontiwachwuthikul et al. [56, 110], while the second one was the CESAR (CO_2 Enhanced Separation and Recovery) large-scale absorption/desorption system described by Razi et al. [44]. The two systems were chosen because of their differences in the dimensions (laboratory- vs large-scale) and in the packing type (random vs structured). In the following two sections, a brief description of the two facilities is reported.

4.1.1 Laboratory-scale pilot-plant

The pilot-plant facility described in the works of Tontiwachwuthikul et al. [56,110] consists in the packed absorption column schematized in Figure 4.1.

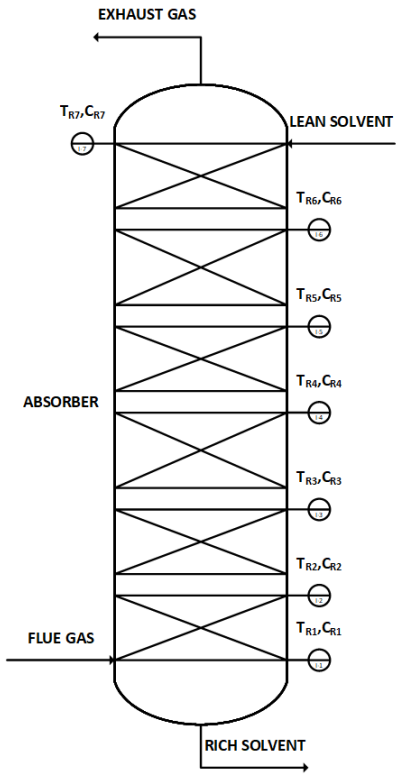

Figure 4.1: Laboratory-scale plant flowsheet

The flue gas containing the CO_2 enters the bottom of the column and flows

countercurrent with the aqueous MEA solution. Within the packing, the CO_2 is transferred from the gaseous phase to the liquid one where it reacts with the amine. The exhaust gas from the top and the rich solvent from the bottom exit the column. The column is packed with 12.7 mm Ceramic Berl Saddles divided in six sections separated by redistributors. The column and packing features are reported in Table 4.1. Each section is equipped with sample points for the measurement of the liquid temperature and the CO_2 concentration in the gaseous phase. In particular, two runs, Run 20 and Run 22, of which the feed characterization is reported in Table 4.2, were chosen in this work to validate the model. The experimental data available for the two runs are reported in Table 4.3, where the height 0 m corresponds to the column bottom [56].

Variable	**Value**
Packing height [m]	6.55
Column diameter [m]	0.1
Void fraction [m^3/m^3]	0.62
Dry specific surface area [m^2/m^3]	465

Table 4.1: Lab-scale plant column and packing features

Run	*T20*		*T22*	
Stream	*Flue Gas*	*Lean Solvent*	*Flue Gas*	*Lean Solvent*
Temperature [K]	288.15	292.15	288.15	292.15
Molar flow [mol/s]	0.14	1.04	0.14	1.04
CO_2 [mol frac]	0.192	0	0.191	0
MEA [mol frac]	0	0.0497	0	0.055
H_2O [mol frac]	0.1	0.9503	0.1	0.945
N_2 [mol frac]	0.708	0	0.709	0
Pressure [kPa]	103.15	103.15	103.15	103.15

Table 4.2: Feed characterization for Run T20 and T22 from the lab-scale plant

Run		*T20*		*T22*	
Sample	**H [m]**	**T^L [K]**	**y_{CO_2} [mol frac]**	**T^L [K]**	**y_{CO_2} [mol frac]**
1	0.00	321.15	0.192	320.15	0.191
2	1.05	330.15	0.177	318.15	0.128
3	2.15	320.15	0.142	302.15	0.053
4	3.25	305.15	0.077	294.15	0.012
5	4.35	295.15	0.028	292.15	0.001
6	5.45	293.15	0.006	292.15	0.000
7	6.55	292.15	0.000	292.15	0.000

Table 4.3: Experimental data for Run T20 and T22 from the lab-scale plant

4.1.2 Large-scale pilot-plant

The CESAR pilot plant described in the work of Razi et al. [44] is a large-scale plant which treats part of the flue gas coming from the Dong Esbjerg power station (power plant fed with 400 MW_e pulverized bituminous coal) extracted directly from the desulfurization section without any pretreatment. A flowsheet of the absorption section of the plant is reported in Figure 4.2.

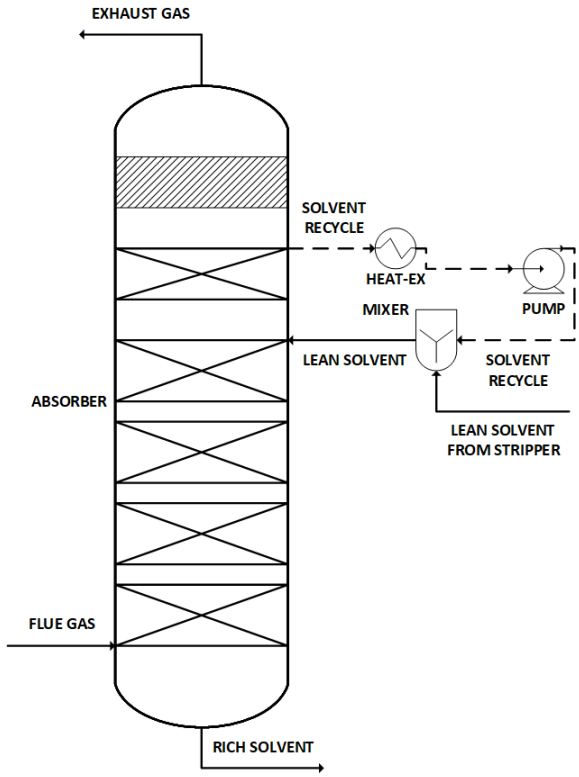

Figure 4.2: Large-scale plant flowsheet

In this case the packing height is divided into four identical sections containing structured Mellapak 2X. After the absorption zone, a waterwash section is present at the top of the column to recover the volatilized MEA from the gas phase. The recovered solvent is then recycled back to the top of the absorption section after cooling. In the simulations the waterwash section was not included, since no informations on the recycle stream was reported in the work of Razi et al. [44].
The column and packing features are reported in Table 4.4. Each section is equipped with sample points for the measurement of the temperature. One run, Run 1-A2, of which the feed characterization is reported in Table 4.5,

was chosen in this work to validate the model. The experimental data available for the runs are reported in Table 4.6, where the height 0 m corresponds to the column bottom.

Variable	**Value**
Packing height [m]	17
Column diameter [m]	1.1
Void fraction [m^3/m^3]	0.99
Dry specific surface area [m^2/m^3]	205

Table 4.4: Large-scale plant column and packing features

Run	*1-A2*	
Stream	*Flue Gas*	*Lean Solvent*
Temperature [K]	326.92	332.57
Molar flow [mol/s]	52.33	214.55
CO_2 [mol frac]	0.12	0.0263
MEA [mol frac]	0	0.102
H_2O [mol frac]	0.12	0.8717
N_2 [mol frac]	0.76	0
Pressure [kPa]	106.391	101.325

Table 4.5: Feed characterization for Run 1-A2 from the large-scale plant

Run		*1-A2*
Sample	**H [m]**	**T [K]**
1	0.00	326.92
2	4.25	333.47
3	8.50	339.95
4	12.75	346.55
5	17	332.57

Table 4.6: Experimental data for Run 1-A2 from the large-scale plant

4.2 The temperature bulge

As discussed previously in Chapter 2, the absorption process is characterized by several heat transfer phenomena, including those due to the reactions (exothermic in the case of the absorption) and water vaporization/condensation. For this reason, the absorber temperature profiles show

a pronounced bulge. The position and magnitude of this bulge give important indications on the behavior of the process which have fundamental implications in the design of the absorber, as it is going to be discussed in detail in Chapter 6, and it is influenced by different factors, as it was extensively studied in the work of Kvamsdal & Rochelle [39]. In particular, one of the main factors is represented by the molar L/V ratio. Three situations are possible depending on the value of this parameter:

- $L/V < 5$: the bulge is located at the top of the column;
- $5 < L/V < 6$: the bulge is located in the middle of the column;
- $L/V > 6$: the bulge is located at the bottom of the column.

The first situation is usually verified in columns containing structured packing, since due to the higher surface area, the required performance can be achieved with a low L/V ratio value. On the other hand, when columns containing random packing are considered, a higher L/V ratio is required to obtain the requested performance. In this work, the three runs were chosen according to the possibility of different temperature bulge positions. In particular, in the lab-scale plant, packed with random packing, the L/V ratio was equal to 7.43 for both Run T20 and T22, then a bottom temperature bulge was expected, while in the large-scale plant a 4.1 L/V ratio was used for Run 1-A2 and a top temperature bulge was awaited [2].

4.3 Peclet number analysis

Prior to the simulations, the Peclet number analysis was performed for all the runs. In Subsection 2.4.4.1 it was outlined how the evaluation of the dimensionless group gives indication on the influence of the axial diffusion/dispersion on the process, which is a fundamental factor in the choice of a proper number of segments for the discretization of the axial domain. The Peclet number was evaluated for all the runs for both the material (single components and mixture) and energy transport in each phase and with reference to both the packing height and the packing equivalent diameter using Aspen Custom Modeler®. The inlet conditions (column top for the liquid phase, column bottom for the gaseous phase) were used as reference conditions. The results of the computations are reported in Tables 4.7-4.9.

Run	*T20*			
Phase	*Liquid*		*Gaseous*	
Characteristic length	H	d_{eq}	H	d_{eq}
$Pe_{M,i}$				
CO_2	$3.54 \cdot 10^8$	$2.65 \cdot 10^5$	$3.05 \cdot 10^5$	228.03
CO_3^{--}	$3.84 \cdot 10^8$	$2.87 \cdot 10^5$	–	–
H_2O	$3.04 \cdot 10^9$	$2.27 \cdot 10^6$	$2.32 \cdot 10^5$	173.87
H_3O+	$3.80 \cdot 10^7$	$2.84 \cdot 10^4$	–	–
HCO_3^-	$2.44 \cdot 10^8$	$1.83 \cdot 10^5$	–	–
MEA	$3.32 \cdot 10^8$	$2.49 \cdot 10^5$	$5.19 \cdot 10^5$	388.64
MEA^+	$2.66 \cdot 10^8$	$1.99 \cdot 10^5$	–	–
$MEACOO^-$	$2.66 \cdot 10^8$	$1.99 \cdot 10^5$	–	–
N_2	$3.52 \cdot 10^8$	$2.63 \cdot 10^5$	$2.75 \cdot 10^5$	205.82
OH^-	$6.71 \cdot 10^7$	$5.02 \cdot 10^4$	–	–
$Mixture$	$2.15 \cdot 10^9$	$1.61 \cdot 10^6$	$2.75 \cdot 10^5$	$2.05 \cdot 10^2$
Pe_T				
$Mixture$	$3.1 \cdot 10^6$	2319.71	$2.92 \cdot 10^5$	$2.19 \cdot 10^2$

Table 4.7: Peclet number evaluation for Run T20

Run	*T22*			
Phase	*Liquid*		*Gaseous*	
Characteristic length	H	d_{eq}	H	d_{eq}
$Pe_{M,i}$				
CO_2	$3.71 \cdot 10^8$	$2.78 \cdot 10^5$	$3.05 \cdot 10^5$	228.03
CO_3^{--}	$3.85 \cdot 10^8$	$2.88 \cdot 10^5$	–	–
H_2O	$3.05 \cdot 10^9$	$2.28 \cdot 10^6$	$2.32 \cdot 10^5$	173.91
H_3O+	$3.81 \cdot 10^7$	$2.85 \cdot 10^4$	–	–
HCO_3^-	$2.45 \cdot 10^8$	$1.83 \cdot 10^5$	–	–
MEA	$3.34 \cdot 10^8$	$2.50 \cdot 10^5$	$5.19 \cdot 10^5$	388.72
MEA^+	$2.67 \cdot 10^8$	$2.00 \cdot 10^5$	–	–
$MEACOO^-$	$2.67 \cdot 10^8$	$2.00 \cdot 10^5$	–	–
N_2	$3.69 \cdot 10^8$	$2.76 \cdot 10^5$	$2.75 \cdot 10^5$	205.87
OH^-	$6.73 \cdot 10^7$	$5.04 \cdot 10^4$	–	–
$Mixture$	$2.09 \cdot 10^9$	$1.57 \cdot 10^6$	$2.75 \cdot 10^5$	205.93
Pe_T				
$Mixture$	$3.16 \cdot 10^6$	2364.74	$2.92 \cdot 10^5$	$2.19 \cdot 10^2$

Table 4.8: Peclet number evaluation for Run T22

Run	*1-A2*			
Phase	*Liquid*		*Gaseous*	
Characteristic length	H	d_{eq}	H	d_{eq}
$Pe_{M,i}$				
CO_2	$9.72 \cdot 10^8$	$1.14 \cdot 10^5$	$1.30 \cdot 10^6$	1525.2
CO_3^{--}	$2.68 \cdot 10^9$	$3.15 \cdot 10^6$	–	–
H_2O	$4.03 \cdot 10^9$	$4.74 \cdot 10^6$	$9.49 \cdot 10^5$	1116.78
H_3O+	$2.65 \cdot 10^8$	$3.12 \cdot 10^5$	–	–
HCO_3^-	$1.70 \cdot 10^9$	$2.00 \cdot 10^6$	–	–
MEA	$1.00 \cdot 10^9$	$1.18 \cdot 10^6$	$2.13 \cdot 10^6$	2500.37
MEA^+	$1.86 \cdot 10^9$	$2.18 \cdot 10^6$	–	–
$MEACOO^-$	$1.86 \cdot 10^9$	$2.18 \cdot 10^6$	–	–
N_2	$9.66 \cdot 10^8$	$1.14 \cdot 10^6$	$1.11 \cdot 10^6$	1300.85
OH^-	$4.68 \cdot 10^8$	$3.90 \cdot 10^6$	–	–
$Mixture$	$3.31 \cdot 10^9$	$3.90 \cdot 10^6$	$1.10 \cdot 10^6$	1298.1
Pe_T				
$Mixture$	$2.03 \cdot 10^7$	$2.39 \cdot 10^4$	$1.19 \cdot 10^6$	$1.40 \cdot 10^3$

Table 4.9: Peclet number evaluation for Run 1-A2

As it is possible to notice from the analysis of Tables 4.7-4.9, the values of the Peclet number are quite large. Tables 4.7 and 4.8 show the results for the lab-scale plant. When the liquid phase is considered and the column height is used as characteristic length, the material Peclet number values are in the order of 10^9. If the packing equivalent diameter is used, this value is reduced to about 10^6. For what concerns the gaseous phase, the material Peclet number is in the order of 10^5 and 10^2 when the column height and the packing equivalent diameter are considered, respectively. On the other hand, the thermal Peclet number for the liquid phase is in the range of 10^6 when the packing height is used and 10^3 with the packing equivalent diameter as characteristic length. With regards to the gaseous phase, the thermal Peclet number is in the order of 10^5 with the packing height as characteristic length, while the same value is reduced to 10^2 when the packing equivalent diameter is considered.
For what concerns the large-scale plant, as expected, the values of the Peclet number shown in Table 4.9 are higher compared to the lab-scale plant due to the higher column dimensions and molar flows involved. For the liquid phase, the material Peclet number is in the order of 10^9 when the column height is considered and 10^6 for the packing equivalent diameter. For the gaseous phase, values in the range of 10^6 with the column height and 10^3 considering the packing equivalent diameter are observed. The liquid thermal Peclet number is in the order of 10^7 and 10^4 considering the column height and the packing equivalent diameter, respectively. For the gaseous phase, similarly

to the material Peclet number, values of the thermal Peclet number in the order of 10^6 considering the column height to 10^3 considering the packing equivalent diameter are obtained.
Since the lowest value of the dimensionless group was in the order of 10^2, it could be concluded that the axial diffusion/dispersion had no effect on the process and that the column fluid dynamics resembled that of an ideal plug-flow [2]. This meant that the process was represented by a system of ODEs at steady-state. Since the axial diffusion/dispersion effect could be neglected, from a mathematical point of view a sufficiently high number of segments for the discretization of the axial domain was required to achieve a correct representation of the system.

4.4 Backmixing due to the countercurrent effect

The results obtained in Section 4.3 with the Peclet number analysis led to the conclusion that the axial diffusion/dispersion could be neglected and, consequently, the column behavior from a fluid dynamics point of view resembled that of an ideal plug-flow.
However, in the reality, the countercurrent generates a backmixing effect that can deviate the real column behavior from the ideal plug-flow one. Being a macroscale phenomenon, the backmixing is not taken into account in the Peclet number analysis, since the dimensionless group contains the axial diffusion/dispersion, which is a microscale phenomenon. The backmixing due to the countercurrent is implicitly present in the material and energy balances describing the process and its possible effect can be analyzed only after the obtainment of the correct numerical solution of the system. In particular, if a high number of segments was needed to find the correct solution, then it could be concluded that the backmixing did not play an important role on the process.
Finally, it is worth to remember that in this work the plug-flow was approximated as a series of n-CSTRs, where the number of CSTR corresponds to the number of segments. This approximation could be done since, according to the high values of the Peclet number, there was no need to include the axial diffusion/dispersion in the model.
Keeping constant the input parameters reported in Tables 4.1-4.2 and Tables 4.4-4.5, the number of segments was increased until the difference between two consecutive profiles became negligible [107–109].

4.5 Absorber simulation and analysis

4.5.1 Lab-scale plant: Run T20

4.5.1.1 *RadFrac*™ model - Rate-Based mode set-up

As discussed in Subsection 3.4.2.3, since the option *Discrxn* was activated in the *RadFrac*™ model for the discretization of the liquid film, three parameters had to be defined for the setup of the rate-based model. In particular:

- the *Reaction Condition Factor* was set to 0.9 in order to give more weight to the bulk conditions in the evaluation of the film reaction rates, due to the high rate of the reactions in the liquid film. This value was in agreement with the work of Zhang et al. [38];
- after a significant number of simulations, it was found that 5 non-equidistant *Discretization Points* in the liquid film were sufficient for the correct description of the profiles on the basis of the comparison between the model results and the experimental data. This value was in agreement with the work of Kucka et al. [79];
- the *Film Discretization Ratio* was fixed to 10, value that was found to be a good compromise between the placing of the discretization points and the discretization steps for the numerical solution of the system. The location of the discretization points is reported in Table 4.10 [2].

Point	**Location**
1	$9 \cdot 10^{-6}$
2	$9 \cdot 10^{-5}$
3	$9 \cdot 10^{-4}$
4	$9 \cdot 10^{-3}$
5	$9 \cdot 10^{-2}$

Table 4.10: Location of the discretization points in the liquid film

Moreover, in the case of the random packing, since Zhang et al. [38] demonstrated that the correlation by Onda et al. [91] underestimated the wetted surface area, the *Interfacial Area Factor* available in the simulator to correct the evaluation of the parameter was set to 1.2. This factor was coherent with the dry specific area for the ceramic Berl saddles reported by Mores et al. [27]. For what concerns the fluid dynamics, the *Mixed* flow model was used in the simulations, since in this way it was possible to model the column as a series of CSTRs. A comparison between the *Mixed* flow model and the other flow models present in the software is reported in Subsection 4.5.1.5.

4.5.1.2 Kinetic parameters

As already reported in Section 3.3, two kinetic reversible reactions involving carbon dioxide were considered in this work: the formation of the carbamate ion and the formation of the bicarbonate ion. For what concerns the first reaction, the kinetic parameters were taken from the work of Hikita et al. [66], while for the latter reactions the values reported in Pinsent et al. [60] were used. Table 4.11 resumes the kinetic parameters for the forward and reverse reactions.

Reaction	*Forward reaction*		*Reverse reaction*	
	$k^0_{f,j}\left[\frac{kmol}{m^3 s}\right]$	$E_{a,f_j}\left[\frac{cal}{mol}\right]$	$k^0_{r,j}\left[\frac{kmol}{m^3 s}\right]$	$E_{a,r_j}\left[\frac{cal}{mol}\right]$
3.13	$9.77 \cdot 10^{10}$	9855.8	$3.23 \cdot 10^{19}$	15655
3.14	$4.32 \cdot 10^{13}$	13249	$2.38 \cdot 10^{17}$	29451

Table 4.11: Kinetic reversible reactions parameters

4.5.1.3 Number of segments analysis

The first analyzed case was Run T20 from the lab-scale plant. The absorber was simulated varying the number of segments until two consecutive profiles were overlapped. The liquid temperature and the CO_2 in the vapor phase profiles are reported in Figure 4.4.

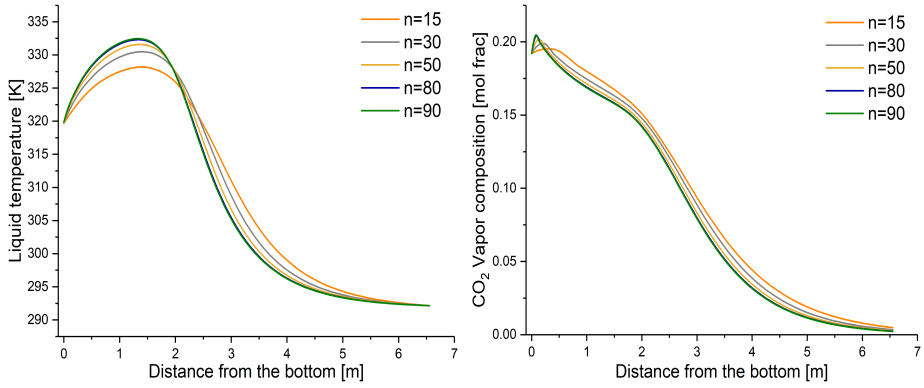

(a) Liquid temperature (b) CO_2 vapor phase composition

Figure 4.3: Run T20 - Absorber (a) liquid temperature profile and (b) CO_2 vapor composition profile variation with the number of segments

From the analysis of Figure 4.4 it is possibile to notice that the profiles with 80 and 90 segments are overlapped. Then 90 segments are sufficient to obtain the correct system solution. In particular, in Figure 4.4(a) it can be observed that the temperature bulge, which as expected is placed in the bottom of the column, is correctly described only after 30 segments. This result proves the correctness of the previous Peclet number analysis and it leads to the conclusion that the backmixing effect can be neglected. It must be noticed that only with an appropriate number of segments it is possible to identify a small concentration bulge in the bottom of the column, which is caused by the partial preponderance of the reverse reaction 3.13 of carbamate to CO_2. The number of segments analysis was needed to obtain a model which was robust and correct from a numerical point of view. Only at this point it was possible to make the comparison between the 90 segments model and the experimental data, which is reported in Figure 4.3 for both the liquid temperature and the CO_2 vapor composition.

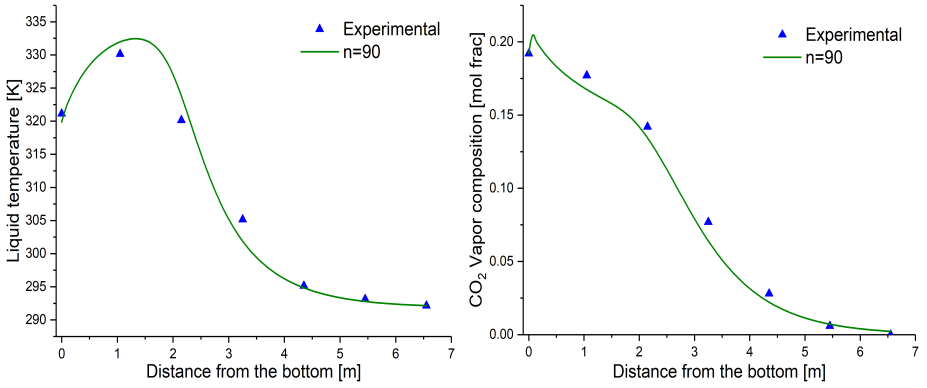

(a) Liquid temperature (b) CO_2 vapor phase composition

Figure 4.4: Run T20 - Comparison between absorber (a) liquid temperature profile and (b) CO_2 vapor composition profile with the experimental data

From Figure 4.3 it is possible to observe the good agreement between the model and the experimental data profiles and this result was obtained with a model correct from a numerical point of view. However, the agreement between the model and the experimental data can be furtherly improved, as it is going to be shown in Subsection 4.5.1.4.
From the point of view of the column performance, which are represented by the CO_2 removal and the loading in the outlet liquid stream, the results are reported in Table 4.12.

Performance	**Experimental**	**Number of segments**				
		15	30	50	80	90
CO_2 Removal %	100	98.2	98.8	99	99.1	99.1
Loading out	0.514	0.507	0.511	0.515	0.516	0.516

Table 4.12: Run T20 - Absorber performance variation with the number of segments

It can be noticed that when the number of segments is increased higher values of both the CO_2 removal and the loading are obtained. This fact can be explained analyzing the variation of the CO_2 interphase molar flow rate profile with the number of segments, reported in Figure 4.5.

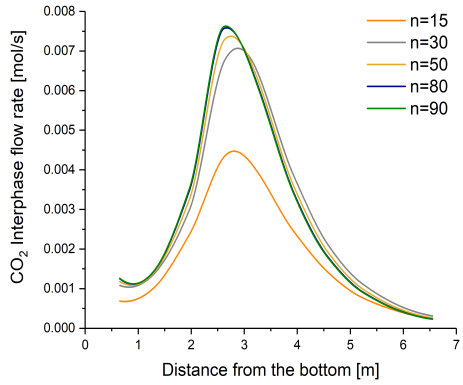

Figure 4.5: Run T20 - Absorber CO_2 interphase molar flow rate profile variation with the number of segments

It is possible to notice from Figure 4.5 that with the increase in the number of segments the simulator is always able to evaluate a higher mean CO_2 transfer from the gaseous to the liquid phase since, due the more detailed discretization of the axial domain, the calculations are performed in more points.
From these first results, it was highlighted the need of a sufficiently high number of segments to discretize the axial domain. This necessity could be explained also by the fact the along the column several transitions happen between the absorption and the desorption process regimes and between water evaporation and condensation [108]. Using an inadequate number of segments, the net fluxes, especially for water, between liquid and vapor could be under/over-estimated, as shown in Figure 4.6, leading to different temperature and composition profiles. It must be noticed that in Figure 4.6 a *negative* flow rate indicates a transfer from the liquid to the vapor phase (evaporation), while a *positive* flow rate indicates a transfer from the vapor

to the liquid phase (condensation).

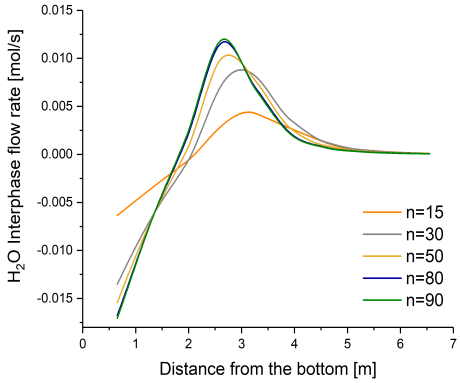

Figure 4.6: Run T20 - Absorber H_2O interphase molar flow rate profile variation with the number of segments

4.5.1.4 Kinetic parameters calibration

After the identification of an appropriate number of segments for the discretization of the axial domain, it was possible to assure that the proposed model was numerically robust and it was in agreement with the fluid dynamics predicted by the Peclet number.
At this point, it was possible to improve the model focusing on the physical parameters involved. After a literature review and comparing different models, it was possible to conclude that some parameters are affected by uncertainty. In particular, the attention was concentrated on the kinetic parameters of the forward reaction 3.13, of which Table 4.13 reports the range of variation found in the literature.

$k^0_{f,j}\left[\frac{kmol}{m^3 s}\right]$	$E_{a,f_j}\left[\frac{cal}{mol}\right]$	**Reference**
$4.495 \cdot 10^{11}$	10733.22	Kucka et al. [79]
$9.77 \cdot 10^{10}$	9855.8	Hikita et al. [66]
$1.17 \cdot 10^{6}$	1797.1	Kvamsdal & Rochelle [39]

Table 4.13: Kinetic reversible reactions parameters

In general it is known that to evaluate the influence of uncertain parameters a sensitivity analysis is required [111]. Moreover, as reported by Rodriguez-Aragon & Lopez-Fidalgo [112], the kinetic parameters are essential in the modeling of the phenomena and the most accurate estimation will produce

the best results in the use of the model. Different studies [113–115] dealt with the uncertainty related to the parameters of the Arrhenius equation and in the present work the pre-exponential factors of both the forward and reverse reactions 3.13 were calibrated, assuming the correctness of the equilibrium constant of the overall reaction. The pre-exponential factor was optimized minimizing the standard error (SE) between the experimental data and model values. The SE is defined, according to Eq. 4.1, as the square root of the mean squared error (MSE):

$$SE = \sqrt{MSE} \tag{4.1}$$

The optimization led to a 30% reduction of the pre-exponential factor of the forward reaction. Remembering that the equilibrium constant must be always respected for the reaction, the pre-exponential factor for the reverse reaction was evaluated consequently using the relation:

$$K_{eq} = \frac{k_f}{k_r} \tag{4.2}$$

The new set of kinetic parameters is reported in Table 4.14 [2].

Set	**Forward reaction**		**Reverse reaction**	
	$k^0_{f,j}\left[\frac{kmol}{m^3 s}\right]$	$E_{a,f_j}\left[\frac{cal}{mol}\right]$	$k^0_{r,j}\left[\frac{kmol}{m^3 s}\right]$	$E_{a,r_j}\left[\frac{cal}{mol}\right]$
Hikita et al. [66]	$9.77 \cdot 10^{10}$	9855.8	$3.23 \cdot 10^{19}$	15655
Proposed model	$6.839 \cdot 10^{10}$	9855.8	$2.261 \cdot 10^{19}$	15655

Table 4.14: Modified kinetic parameters

The optimized parameters of reaction 3.13 together with the parameters of reaction 3.14 were varied of ±10% in order to verify the robustness of the system. The effect on the temperature and composition profiles for Run T20 are reported in Figure 4.7.

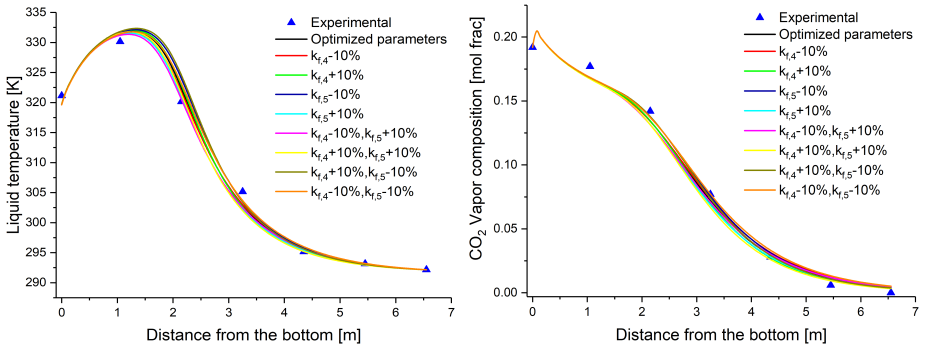

(a) Liquid temperature (b) CO_2 vapor phase composition

Figure 4.7: Run T20 - Absorber (a) liquid temperature profile and (b) CO_2 vapor composition profile for a ±10% variation of the kinetic parameters

It must be noticed that in Figure 4.7 the profiles were obtained varying the modified pre-exponential factors of the forward reaction 3.13 and the pre-exponential factors of the forward reaction 3.14 by ±10% and obtaining the pre-exponential factors of the reverse reaction using the corresponding equilibrium constants. In the first four cases the parameters of one reaction were changed while the other reaction parameters were kept at the optimized values. Then, all the possible combinations were considered, for a total of eight profiles. The results reported in Figure 4.7 demonstrate the robustness of the system for small variations of the modified kinetic parameters set, since no significant variations are observed in the profiles.
Figure 4.8 reports the comparison between the absorber profiles with the initial set of kinetic parameters from Hikita et al. [66] and the modification proposed in this thesis.

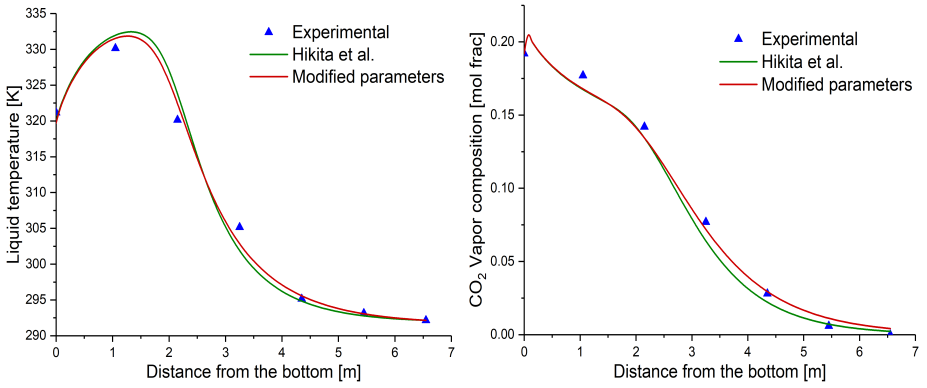

(a) Liquid temperature (b) CO_2 vapor phase composition

Figure 4.8: Run T20 - Absorber (a) liquid temperature profile and (b) CO_2 vapor composition profile before and after the modification of the kinetic parameters

An effective improvement can be immediately observed in the description of the experimental data for both the liquid temperature and the CO_2 molar fraction.
In order to quantify this improvement, the standard error defined in Eq. 4.1 was evaluated and reported in Table 4.15. A reduction of more than 0.5 degree was obtained for the temperature, while a slightly reduction of about $1.5 \cdot 10^{-3}$ was obtained for the CO_2 composition.

Set	$\mathbf{SE_T}$	$\mathbf{SE_x}$
Hikita et al. [66]	2.03	$7.12 \cdot 10^{-3}$
Proposed model	1.44	$5.5 \cdot 10^{-3}$

Table 4.15: Run T20 - Standard error using the two different sets of kinetic parameters

Following the modification of the kinetic parameters, as expected, a slightly reduction of both the CO_2 removal and loading were obtained, as shown in Table 4.16. Anyway, the results remained coherent with the experimental values.

Performance	**Experimental**	**Hikita et al.** [66]	**Proposed model**
CO_2 Removal %	100	99.1	98.4
Loading out	0.514	0.516	0.512

Table 4.16: Run T20 - Performance of the absorber before and after the modification of the kinetic parameters

4.5.1.5 Influence of the different flow models

In Subsection 3.4.1.2 the five flow models included in the *RadFrac*^{TM} model for the evaluation of the bulk properties were presented. All the models were tested in this thesis to investigate their possible influence on the simulations. The results of this analysis related to Run T20 for both the liquid temperature and the CO_2 vapor composition are reported in Figure 4.9.

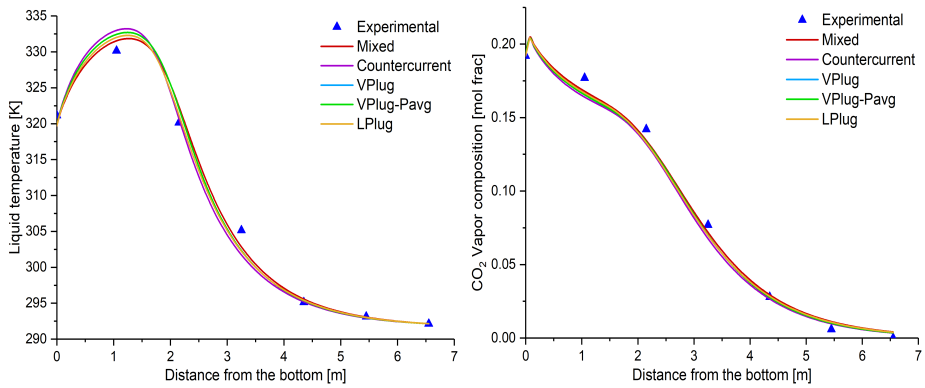

(a) Liquid temperature (b) CO_2 vapor phase composition

Figure 4.9: Run T20 - Absorber (a) liquid temperature profile and (b) CO_2 vapor composition profile using different flow models

No significant differences in the profiles are observed using the different flow models in this case. To corroborate this conclusion, the values of the standard error are reported in Table 4.17, while the performance of the absorber are reported in Table 4.18.

Variable	**Mixed**	**Countercurrent**	**VPlug**	**VPlug-Pavg**	**LPlug**
$\mathbf{SE_T}$	1.44	1.77	1.65	1.65	1.47
$\mathbf{SE_x}$	$5.5 \cdot 10^{-3}$	$7.4 \cdot 10^{-3}$	$6.42 \cdot 10^{-3}$	$6.42 \cdot 10^{-3}$	$6.35 \cdot 10^{-3}$

Table 4.17: Run T20 - Standard error using the different flow models

Variable	**Mixed**	**Countercurrent**	**VPlug**	**VPlug-Pavg**	**LPlug**
CO_2 Removal %	98.4	98.7	98.6	98.6	98.5
Loading out	0.512	0.513	0.513	0.513	0.512

Table 4.18: Run T20 - Absorber performance using the different flow models

The results from Table 4.17 indicate that the minimum SE is obtained using the *Mixed* model; on the other hand, the performance of the absorber remain practically constant varying the flow models.

4.5.2 Lab-scale plant: Run T22

The procedure used to validate the model in the case of Run T20 was next applied to another run from the same lab-scale facility, Run T22. This run is characterized by a higher amount of MEA in the liquid entering the top of the absorber. First, it was verified the correctness of the previously defined number of segments due to the change in the operating conditions. Again 90 segments were sufficient to correctly simulate the plant. This result was somewhat expected since the column is the same as Run T20. For what concerns the performance of the absorber, the trend was similar to that of Run T20. Subsequently to the choice of an appropriate number of segments, the plant was simulated using the new set of kinetic parameters reported in Table 4.14. The comparison between the model and the experimental data is reported in Figure 4.10.

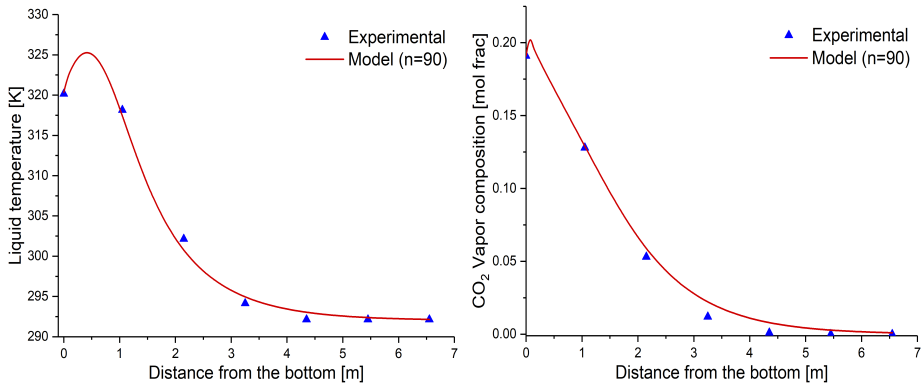

(a) Liquid temperature (b) CO_2 vapor phase composition

Figure 4.10: Run T22 - Comparison between absorber (a) liquid temperature profile and (b) CO_2 vapor composition profile with the experimental data

In this case the temperature bulge is more squashed towards the bottom of the column, while the concentration bulge remains similar to that of Run T20, although the profile becomes steeper. This behavior can be explained by the higher amount of MEA in the liquid solution that makes the reactions faster. Even in this case the agreement between the 90 segments model and the experimental data is good. The standard error was evaluated for Run T22 before and after the modification of the kinetic parameters and the results are shown in Table 4.19.

Set	$\mathbf{SE_T}$	$\mathbf{SE_x}$
Hikita et al. [66]	1.59	$4 \cdot 10^{-3}$
Proposed model	0.74	$5 \cdot 10^{-3}$

Table 4.19: Run T22 - Standard error using the two different sets of kinetic parameters

It is possible to notice from Table 4.19 that for what concerns the liquid temperature the SE is reduced by almost 1K, which is higher compared to Run T20. On the other hand, the composition SE is increased by $1 \cdot 10^{-3}$, which can be considered negligible.
Finally, the performance of the absorber following the modification of the kinetic parameters are reported in Table 4.20.

Performance	**Experimental**	**Hikita et al.** [66]	**Proposed model**
CO_2 Removal %	100	99.85	99.6
Loading out	0.443	0.458	0.457

Table 4.20: Run T22 - Performance of the absorber before and after the modification of the kinetic parameters

The results obtained proved the ability of the proposed model to describe different sets of experimental data from the same plant. In the next Subsection the model is going to be tested for the large-scale pilot-plant.

4.5.3 Large-scale plant: Run 1A2

With the purpose of proving the general validity of the proposed method, the developed model was tested on another pilot-plant facility. In this case a large-scale facility, equipped with structured packing and with an L/V ratio leading to a top temperature bulge was considered. Since the column dimensions and the molar flows involved were higher compared to the lab-scale pilot-plant, in the light of the Peclet number values obtained and reported in Table 4.9, a higher number of segments was expected in this case. The model with the modified kinetic parameters was directly applied to find the proper number of segments. For this plant, only temperature measurements were available and the phase was not specified. For this reason, Figure 4.11 reports the profiles for the liquid and vapor/gas temperature with different number of segments.

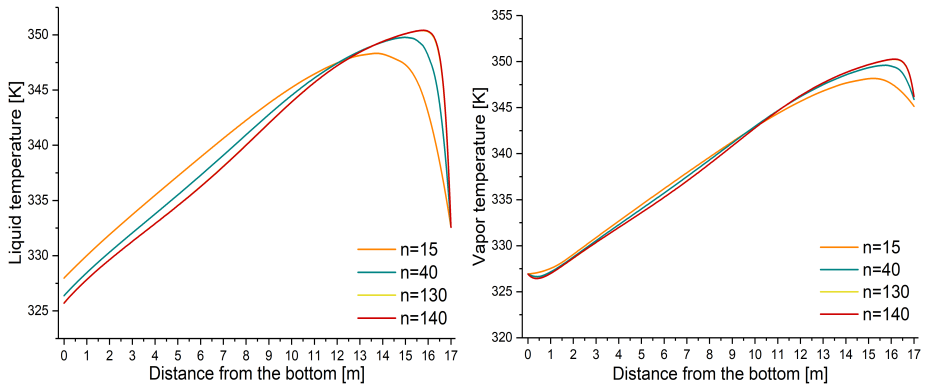

(a) Liquid temperature (b) Vapor temperature

Figure 4.11: Run 1-A2 - Absorber (a) liquid temperature profile and (b) vapor temperature profile variation with the number of segments

As it is possible to notice, 140 segments are needed in this case to obtain a numerically robust solution of the system. The temperature bulge, due to the L/V ratio less than 5, appears in the top of the column.
After the evaluation of a proper number of segments, the comparison between the model and the experimental data is reported in Figure 4.12.

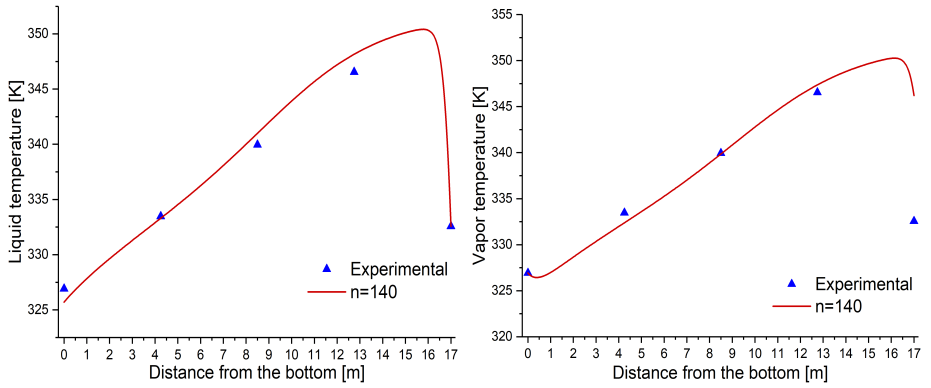

(a) Liquid temperature (b) Vapor temperature

Figure 4.12: Run 1-A2 - Comparison between absorber (a) liquid temperature profile and (b) CO_2 vapor composition profile with the experimental data

A good agreement is found between the model with 140 segment and the experimental data.
From the point of view of the column performance, only the CO_2 removal % was available in the work of Razi et al. [44]. The comparison between the experimental values and the model estimations is reported in Table 4.21.

Performance	**Experimental**	**Number of segments**		
		15	40	140
CO_2 Removal %	90	85.2	86.6	87.2

Table 4.21: Run 1-A2 - Absorber performance

In the light of these results, it was validated again the necessity of an appropriate number of segments to obtain a numerically correct and robust solution of the resulting system of algebraic equation.
Using a too low number of segments leads to an incorrect description of the critical temperature bulge zone and can bring to incorrect evaluations especially if the model is extended to describe the dynamic behavior of the absorber.

4.6 Chapter 4 Summary

In this chapter the model developed in Aspen Plus® using the *RadFrac*™ model - Rate-Based mode and described in Chapter 3 was tested on two pilot-plant facilities for validation purposes. In particular, the two plants were chosen for their differences in dimensions and amount of streams involved (lab- vs large-scale), packing type (random vs structured) and position of the temperature bulge (bottom vs top). Before the simulations, the analysis of the Peclet number was performed for all the case studies. The smallest dimensionless number value obtained was in the order of the 10^2, and this results led to the conclusion that the axial diffusion/dispersion had no effect on the process. Consequently, the column behavior resembles that of an ideal plug-flow and then there was the need for a sufficiently high number of segments for the correct mathematical description of the process. The Peclet number does not take into account the backmixing due to the countercurrent, which is included in the material and energy balances describing the system. So, to investigate the possible effect of the backmixing on the process, it was necessary to simulate the column varying the number of segments. For what concerns the lab-scale plant, it was found the 90 segments for the discretization of the axial domain, corroborating the results previously obtained with the Peclet number analysis. After the identification of a proper number of segments, the uncertainty on the evaluation of the kinetic parameters of the reaction involving carbon dioxide and MEA was considered. In particular, the pre-exponential factors of both the forward and the reverse reaction were optimized in order to minimize the standard error between the experimental data and the model results. The results showed

an improvement in the profiles both for what concerns the liquid temperature and the CO_2 vapor composition. Moreover, the influence of different flow models for the calculation of the bulk properties was considered and no substantial differences were observed in the results. The proposed model with the modified parameters was then tested on another run of the lab-scale plant, validating again the proposed procedure. In the end, one run of the large-scale absorber was simulated in order to generalize the validity of the procedure, founding the necessity of using 140 segments due to the higher column dimensions and molar flow rates included. In all the cases it was found that the model is able to accurately describe the experimental data, independently from the column dimensions and the position of the temperature bulge.

From the results included in this chapter, it should be highlighted the importance of the profiles in the steady-state modeling of the absorption section. The profiles should be considered as important as the final purities in the design of an absorber, since they give significant indications on the column behavior. Moreover, the internal profiles are fundamental when a study of the dynamic behavior is conducted or when a new control structure is to be implemented. Then, great attention should be put on the proper choice of the number of segments, since it was demonstrated that a wrong definition of this parameter would lead to an incorrect numerical solution of the system. This fact would eventually lead to an incorrect description of the system profiles, especially for what concerns the critical temperature bulge. In the next chapter, the procedure used to validate the model for the absorber is applied to the stripping section.

Chapter 5

Model validation for the stripper

In this chapter the stripping section is taken into account to test the model proposed in Chapter 3. Similarly to the absorber case, two different pilot-plant facilities are considered. Two different sets of degrees of freedom are chosen for the two plants in order to study the effect of the number of segments on the evaluation of the output streams features in one case and on the evaluation of the reboiler duty in the other case. After the Peclet number evaluation for all the case studies, the number of segments analysis is performed. The obtained model is again able to describe correctly the experimental data, validating the proposed procedure for the stripper.

5.1 Introduction to the stripping section modeling

After the model validation for the absorber in Chapter 4, this chapter was dedicated to the validation of the proposed model for what concerns the stripping section. Up to now in the open literature more attention has been given to the absorption process compared to the stripping one since, as stated by Zhang et al. [38], the absorber is more sensitive to accurate modeling of the transport phenomena and rates compared to the stripper.
At the same time, the stripper represents undoubtedly the most critical part of the system from an economical point of view, and its optimization is crucial in order to minimize the energy consumption in the capture plant. As the reboiler duty represents by far the highest operating cost of the plant, as it drives the entire thermal swing, it is also the value that has the largest potential for improvement. Different works on the stripper have been focused mainly on the search for the operative conditions that minimize the reboiler duty or in the search for new plant schemes to improve the energy utilisation through Process Integration [53].
The development of a model able to correctly describe the behavior of the stripper is an essential step to successively identify new possible ways to minimize the energy consumption. As highlighted by Tobiesen et al. [49], the solvent regeneration section is more complex than the absorption one due to the presence of condenser and reboiler. For this reason, a detailed model of this section is needed to have a better description of the phenomena happening inside the equipment and to improve the interpretation of the results obtained from the experimental campaign. At the same time, only few experimental data sets for the stripper are available in the open literature. This makes model validation and verification more difficult.
In this thesis, like the case of the absorber, two different pilot-plant facilities were taken into account to test the model proposed in Chapter 3. In particular, the first plant considered was the CO_2 capture facility from SINTEF Materials and Chemistry described in the work of Tobiesen et al. [49], while the second one was the pilot-plant from the University of Texas at Austin described in the work of Dugas [106]. A brief description of both the plants is reported in the following Section.

5.2 Stripping section case studies

5.2.1 SINTEF pilot-plant

The pilot-plant facility from the SINTEF Materials and Chemistry of Norway described in the work of Tobiesen et al. [49] consists in the packed column equipped with both condenser and reboiler of which a schematic

flowsheet is reported in Figure 5.1.

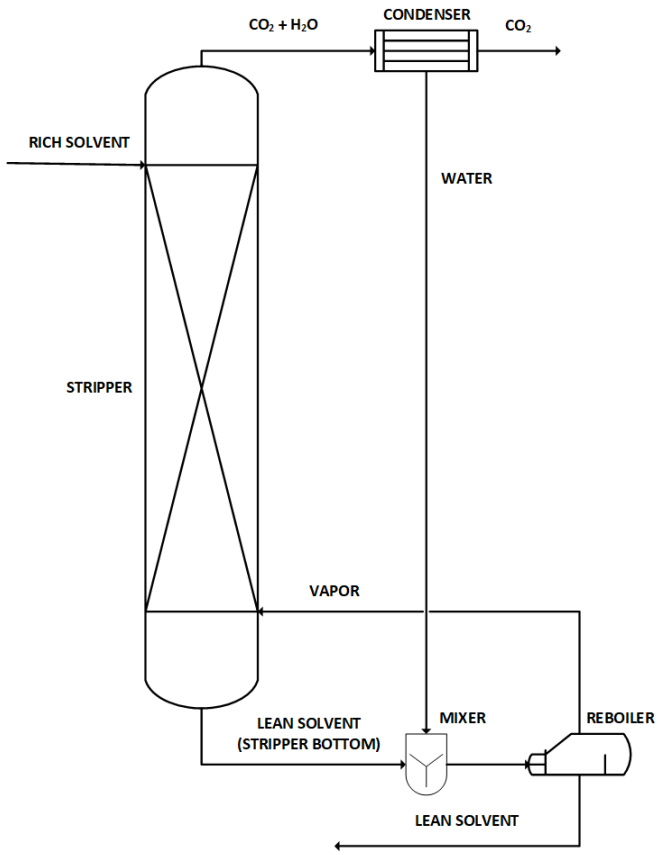

Figure 5.1: SINTEF plant flowsheet

The rich solvent coming from the absorption section is fed to the top of the stripper where it flows countercurrent with the vapor stream generated by the reboiler. From the top of the column, a vapor/gas mixture containing mainly CO_2 and water is sent to a partial condenser where the CO_2 is concentrated in the gas phase. The water recovered from the condenser is mixed with the liquid exiting the bottom of the column and the obtained liquid is sent to the reboiler. In the reboiler, part of this liquid is vaporized, while the remaining part is recycled back to the absorption section.
The column is packed with Mellapak 250Y and it is equipped with five sensors for the measurement of the liquid temperature. Moreover, different streams features measurements are available. In this thesis, two runs from this facility, Run 1 and Run 14, were chosen to validate the model on the basis of different rich solvent loadings and operating conditions. The column

and packing features are reported in Table 5.1, while the feed input data for each run are shown in Table 5.2. Furthermore, the operating conditions for each run are shown in Table 5.3. Then, the experimental data concerning the liquid temperature and the output streams features are reported in Table 5.4, where the height 0 m corresponds to the column bottom, and Table 5.5, respectively.

Variable	**Value**
Packing height [m]	3.89
Column diameter [m]	0.1
Void fraction [m^3/m^3]	0.987
Dry specific surface area [m^2/m^3]	256

Table 5.1: SINTEF plant column and packing features

Run	1	14
Temperature [K]	389.81	381.454
Molar flow [kmol/h]	10.7121	24.281
CO_2 [mol frac]	0.03484	0.0518
MEA [mol frac]	0.11023	0.1134
H_2O [mol frac]	0.8549	0.8348
Loading [mol CO_2/mol MEA]	0.3161	0.4571
Pressure [kPa]	196.96	215.3588

Table 5.2: Feed characterization for Run 1 and 14 from the SINTEF plant

Run	1	14
Condenser/Top pressure [kPa]	196.96	215.3588
Pressure drop [kPa]	1	0.001
Condenser temperature [K]	288.15	292.15
Reboiler duty [kW]	11.6	11.6

Table 5.3: Operating conditions for Run 1 and 14 from the SINTEF plant

Run		1	14
Sample	**H [m]**	**T^L [K]**	**T^L [K]**
1	0.01	393.59	383.73
2	1.05	392.41	381.93
3	2.15	391.5	381.66
4	3.25	391	382.02
5	4.35	389.81	381.45

Table 5.4: Temperature profile experimental data for Run 1 and 14 from the SINTEF plant

Run	1	14
Lean solvent		
Temperature [K]	394.15	394.91
CO_2 [mol frac]	0.02372	0.025405
MEA [mol frac]	0.10855	0.10751
H_2O	0.86773	0.86708
Loading [mol CO_2/mol MEA]	0.21852	0.2363
Gas from condenser		
Molar flow [kmol/h]	0.11588	0.0939

Table 5.5: Output streams experimental data for Run 1 and 14 from the SINTEF plant

5.2.2 University of Texas at Austin pilot-plant

The stripping section within the pilot-plant facility of the University of Texas at Austin and described in the work of Dugas [106] is represented by the classic configuration with partial condenser and reboiler schematized in Figure 5.2. In this case the packing height is divided into two sections packed with structured Flexipac 1Y separated by a liquid redistribution zone. The main difference with the SINTEF plant is represented by the fact that the water recovered in the condenser is sent back to the top of the column as reflux. The column and packing features are reported in Table 5.6. For this plant, one run, Run 47, from the experimental campaign reported in [106] is considered. The feed characterization is shown in Table 5.7. Six sensors for the measurement of the liquid temperature are present along the column but only four of them are inside the packing. For this reason, the two measurement outside the packing are not considered in the model validation. The available experimental data for the liquid temperature and the output streams features are reported in Table 5.8 and Table 5.9.

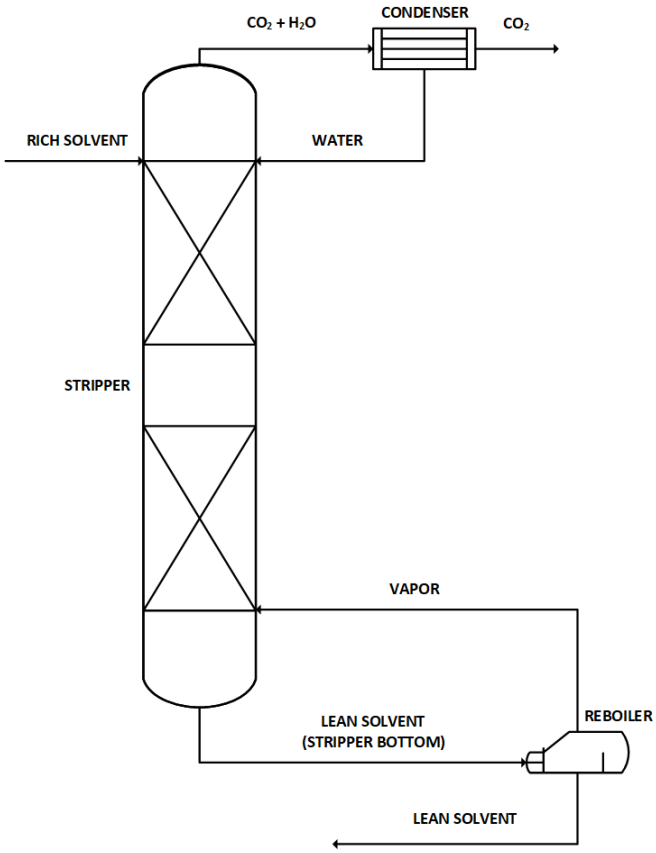

Figure 5.2: University of Texas at Austin plant flowsheet

Variable	**Value**
Packing height [m]	6.1
Column height [m]	11.1
Column diameter [m]	0.427
Void fraction [m^3/m^3]	0.91
Dry specific surface area [m^2/m^3]	420

Table 5.6: University of Texas at Austin plant column and packing features

Run	47
Temperature [K]	356
Molar flow [kmol/h]	90.9912
CO_2 [mol frac]	0.0534
MEA [mol frac]	0.1181
H_2O [mol frac]	0.828
N_2 [mol frac]	0.0005
Loading [mol CO_2/mol MEA]	0.3161
Pressure [kPa]	196.96

Table 5.7: Feed characterization for Run 47 from the University of Texas at Austin plant

Run		47
Sample	**H [m]**	**T^L [K]**
1	1.75	365.16
2	3.05	363.98
3	4.72	363.47
4	6.245	361.16

Table 5.8: Temperature profile experimental data for Run 47 from the University of Texas at Austin plant

Run	47
Reboiler duty [MJ/h]	738
Lean solvent	
Loading [mol CO_2/mol MEA]	0.28
Gas from condenser	
CO_2 mass flow [kg/h]	92

Table 5.9: Output streams experimental data for Run 47 from the University of Texas at Austin plant

5.2.3 Stripper degrees of freedom

Differently from the absorber, due to the presence of the condenser and the reboiler, two degrees of freedom must be defined for the stripper in order to perform the simulations. In order to analyze different possibilities, two different sets of degrees of freedom were chosen for the two plants studied. In particular:

- in the case of the SINTEF plant, the condenser temperature and the reboiler duty were fixed;
- in the case of the University of Texas at Austin, the condenser tem-

perature and the CO_2 gas molar flow rate were fixed.

This choice of the degrees of freedom was done to prove the validity of the proposed model in the case of different experimental data sets available. Moreover, as it will be shown in the next sections, this kind of analysis explains once again the importance of having a correct model of the process, with outcomes that have important implications both at a design and dynamic level.

5.3 Peclet number analysis

The first step in the procedure shown in Chapter 4 regarded the Peclet number analysis, which was performed for all the runs examined for the stripping section. Like the absorber, the Peclet number was evaluated for all the runs for both the material (single components and mixture) and energy transport in each phase and with reference to both the packing height and the packing equivalent diameter using Aspen Custom Modeler®. The inlet conditions (column top for the liquid phase, column bottom for the gaseous phase) are used as reference conditions. The results of the computation are reported in Tables 5.10-5.12.

Run	1			
Phase	*Liquid*		*Gaseous*	
Characteristic length	H	d_{eq}	H	d_{eq}
$Pe_{M,i}$				
CO_2	$8.00 \cdot 10^7$	$2.63 \cdot 10^5$	$1.31 \cdot 10^5$	431.43
CO_3^{--}	$5.20 \cdot 10^8$	$1.71 \cdot 10^6$	–	–
H_2O	$2.03 \cdot 10^8$	$6.68 \cdot 10^5$	$1.38 \cdot 10^5$	454.25
H_3O+	$5.15 \cdot 10^7$	$1.69 \cdot 10^5$	–	–
HCO_3^-	$3.31 \cdot 10^8$	$1.09 \cdot 10^6$	–	–
MEA	$9.44 \cdot 10^7$	$3.10 \cdot 10^5$	$2.25 \cdot 10^5$	738.71
MEA^+	$3.61 \cdot 10^8$	$1.18 \cdot 10^6$	–	–
$MEACOO^-$	$3.61 \cdot 10^8$	$1.18 \cdot 10^6$	–	–
N_2	$7.95 \cdot 10^7$	$2.61 \cdot 10^5$	$9.93 \cdot 10^4$	326.08
OH^-	$9.09 \cdot 10^7$	$2.98 \cdot 10^5$	–	–
$Mixture$	$2.00 \cdot 10^8$	$6.55 \cdot 10^5$	$1.38 \cdot 10^5$	453.98
Pe_T				
$Mixture$	$4.22 \cdot 10^6$	$1.38 \cdot 10^4$	$1.69 \cdot 10^5$	554.6

Table 5.10: Peclet number evaluation for Run 1

Run	1			
Phase	*Liquid*		*Gaseous*	
Characteristic length	H	d_{eq}	H	d_{eq}
$Pe_{M,i}$				
CO_2	$1.19 \cdot 10^8$	$3.90 \cdot 10^5$	$9.28 \cdot 10^4$	304.77
CO_3^{--}	$9.78 \cdot 10^8$	$3.21 \cdot 10^6$	–	–
H_2O	$1.14 \cdot 10^8$	$3.73 \cdot 10^5$	$9.32 \cdot 10^4$	305.76
H_3O+	$9.68 \cdot 10^7$	$3.18 \cdot 10^5$	–	–
HCO_3^-	$6.22 \cdot 10^8$	$2.04 \cdot 10^6$	–	–
MEA	$1.83 \cdot 10^8$	$5.99 \cdot 10^5$	$1.70 \cdot 10^5$	558.81
MEA^+	$6.78 \cdot 10^8$	$2.23 \cdot 10^6$	–	–
$MEACOO^-$	$6.78 \cdot 10^8$	$2.23 \cdot 10^6$	–	–
N_2	$1.16 \cdot 10^8$	$3.82 \cdot 10^5$	$7.40 \cdot 10^4$	243.04
OH^-	$1.71 \cdot 10^8$	$5.61 \cdot 10^5$	–	–
$Mixture$	$1.26 \cdot 10^8$	$4.12 \cdot 10^5$	$9.31 \cdot 10^4$	305.76
Pe_T				
$Mixture$	$6.43 \cdot 10^6$	$2.11 \cdot 10^4$	$1.20 \cdot 10^5$	392.66

Table 5.11: Peclet number evaluation for Run 14

Run	1			
Phase	*Liquid*		*Gaseous*	
Characteristic length	H	d_{eq}	H	d_{eq}
$Pe_{M,i}$				
CO_2	$1.77 \cdot 10^7$	$2.62 \cdot 10^4$	$3.91 \cdot 10^5$	576.64
CO_3^{--}	$1.05 \cdot 10^8$	$1.55 \cdot 10^5$	–	–
H_2O	$3.77 \cdot 10^7$	$5.57 \cdot 10^4$	$4.36 \cdot 10^5$	643.87
H_3O+	$1.04 \cdot 10^7$	$1.53 \cdot 10^4$	–	–
HCO_3^-	$6.67 \cdot 10^7$	$9.84 \cdot 10^4$	–	–
MEA	$2.71 \cdot 10^7$	$4.00 \cdot 10^4$	$6.80 \cdot 10^5$	1003
MEA^+	$7.27 \cdot 10^7$	$1.07 \cdot 10^5$	–	–
$MEACOO^-$	$7.27 \cdot 10^7$	$1.07 \cdot 10^5$	–	–
N_2	$1.75 \cdot 10^7$	$2.58 \cdot 10^4$	$2.90 \cdot 10^5$	427.75
OH^-	$1.83 \cdot 10^7$	$2.26 \cdot 10^4$	–	–
$Mixture$	$3.96 \cdot 10^7$	$5.85 \cdot 10^4$	$4.36 \cdot 10^5$	643.57
Pe_T				
$Mixture$	$5.56 \cdot 10^5$	819.71	$4.92 \cdot 10^5$	725.96

Table 5.12: Peclet number evaluation for Run 47

As it is possible to notice from the analysis of Tables 5.10-5.12, the values of the Peclet number are quite large. Tables 5.10 and 5.11 show the results for the lab-scale plant. When the liquid phase is considered and the column height is used as characteristic length, the material Peclet number values are in the order of 10^8. If the packing equivalent diameter is used, this value

is reduced to about 10^5. For what concerns the gaseous phase, the material Peclet number is in the order of 10^5 and 10^2 when the column height and the packing equivalent diameter are considered, respectively. On the other hand, the thermal Peclet number for the liquid phase is in the range of 10^6 when the packing height is used and 10^4 with the packing equivalent diameter as characteristic length. With regards to the gaseous phase, the thermal Peclet number is in the order of 10^5 with the packing height as characteristic length, while the same value is reduced to 10^2 when the packing equivalent diameter is considered.
For what concerns the University of Texas at Austin plant, as expected, the values of the Peclet number shown in Table 5.12 are higher compared to the lab-scale plant due to the higher column dimensions and molar flows involved. For the liquid phase, the material Peclet number is in the order of 10^7 when the column height is considered and 10^4 for the packing equivalent diameter. For the gaseous phase, values in the range of 10^5 with the column height and 10^2 considering the packing equivalent diameter are observed. The liquid thermal Peclet number is in the order of 10^5 and 10^2 considering the column height and the packing equivalent diameter, respectively. For the gaseous phase, similarly to the material Peclet number, values of the thermal Peclet number in the order of 10^5 considering the column height to 10^2 considering the packing equivalent diameter are obtained.
Like the absorber, since the lowest value of the dimensionless group was in the order of 10^2, it could be concluded that the axial diffusion/dispersion had no effect on the process and that the column fluid dynamics resembled that of an ideal plug-flow [2, 46]. Consequently, even in the case of the stripper, a sufficiently high number of segments was needed for the mathematical solution of the resulting system of algebraic equations.

5.4 SINTEF plant: Run 1

After the evaluation of the Peclet number, the SINTEF plant was simulated varying the number of segments until two consecutive profiles were overlapped to obtain a correct solution of the system from a numerical point of view. It must be remembered that in this case the condenser temperature and the reboiler duty are fixed to saturate the stripper degrees of freedom. Since the water from the condenser is not sent to the top of the column as reflux but it is mixed with the liquid from the stripper bottom, as reported in Figure 5.1, both condenser and reboiler were modeled separately from the column using the *Flash2* model on Aspen Plus®. For this reason it was possible to fix the degrees of freedom directly on the software. The variation of the liquid temperature profile with the number of segments is reported in

Figure 5.3.

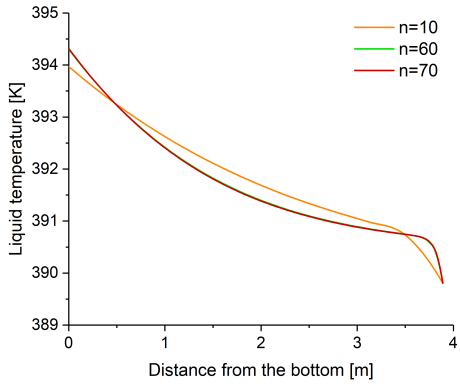

Figure 5.3: Run 1 - Stripper temperature profile variation with the number of segments

As it is possibile notice from Figure 5.3, the asymptotic behavior is reached with 70 segments. After the evaluation of a proper number of segments it was possible to make the comparison between the model and the experimental data, reported in Figure 5.4.

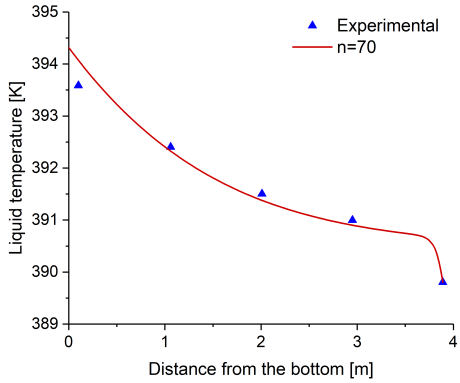

Figure 5.4: Run 1 - Comparison between the model liquid temperature profile and the experimental data

The good agreement between the model and the experimental data is demonstrated by the evaluation of the standard error, which is 0.23 K for the profile with 70 segments. The same good agreement is observed for what concerns the output measured variables, as reported in Table 5.13.

Variable	**Experimental**	**Model (n=70)**
Lean solvent		
Temperature [K]	394.15	395.24
CO_2 [mol frac]	0.02372	0.02601
MEA [mol frac]	0.10855	0.11125
H_2O	0.86773	0.86274
Loading [mol CO_2/mol MEA]	0.21852	0.2338
Gas from condenser		
Molar flow [kmol/h]	0.11588	0.09809

Table 5.13: Run 1 - Comparison between the output streams experimental data and the model results with n=70

In the case of the stripper, differently from the absorber, since no significant gradients are present, the differences between the model with 10 segments and the model with 70 segments might not seem evident from the analysis of the liquid temperature profiles reported in Figure 5.3. Anyway, considering the variation of the CO_2 vapor molar fraction with the number of segments, reported in Figure 5.5, it becomes clear how the parameter influences the description of the system.

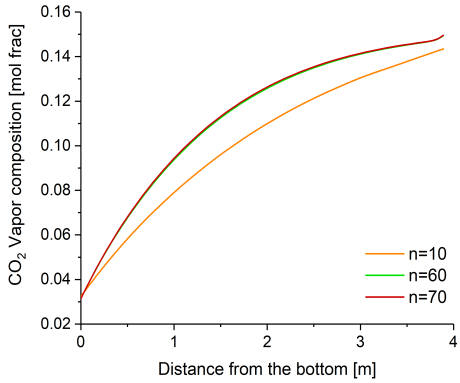

Figure 5.5: Run 1 - Stripper CO_2 vapor composition profile variation with the number of segments

In particular, it can be observed that the profile with a higher number of segments highlights a higher extent of the stripping reaction, as demonstrated by the higher value of the CO_2 vapor molar fraction along the column. This result has important implications both at a design and dynamic extension level and it was obtained thanks to the better discretization of the axial domain that led to a better evaluation of the internal fluxes in the stripper. In fact, remembering the definition of CSTR, a more detailed discretization

permits to evaluate the internal fluxes in more points, and this generates more precise results. This fact is further demonstrated by the obtained CO_2 and H_2O interphase molar flow profiles reported in Figure 5.6.

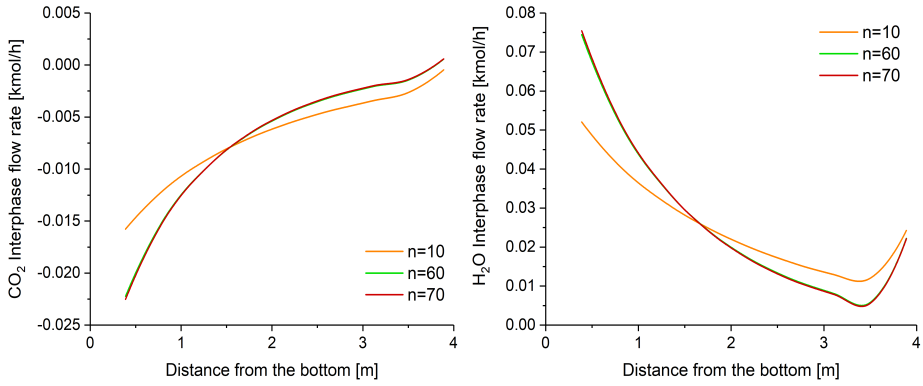

(a) CO_2 Interphase flow rate (b) H_2O Interphase flow rate

Figure 5.6: Run 1 - Stripper (a) CO_2 and (b) H_2O interphase molar flow rate profile variation with the number of segments

It can clearly be seen that the profiles obtained with 10 segments are significantly different from those at 70 segments, testifying the influence of the number of segments on the system and justifying this analysis. Moreover, the profile with 70 segments allows to identify an initial part of the column where the absorption process takes place instead of the stripping one. The process is characterized by an interphase transfer of water from the vapor to the liquid phase throughout the column, as a consequence of the condensation.
This result has evident implications in design, because an inadequate discretization of the axial domain can lead to an under-/over-estimation of the column dimensions and required duty, and in the assessment of a control system structure, because the profiles would be different from the real ones.

5.5 SINTEF plant: Run 14

After the validation of the model for Run 1, Run 14 from SINTEF plant was analyzed. Differently from the previous run, this one is characterized by a substantially higher loading and molar flow rate in the rich solvent entering the top of the column. Some issues were found for what concerns the inlet feed temperature and for this reason two different cases were studied:

1. the inlet feed temperature was fixed at 381.45 K as reported in the

experimental data. In this case the feed was liquid phase only;

2. the inlet feed temperature was fixed at 386.15 K. In this case the feed was a vapor-liquid mixture.

Figure 5.7 reports the liquid temperature profile using the model obtained in Section 5.4 for the two situations. The first thing to be noticed is that, independently from the case, the profiles have not the typical behavior of a stripper liquid temperature profile. In fact, starting from the top, the temperature diminishes, then remains constant and finally rises again.

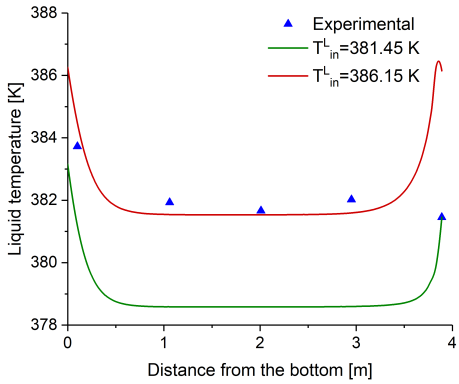

Figure 5.7: Run 14 - Comparison between the stripper liquid temperature profile for two different values of the inlet temperature and the experimental data

When the temperature of the rich solvent was set to 381.45 K, the feed was liquid only and, as previously reported in the work of Tobiesen et al. [49], it was inadequate for the description of the temperature profile, probably due to a flash that took place before the feed entered the stripper. Tobiesen et al. also indicated that for this run a feed pre-heater was used and this probably caused the flash. So, this feed temperature was probably not correct. In the work of Tobiesen et al. the new feed temperature value seemed to be around 390.15 K, obtaining a good agreement with the experimental data using a model based on the enhancement factor. Using the model developed in this work, which is based on the rigorous Maxwell-Stefan equations, when the rich solvent temperature was set to 390.15 K the results led again to an inadequate temperature profile, since the temperature seemed to be too high. For this reason, the inlet temperature was set at 386.15 K, value that still ensured the stream to be a vapor-liquid mixture. As it is possible to observe in Figure 5.7, with the higher feed temperature the agreement between the experimental data and the model profile becomes very good.
In Figure 5.8 the CO_2 vapor composition profile is shown for the case when

the rich solvent temperature was set to 386.15 K.

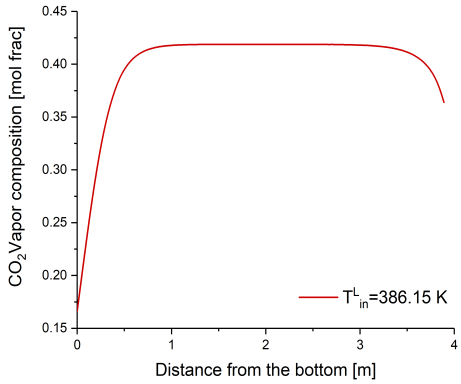

Figure 5.8: Run 14 - Stripper CO_2 vapor composition profile

The profile is characterized by a reduction of the CO_2 molar fraction at the top of the stripper. This fact can be explained by two possible situations:

- an absorption process is present. In this case the CO_2 in the vapor is reduced by chemical reaction;
- the enthalpy of the inlet stream is high enough to determine an evaporation process. In this case the CO_2 in the vapor is reduced by dilution.

The answer can be given analyzing the CO_2 and H_2O interphase molar flow rate profiles, reported in Figure 5.9.

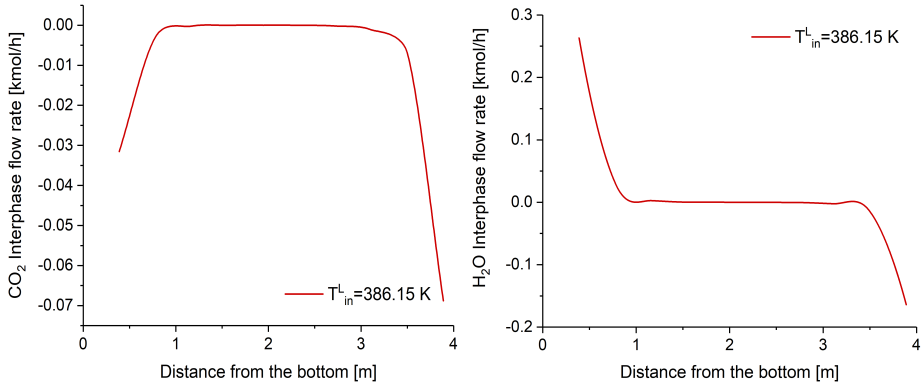

(a) CO_2 Interphase flow rate (b) H_2O Interphase flow rate

Figure 5.9: Run 14 - Stripper (a) CO_2 and (b) H_2O interphase molar flow rate profile

As the CO_2 is always involved in the desorption process (no positive molar flow is observed), the evaporation of water is due to the high enthalpy of the inlet flow. The H_2O evaporation at the top dilutes the CO_2 concentration in the vapor phase, justifying the profile behavior in Figure 5.8. This fact also explains the initial reduction of the temperature at the top in Figure 5.7. Finally, in order to conclude the analysis of Run 14, Table 5.14 reports the comparison between the experimental data and the model results for what concerns the output streams features.

Variable	**Experimental**	**Model (n=70)**
Lean solvent		
Temperature [K]	389.04	392.66
CO_2 [mol frac]	0.0408	0.0437
MEA [mol frac]	0.1117	0.1143
H_2O	0.8475	0.8419
Loading [mol CO_2/mol MEA]	0.3656	0.3818
Gas from condenser		
Molar flow [kmol/h]	0.2618	0.209

Table 5.14: Run 14 - Comparison between the output streams experimental data and the model results with n=70

5.6 University of Texas at Austin plant: Run 47

After the validation of the model for what concerns the SINTEF plant, the stripping section of the University of Texas at Austin was taken into account. As already mentioned in Subsection 5.2.3, in the case of Run 47 the condenser temperature and the CO_2 output gas mass flow rate were fixed to saturate the degrees of freedom. This choice was made to highlight the effect of the number of segments analysis in the evaluation of the reboiler duty. It must be noticed that in this case, since the classic stripper configuration with reflux from the condenser was involved, both condenser and reboiler were modeled within the *RadFrac*^{TM} model. Differently from the previous case studied, it was not possible to fix the chosen degrees of freedom directly. In particular, the mass reflux ratio, R_{mass}, was used to fix the condenser temperature, T_{cond}, while the total gas molar flow rate from the condenser, V_{cond}, was used to fix the CO_2 output gas mass flow rate, $V_{CO_2,cond}$, by means of the *Design Specification* tool included in the *RadFrac*^{TM} module. The plant was simulated varying the number of segments and the results are reported in Figure 5.10.

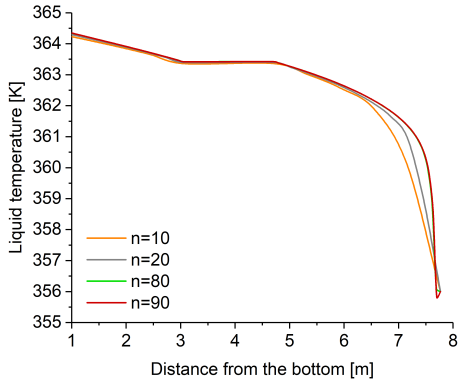

Figure 5.10: Run 47 - Stripper temperature profile variation with the number of segments

The flat part in the middle of the profile corresponds to redistribution zone. Since the column is higher than the SINTEF plant one, the asymptotic behavior was reached only after 90 segments. The comparison between the experimental profile and the model profiles for what concerns the liquid temperature is reported in Figure 5.11.

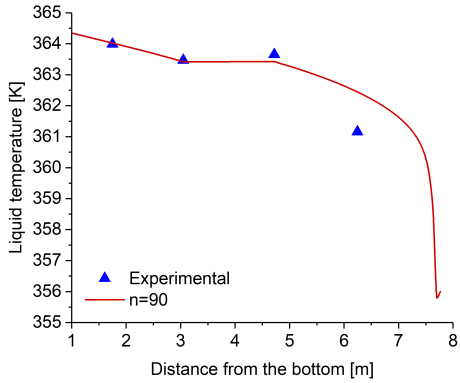

Figure 5.11: Run 47 - Comparison between the model liquid temperature profile and the experimental data

As it is possible to observe from the analysis of Figure 5.11 the model is able to describe adequately the experimental data, as further demonstrated by the value of the standard, which is about 0.7 K when 90 segments are used. For what concerns the CO_2 vapor composition, the variation of the profiles with the number of segments is shown in Figure 5.12.

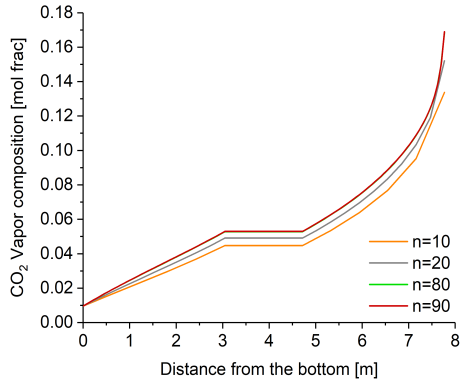

Figure 5.12: Run 47 - Stripper CO_2 vapor composition profile variation with the number of segments

Similarly to Run 1 from the SINTEF plant, the model with a higher number of segments always highlights a higher extent of the stripping reaction. Again, this is a consequence of the better discretization of the axial domain, which is corroborated by the analysis of the CO_2 and H_2O interphase molar flow rate profiles, reported in Figure 5.13.

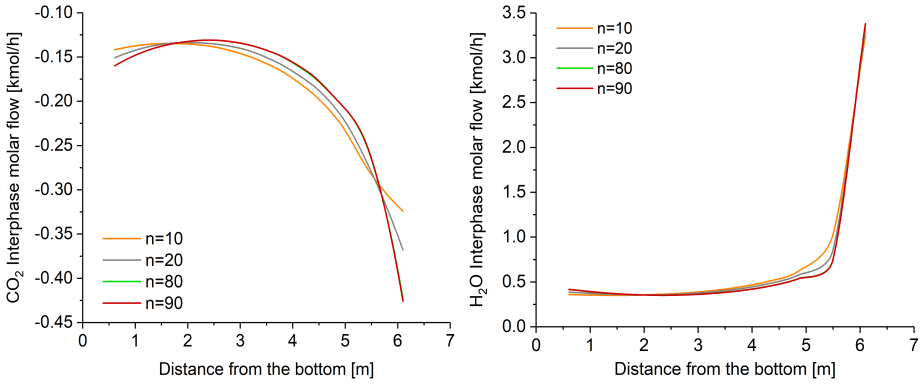

(a) CO_2 Interphase flow rate (b) H_2O Interphase flow rate

Figure 5.13: Run 47 - Stripper (a) CO_2 and (b) H_2O interphase molar flow rate profile variation with the number of segments

The clear difference between the profiles varying the number of segments justifies the correctness of the analysis even for this case.
Table 5.15 summarizes the stripper performance with the variation of the number of segments.

Performance	**Experimental**	**Number of segments**			
		10	20	80	90
Mass reflux ratio	-	2.57	2.21	1.95	1.94
Lean solvent					
Loading [mol CO_2/mol MEA]	0.286	0.268	0.268	0.268	0.268
Gas from condenser					
Mixture mass flow rate [kg/h]	-	94.89	94.89	94.89	94.89
CO_2 mass flow rate [kg/h]	92	91.8	91.8	91.8	91.8
Reboiler					
Temperature [K]	-	365.4	365.4	365.4	365.4
Duty [MJ/h]	738	895.78	807.04	744.29	742.03

Table 5.15: Run 47 - Stripper performance

From the analysis of Table 5.15 different conclusions can be made:

- the chosen set of degrees of freedom fixes the output conditions on the lean solvent and the gas from the condenser. For this reason, there is no difference in the output values with the variation of the number of segments. At the same time, the reboiler temperature is not influenced by the parameter variation;

- the number of segments has a significant effect on the value of the mass reflux ratio and the reboiler duty. Since the output conditions are fixed by the degrees of freedom, what changes is the internal behavior of the column. From the analysis of Figure 5.12, it was found that the CO_2 molar fraction value with 10 segments was always the lowest all along the column, with the highest difference on the top of the column. But since the output conditions are fixed, in order to respect this constraint, the simulator finds that a high reboiler duty is needed to have that value of the CO_2 mass flow rate from the condenser. For the same reason, the reflux ratio must be high. This is a consequence of the poor description of the column internal fluxes. On the other hand, when a proper number of segments is used, the internal fluxes are described correctly, the CO_2 on the top of the column is higher and then the value of the reboiler duty and the mass reflux ratio are significantly reduced. In particular, for what concerns the reboiler duty, Table 5.16 shows how varying the number of segments it is possible to reduce significantly the error in the estimation of this fundamental variable.

	Experimental	**Number of segments**			
		10	20	80	90
Reboiler duty [MJ/h]	738	895.78	807.04	744.29	742.03
Error [%]	-	21.4	9.4	0.9	0.6

Table 5.16: Run 47 - Variation of the error in the evaluation of the reboiler duty with the number of segments

This result has fundamental implications in the design of the stripper since, once the process targets are fixed, the estimation of the reboiler duty represents a crucial point to quantify the energy requirement. Furthermore, the vapor flow produced in the reboiler influences the column and equipment dimensions.

5.7 Chapter 5 Summary

The modeling of the stripping section was the object of this chapter. Two different pilot-plant facilities were chosen to validate the model developed in Chapter 3 and successfully applied for the absorber in Chapter 4. In the first part the Peclet number evaluation was done for all the cases studied, finding out that even in the case of the stripper the column behavior resembles an ideal plug-flow. Then, the number of segments analysis was applied to two runs of the first plant, i.e., the stripping section of the SINTEF CO_2 capture plant in Norway. For this facility, the chosen set of degrees of freedom for the system solution was represented by the condenser temperature and the reboiler duty, in order to investigate the effect of the number of segments on the column profiles and the output streams features. The results obtained highlight the necessity of a high number of segments in order to obtain a correct description of the internal fluxes, which have an important effect on the correct estimation of the extent of the stripping reaction all along the column, and consequently on the output streams features.
Then, the second plant, i.e., the stripping section of the University of Texas at Austin pilot-plant was examined. In this case, the condenser temperature and the CO_2 gas mass flow rate from the condenser were fixed to saturate the degrees of freedom, with the main purpose of analyzing the effect of the number of segments in the estimation of the reboiler duty. With the chosen set of degrees of freedom the output conditions were fixed and, consequently, not influenced by the discretization of the axial domain. From the results obtained it was found that the influence of the number of segments is significant for what concerns both the internal behavior of the column and the

estimation of the reboiler duty. In particular, only with an appropriate discretization of the axial domain the internal fluxes are computed correctly and consequently the CO_2 vapor composition, obtaining a correct evaluation of the energy consumption. This was demonstrated by the fact the moving from a 10 segments model to a 90 segments model the error in the estimation was reduced from 21.4% to 0.6%. This result has fundamental implications at a design level, since the energy consumption represents the main issue in the process development at an industrial level.
The next two and conclusive chapters are dedicated to the analysis of the design of an industrial CO_2 post-combustion capture plant by means of reactive absorption-stripping and using MEA as solvent.

Part III

Industrial-scale plant analysis and design

Chapter 6

Absorption section design analysis

In this first chapter regarding the design of an industrial post-combustion CO_2 capture system using MEA as solvent, the design of the absorption section is taken into account using the model developed in the previous chapters. The absorber design is performed for three values of the lean solvent loading entering the column, in order to analyze the effect of this important parameter. Moreover, the influence of the molar L/V ratio, which affects the amount of solvent to be used in the process, is highlighted by means of the analysis of the liquid temperature profiles.

6.1 Introduction to the design of an industrial CO_2 post-combustion capture plant using MEA

The model developed in Chapter 3 was validated for what concerns the absorber and the stripper in Chapter 4 and Chapter 5, respectively. At this point, this model will be used in this chapter and in the next one with the purpose of analyzing the design of an industrial-scale plant. In general, most of the works concerning the modeling of the CO_2 reactive absorption-stripping process using MEA as solvent have been concentrated on the validation of the model using experimental and pilot-plant facilities data [16, 36–38, 49, 56, 83]. For what concerns the industrial plants, very few experimental data sets are available, mostly reporting values in the extremes of the columns only [116], leading to the impossibility to test models on this scale.

However, industrial plants have been taken into account in different works. For instance, Singh et al. [117] made an economical comparison between a post-combustion capture with MEA system and an O_2/CO_2 recycle combustion. Alie et al. [14] and Abu-Zahra [17] studied the effect of different operating parameters on the process through a number of sensitivity analysis. Cau et al. [12] compared two different power generation systems integrated with a CO_2 post-combustion capture plant. Lawal et al. [118] and Nittaya et al. [84] performed the design of a CO_2 post-combustion capture plant by means of a dynamic model.

The results obtained in the different works were not in agreement in most cases, due to the different amount of flue gases treated and the different operating conditions considered. For instance, the optimal lean solvent loading ranged between 0.25 [14] and 0.32 [17]. The same was observed for the specific reboiler duty, which ranged from 1.7 GJ/t_{CO_2} [117] to 4.1 GJ/t_{CO_2} [84]. Furthermore, except for Abu-Zahra et al. [17], where a sensitivity analysis varying all the most important operating parameters was made, the majority of the works were focused on the effect of few operating parameters only. For example, Lawal et al. [118] and Nittaya et al. [84] investigated the effect of the absorber packing height on the energy consumption, while Cau et al. [12] reported the variation of the CO_2 removal with the L/V ratio and the reboiler duty. Moreover, all of these analysis were made using different mathematical models, from the equilibrium stage model [12, 14, 17] to the rate-based model [84, 118], and the choice of a rigorous model over a simpler one can lead to significant differences in the results.

In general, the approach for the design of the absorption-stripping processes is based on a number of sensitivity analysis, where the columns dimensions and the operating parameters are varied over a certain range of values in

order to obtain the desired final performance. In this analysis the column profiles are usually neglected. This fact could lead to columns that do not work correctly, although the results at the extremes, i.e., product purity, reboiler duty, removal percentage, etc., are those required. Both the output values and the profiles should be considered as equally important in the process study. In this way, it is possible to avoid design results that could be misleading due to the fact that only the final performance are checked.
A design approach based on the contemporary focus on the internal column profiles and the final performance was adopted in this thesis. In particular, the design of both the absorber and the stripper was studied for different loadings in the solvent entering the absorber. Starting from the lean solvent loading, the effect of various important process parameters was analyzed. For what concerns the absorber, the effect of the L/V ratio was taken into account, determining the limits where it was possible to have a column that was consistent both from the output streams and the internal behavior standpoints [119]. When the stripper was considered, an alternative column configuration without reflux from the condenser was used to avoid an unnecessary energy consumption. Moreover, a criterion for the determination of the minimum packing height for the stripper was proposed through the liquid temperature profiles analysis. Finally, the influence of the stripper feed temperature was examined, identifying this parameter as the most important one for what concerns the reduction of the energy consumption in the whole process [119].

6.2 Process description

The absorption-solvent regeneration process reported in Figure 6.1 was considered in this work. The plant is divided into two interconnected sections, i.e., the absorption, where the CO_2 is transferred from the gaseous to the liquid phase and the stripping, where the mass separation agent is recovered. In the absorption section, the CO_2-rich flue gas is sent to the bottom of the absorber, where it flows countercurrent with the lean liquid solvent. The exhaust gas exits the top of the column and is sent to the stack.
The CO_2-rich solvent from the bottom of the absorber is pumped to a cross heat-exchanger, where its temperature is increased, and then to the top of the stripper. The liquid flows countercurrent with the vapor flow generated by the reboiler. In this case, the CO_2 is transferred from the liquid phase to the vapor phase. From the top of the stripper, a gaseous stream composed mainly by CO_2 and water is sent to a partial condenser where the CO_2 is concentrated in the gas phase. The gas is then sent to compression and subse-

quent storage or re-utilization. The lean solvent exiting the stripper bottom is partly vaporized in the reboiler and then sent to the heat-exchanger where it supplies its sensible heat to the stripper feed. The solvent is mixed with the water recovered from the condenser, and then further cooled and recycled to the top of the absorber. This configuration differs from the classic absorption-solvent regeneration process [68, 69], since the water recovered is not sent back to the top of the stripper as reflux. As it is going to be explained in detail in Chapter 7, this choice was made for energy saving reasons.

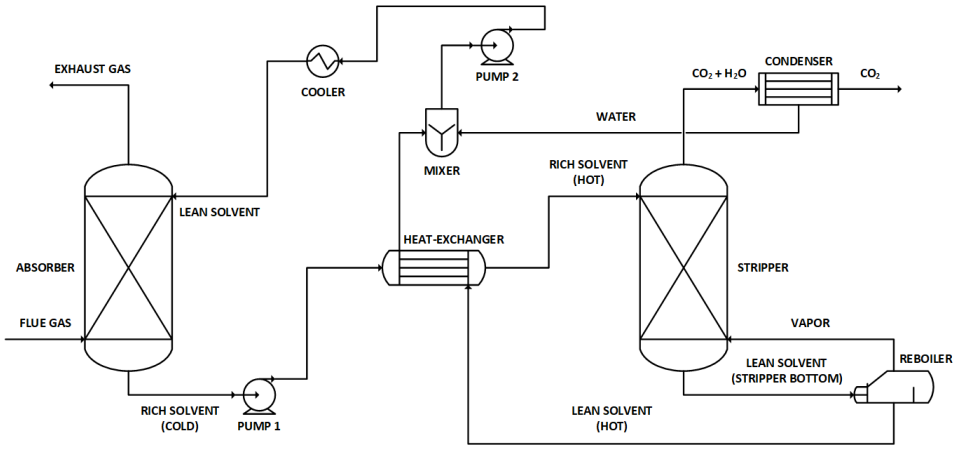

Figure 6.1: Industrial CO_2 post-combustion capture by absorption/stripping plant flowsheet

Both the absorber and the stripper were packed columns, chosen over the plate ones because the packing provides a higher contact area and less pressure drop. In this work Mellapak Plus 252Y was considered as packing.
Monoethanolamine was used as solvent, as it is the most studied and proven to be the most mature one for this process [5, 37, 120, 121]. However, this analysis of the design was independent of the solvent used.
The absorber (this chapter) and the stripper (Chapter 7) were considered separately following the flowsheet decomposition approach proposed by Alie et al. [14]. This method consists in considering each column independently, and then using the results as initial guesses for the coupled system analysis. Typically, although no general rule is present in the literature, packed absorption and stripping columns present packing height/diameter ratio values larger that 1 [84]. For this reason, in this thesis it was decided to impose that both absorber and stripper must have a packing height/diameter ratio higher or equal to 1.

6.3 Feed streams characterization

The purpose of the absorption section is to remove the CO_2 from the flues gas entering the capture plant. It was assumed that other pollutants (H_2S, SO_2, NO_x, etc.) had been previously removed. Typically, before being sent to the stack, the exhaust gas from the top of the absorber goes to a water-wash section, where part of the vaporized solvent is recovered. This section was not considered in this work since it did not influence the scope of the analysis.
The flue gas composition, temperature and pressure reported in the work of Lawal et al. [118] for a coal-fired sub-critical power plant were considered as reference. Differently from Lawal et al., where the flue gas rate was representative of a 500 MWe power plant, in this case it was decided to deal with a 250 MWe power plant, as this is the reference target defined by the European Community for demo-scale CO_2 capture plant [122]. The complete flue gas characterization is reported in Table 6.1.

Variable	**Value**
Mass flow rate [kg/s]	300
Molar flow rate [kmol/s]	10.1413
Temperature [K]	313.15
Pressure [bar]	1
Mass composition	
CO_2 [mass frac]	0.21
H_2O [mass frac]	0.042
N_2 [mass frac]	0.748
Molar composition	
CO_2 [mass frac]	0.1411
H_2O [mass frac]	0.069
N_2 [mass frac]	0.7899

Table 6.1: Flue gas characterization

A CO_2 removal efficiency of 90% was fixed, in agreement with different works [12, 17, 117, 118, 122, 123]. In order to achieve this target, a 30%wt MEA aqueous solution was used [12,17,118,122,123]. Furthermore, the temperature of the solvent was fixed at 30°C, according to the optimum value found by Abu-Zahra et al. [17].
The objective of the absorber design was to determine the amount of solvent and the absorber dimensions, i.e., packing height and diameter. The calculations were done for three different values of the loading in the lean solvent (0.3, 0.25, 0.2), in order to investigate the effect of this parameter

on the whole process. The loading was defined, according to Eq. 6.1, as the ratio between CO_2 and MEA apparent molar fractions:

$$Loading = \frac{x^{app}_{CO_2}}{x^{app}_{MEA}} = \frac{x_{CO_2} + x_{HCO_3^-} + x_{CO_3^{2-}} + x_{MEACOO^-}}{x_{MEA} + x_{MEA^+} + x_{MEACOO^-}} \tag{6.1}$$

The chosen values were in the range generally reported in the literature, as resumed in Table 6.2.

Reference	**Loading [mol CO_2/mol MEA]**
3	0.32
4	0.28
16	0.29
17	0.3
61	0.271

Table 6.2: Different lean solvent loading values in the literature

Once the loading and the MEA concentration were defined, the determination of the solvent composition was straightforward.

6.4 Absorber analysis and design implications

After the definition of the entering streams, a two-step procedure was adopted for the absorber design:

1. evaluation of the number of absorption units required and the minimum solvent flow rate with an infinite packing height;
2. evaluation of the effective packing height with different solvent flow rate.

The two steps are described in detail in Section 6.4.1 and Section 6.4.3.

6.4.1 Evaluation of the minimum number of absorbers and the minimum solvent flow rate

In this section, the minimum solvent solvent flow rate was determined. In this case the packing height was fixed at 100 m. This was done following an approach similar to that used for the plate columns, where a high (theoretically infinite) number of stages is set to determine the minimum reflux

ratio.
In the capture plant, the absorption section is characterized by the highest column diameters, due to the large amount of gas involved in the process. Different works in the literature reported that the diameter should not be higher than 12 m [84, 117, 118]. For this reason, the minimum number of units was determined in this section, since it is intrinsically related to the column diameter.
When the design of a packed column is considered using the *RadFrac*^{TM} model, the *Packing Rating - Design Mode* option must be activated to determine the column diameter. In this case two parameters must be specified:

- base flood: it corresponds to the maximum percentage of flooding velocity allowed for the evaluation of the column diameter. In this work, both for the absorber and the stripper, a gas velocity of 70% of the flooding velocity was fixed;

- base stage: the evaluation of the column diameter is performed with reference to a specific point in the column. Usually, this point corresponds to the part of the column which is more stressed, i.e., the point where the gas/vapor flow rate reaches its maximum value. As the absorption process is characterized by exothermic reactions that cause water vaporization, the maximum vapor flow will most likely not be neither at the top or the bottom of the absorber, but at some point within the column, where the most of the reactions happens. To determine this specific point in the column, the *Packing Sizing* tool, included in the *RadFrac*^{TM} model, was used.

Regarding the simulations, a model with 160 segments was used for the 100 m column, based on the norm of the difference between the interphase CO_2 molar flow vector evaluated at 150 and 160 segments, which was in the order of 10^{-3}. This choice was made because a further increase in the number of segments would have led to an excessive computational cost, which was unnecessary for the scope of the analysis. This criterion was used for all the subsequent simulations to determine the number of segments for the system solution.
For what concerns the minimum number of absorption units, it was found that one absorber led to diameters close to or higher than the imposed limit of 12 m with the infinite packing height. In particular, diameters of 13.1 m, 12.43 m and 12.01 m for lean solvent loading values of 0.3, 0.25 and 0.2 were computed, respectively. Moreover, considering the effective column, the diameter was certainly going to increase due to the higher solvent flow rate involved. For this reason, it could be concluded that at least two units were needed to respect the constraint on the absorber diameter. Consequently, the

flue gas had to be divided into two equal parts that flow into two identical absorbers. At this point, a mass flow rate of 150 kg/s was considered for each unit. Then, to achieve the target of 90% removal of CO_2, 28.35 kg/s of CO_2 had to be removed from the flue gas in each absorber.
The minimum solvent flow rate was evaluated for the three loading values in the lean solvent. The results are reported in Table 6.3, together with the rich solvent characterization and the column features.

	Lean solvent loading [mol CO_2/mol MEA]		
	0.3	0.25	0.2
Lean solvent			
Mass flow [kg/s]	487.2	390.5	332.7
Temperature [K]	303.15	303.15	303.15
Pressure [bar]	1	1	1
L/V ratio [kmol/kmol]	3.86	3.14	2.71
Apparent composition			
CO_2 [mol frac]	0.0354	0.0292	0.0232
MEA [mol frac]	0.1179	0.1169	0.116
H_2O [mol frac]	0.8467	0.8538	0.8608
Rich solvent			
Mass flow [kg/s]	503.7	390.5	332.7
Temperature [K]	317	315.1	314.3
Pressure [bar]	1	1	1
Apparent composition			
CO_2 [mol frac]	0.0672	0.0691	0.0699
MEA [mol frac]	0.1179	0.1179	0.1176
H_2O [mol frac]	0.8149	0.813	0.8125
Loading [mol CO_2/mol MEA]	0.569	0.586	0.595
Column features			
Height [m]	100	100	100
Diameter [m]	9.28	8.91	8.69
Base stage [m]	6	5	4

Table 6.3: Results for the infinite packing height column analysis

From these results it can be noticed that:

- when the loading in the lean solvent decreases, the minimum solvent flow rate decreases. This happens because a cleaner solvent has a higher capture capacity, and then a smaller amount of solvent is needed;

- the less the solvent, the smaller the L/V ratio. This fact has an important effect in the evaluation of the effective solvent flow rate, as it is going to be discussed in Subsection 6.4.3;

- the smaller the loading in the lean solvent, the higher the loading in the rich solvent. This is explained by the fact that, as the minimum solvent flow rate is smaller in the case of low loading values, the resulting rich solvent has a higher CO_2 concentration.

6.4.2 The role of the temperature bulge in the absorber design

Once the minimum solvent flow rate was determined it was possible to shift from the packing height column to the effective packing height column. The first step of this procedure was the evaluation of the effective solvent flow rate which is, in general, a multiple of the minimum solvent flow rate. As reported in the work of Seader et al. [68], the effective solvent flow rate can be computed as:

$$L_0^{eff} = (1 \div 2)\ L_0^{min} \tag{6.2}$$

In the case of a CO_2-MEA absorber, this computation is not immediate. This is because in this kind of system, as already reported in Chapter 4, the molar L/V ratio plays a fundamental role in the quality of the process. In fact, as extensively discussed in the work of Kvamsdal & Rochelle [39], the L/V ratio influences the position of the typical bulge in the temperature profiles. In particular, three situations are possible:

1. $L/V < L/V_{low}$: the bulge is positioned at the top of the absorber; the minimum driving force is present at the bottom of the column. The bulge does not affect the performance of the process.

2. $L/V_{low} < L/V < L/V_{up}$: the temperature profiles do not present a clear bulge neither at the top or the bottom of the absorber; the shape of the curve shows a soft bulge distributed all along the column. The minimum driving force tends to appear somewhere in the middle of the column. In this case, the temperature bulge affects the performance of the absorber. Furthermore, in this situations the temperature gradient is very small along the column and close to be flat in the middle. This is an indication that the absorber is not working correctly, as a large part of the column is practically isothermal, and then not correctly used.

3. $L/V > L/V_{up}$: the bulge is positioned at the bottom of the column; the minimum driving force is present at the top of the absorber. Like Category 1), the temperature bulge does not affect the performance of the absorber.

The values of the L/V interval limits vary based on the examined case. In the plant investigated by Kvamsdal & Rochelle [39], the values of L/V_{low}

and L/V_{up} were found to be around 5 and 6, respectively.
In the light of what was said above, in the case of the absorber design, it is necessary to avoid values of the effective solvent that lead to an L/V ratio inside Category 2). The temperature profile, being closely related to the L/V ratio, highlights the portion of the column where the temperature gradient is close to zero, giving important indications on the quality of the process and should always be checked together with the outputs.

6.4.3 Evaluation of the effective solvent flow rate and the effective packing height

In the following Sections, the effect of the lean solvent loading in the choice of the effective solvent flow rate and on the column dimensions is analyzed.

6.4.3.1 L/V ratio analysis

Firstly, it was examined the value of the L/V ratio for different multiples of the minimum solvent flow rate. According to the values reported by Kvamsdal & Rochelle [39], it was found that the molar L/V ratio was in Category 2) for three different intervals of multiples of the minimum solvent flow rate for the three values of the lean solvent loading. In particular, 1.3 L_0^{min}<L_0^{eff}<1.5 L_0^{min} was the interval for a lean solvent loading value of 0.3, while 1.6 L_0^{min}<L_0^{eff}<1.9 L_0^{min} and 1.9 L_0^{min}<L_0^{eff}<2.0 L_0^{min} were the intervals for what concerns the values of the lean solvent loading 0.25 and 0.2, respectively. Then, for multiples of the minimum solvent flow rate that led to an L/V ratio in these intervals it was expected to have a mild temperature bulge in the absorber. However, since the values reported by Kvamsdal & Rochelle were evaluated in a different pilot-plant facility, these intervals were purely indicative and a deeper analysis based on the column profiles was needed.

6.4.3.2 Absorber liquid temperature profiles

The value of the L/V ratio affects the temperature profiles and limits the choice of the effective solvent flow rate. In this thesis, this effect was investigated with reference to the liquid temperature profiles. To corroborate the correctness of the L/V ratio analysis, the liquid temperature profiles are reported in Figure 6.2. Since for each multiple of the minimum solvent flow rate the effective packing height was different, the relative distance from the bottom of the column was used for the x-axis. For all the subsequent absorber simulations, 100 discretization segments were found to be sufficient

to have a correct model solution.

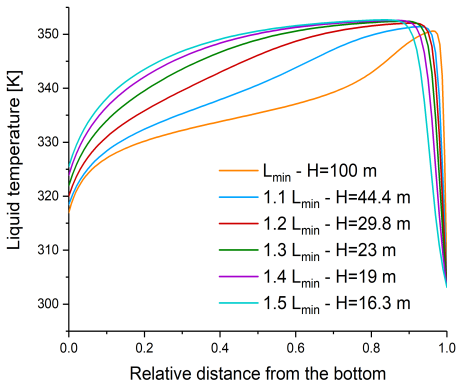

(a) Lean solvent loading = 0.3

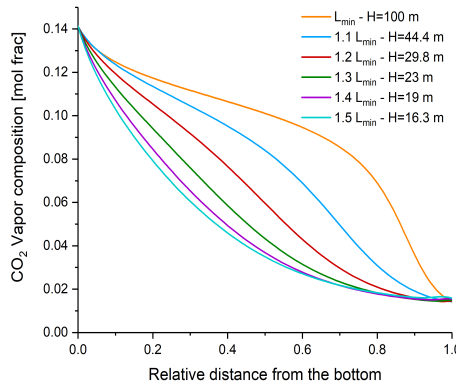

(d) Lean solvent loading = 0.3

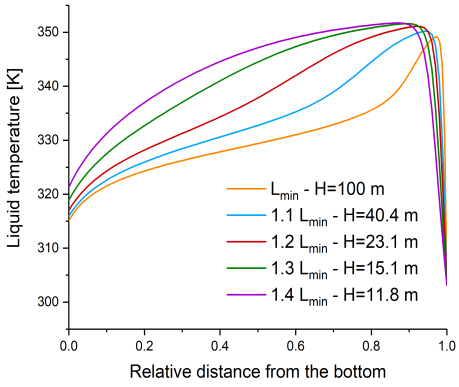

(b) Lean solvent loading = 0.25

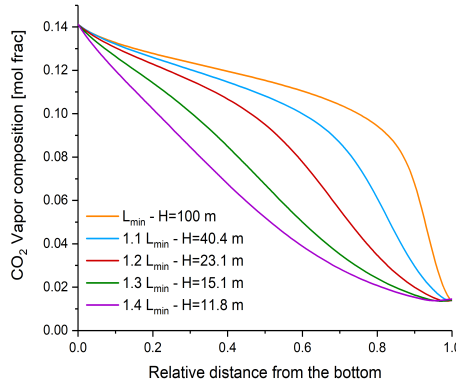

(e) Lean solvent loading = 0.25

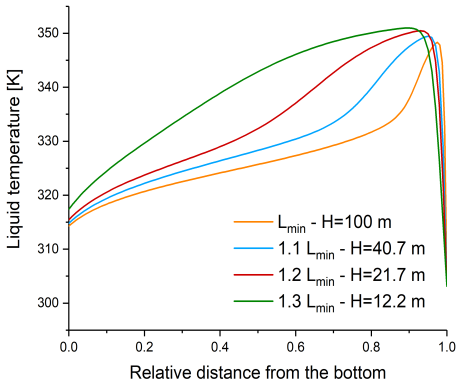

(c) Lean solvent loading = 0.2

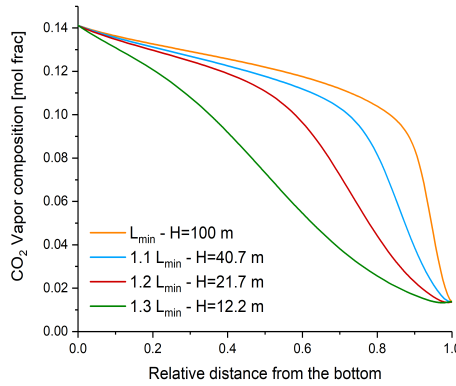

(f) Lean solvent loading = 0.2

Figure 6.2: Variation of the liquid temperature (a-c) and CO_2 vapor composition (d-f) profile for different lean solvent loading values and multiples of the minimum solvent flowrate

As it is shown in Figure 6.2(a), the temperature profile tends to become flatter with the increase of L_0^{eff}, i.e., with the increase of the L/V ratio. In other words, the bulge becomes less evident with the increase of the solvent flow rate. It can be noticed from Figure 6.2(a), correspondent to a lean solvent loading value of 0.3, that moving from L_0^{eff}=1.2 L_0^{min} to L_0^{eff}=1.3 L_0^{min} there is the transition from Category 1) to Category 2). This is highlighted by the fact that an isothermal zone appears between a relative distance from the absorber bottom of 0.7 and 0.9 when L_0^{eff}=1.3 L_0^{min}. For higher multiples of the minimum solvent flow rate this situation is even more evident, since a larger isothermal zone appears. This result is furtherly corroborated by the analysis of the corresponding CO_2 vapor composition profiles, reported in Figure 6.2(d), where it can be observed that the increase of the effective solvent flow rate leads to have a portion of the column where the concentration gradient is close to zero. This fact indicates that in this case the absorber is not working correctly, as in the isothermal part of the column the CO_2 interphase transfer is almost not happening. With respect to the other two lean solvent loading cases, a clear temperature bulge is always present at the top of the column and, consequently, the minimum driving force is always found in the column bottom. For this reason, all the profiles could be considered to appropriately represent the process.

6.4.3.3 Rich solvent and absorber dimensions

For each multiple of the minimum solvent flow rate reported in Figure 6.2 the rich solvent features and the absorber dimensions, i.e., packing height and diameter, were evaluated. It must be noticed that for the case of lean solvent loading fixed to 0.2 it was possible to investigate only up to a multiple of the minimum solvent flow rate of 1.3. This was because for higher values of the effective solvent flow rate, using two absorption units, the columns would have had packing H/D ratio values smaller than 1. For the same reason, it was not possible to investigate over a multiple of the minimum solvent flow rate of 1.4 when the lean solvent loading was fixed to 0.25. In order to study the behavior of the system for higher multiples of the minimum solvent flow rate, a higher number of units would be needed, since in that case there would be a lower volume of gas to be treated per absorption unit and, consequently, smaller diameters.
Table 6.4 summarizes the column features, while the results for the rich solvent characterization are reported in Table 6.5.

	Lean solvent loading mol CO_2/mol MEA		
	0.3	0.25	0.2
$\boldsymbol{L_0^{eff} = 1.1\ L_0^{min}}$			
Packing height [m]	44.4	40.4	40.7
Diameter [m]	9.47	9.09	8.88
Reference segment	7	6	4
$\boldsymbol{L_0^{eff} = 1.2\ L_0^{min}}$			
Packing height [m]	29.8	23.1	21.6
Diameter [m]	9.67	9.3	9.07
Reference segment	9	7	7
$\boldsymbol{L_0^{eff} = 1.3\ L_0^{min}}$			
Packing height [m]	23	15.1	12.2
Diameter [m]	9.83	9.46	9.21
Reference segment	11	10	10

Table 6.4: Column features for the three values of the lean solvent loading and different values of the effective of the solvent flow rate

	Lean solvent loading mol CO_2/mol MEA		
	0.3	0.25	0.2
$\boldsymbol{L_0^{eff} = 1.1\ L_0^{min}}$			
Mass flow [kg/s]	553.8	444.2	379.2
Temperature [K]	318	315.9	314.8
Pressure [bar]	1	1	1
Apparent composition			
CO_2 [mol frac]	0.0641	0.0653	0.0656
MEA [mol frac]	0.1175	0.1176	0.1173
H_2O [mol frac]	0.8241	0.8171	0.8171
Loading [mol CO_2/mol MEA]	0.545	0.556	0.559
$\boldsymbol{L_0^{eff} = 1.2\ L_0^{min}}$			
Mass flow [kg/s]	604.1	484	412.7
Temperature [K]	320	317	315.4
Pressure [bar]	1	1	1
Apparent composition			
CO_2 [mol frac]	0.0614	0.062	0.0619
MEA [mol frac]	0.1171	0.1172	0.1171
H_2O [mol frac]	0.8214	0.8206	0.8171
Loading [mol CO_2/mol MEA]	0.525	0.53	0.529
$\boldsymbol{L_0^{eff} = 1.3\ L_0^{min}}$			
Mass flow [kg/s]	654.89	525.03	447.22
Temperature [K]	321.97	318.87	317.38
Pressure [bar]	1	1	1
Apparent composition			
CO_2 [mol frac]	0.0592	0.0593	0.0587
MEA [mol frac]	0.1166	0.1168	0.1165
H_2O [mol frac]	0.8242	0.8239	0.8248
Loading [mol CO_2/mol MEA]	0.507	0.509	0.504

Table 6.5: Rich solvent characterization for the three values of the lean solvent loading and different values of the effective solvent flow rate

From the analysis of Table 6.5 it is possible to notice that, for the same multiple of the minimum solvent flow rate, there is always a decrease in the rich solvent flow rate when the lean solvent loading decreases. At the same time, the loading in the rich solvent remains practically constant with the variation of the lean solvent loading. Then, it can be concluded that the quality of the solvent exiting the absorber is not influenced by the quality of the entering one and only the amount of solvent involved changes, once the absorption target is fixed.
It is evident that working with lower lean solvent loading leads to benefits either for the absorber dimensions (Table 6.4) and the amount of solvent involved in the subsequent stripping process (Table 6.5).

In the next chapter regarding the stripper, the three simulations corresponding to $L_0^{eff} = 1.2\ L_0^{min}$ were considered for the design, pointing out that this value was chosen as an example in this work. In order to choose the best case among the previous absorber simulations, an optimization problem should have been solved to find the optimal values packing height and the effective solvent flow rate to operate the absorber, but this was not the scope of the analysis and then it was not considered in this work.

6.5 Chapter 6 Summary

In this chapter the design of the absorption section of an industrial CO_2 capture system using MEA as solvent was performed by means of a two-step procedure. In the first step, the evaluation of the minimum number of absorption units and the minimum solvent flow rate were done using an infinite packing height column. In particular, it was found that at least two absorbers were needed in order to respect the constraint on the maximum value of the column diameter. Then, the effective solvent flow rate and effective packing height were computed starting from the results of the first step. The design was made for three values of the lean solvent loading entering the absorber, in order to investigate the effect of this fundamental parameter. Moreover, the role of the L/V ratio, which affects the internal behavior of the column and is strongly related to the typical temperature bulge in the absorber, was studied by means of the liquid temperature profiles. The results highlighted that the L/V ratio limits the choice of the effective solvent flow rate and it must be chosen in order to avoid isothermal zones in the absorber. In this way, it is possible to ensure the correct operativity of the column, contemporarily respecting the performance required. Finally, it was obtained that a low lean solvent loading leads to the best results both in terms of column dimensions and amount of circulating solvent involved in the process.
The next chapter deals with the design of the stripping section.

Chapter 7

Stripping section design analysis

In this second chapter regarding the design of an industrial post-combustion CO_2 capture system using MEA as solvent, the stripping section is considered. After the introduction of an alternative configuration without the reflux, the most important operating process parameters are described in detail. Then, the effect of the packing height on the reboiler duty and the column diameter is analyzed and a criterion for the definition of the minimum packing height is proposed. Then, the effect of the rich solvent temperature, which strongly influences the energy consumption, is studied and the conditions leading to the minimum reboiler duty are presented.

7.1 Stripper configuration

The role of the stripping section is the regeneration of the CO_2-rich solvent which arrives from the absorber. The separating agent in this case is the vapor flow rate produced in the reboiler, since the reactions in the stripping process are endothermic. Furthermore, in the case of the CO_2-MEA system, as carbon dioxide is a gas, its mass transfer from the liquid to the vapor phase is no-heat consuming and, consequently, the duty is needed to reverse the absorption chemical reactions only. In general, the process must be operated at the highest possible temperature once the feed conditions are fixed. In order to achieve this objective, the configuration of the stripper was analyzed before the design. Different works dealing with the design problem report the possibility to send part of the water recovered in the condenser back to the column top as reflux [14,17,68,69,84,117,122,124]. Since the reflux would enter the column at a considerably lower temperature compared to the stripper feed, this configuration would lead to a decrease in the column top temperature and, consequently, to the need for a higher duty from the reboiler to heat the cold reflux. For this reason, as already reported in Section 6.2, in this thesis it was proposed to mix the cold water recovered in the condenser with the lean solvent exiting from the heat-exchanger (Figure 7.1), as it was previously done in the work of Oexmann & Kather [40].

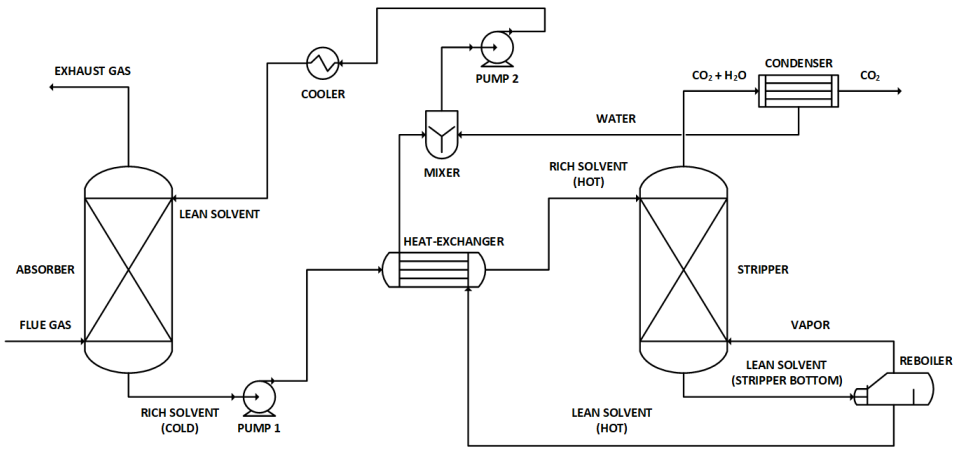

Figure 7.1: Industrial CO_2 post-combustion capture by absorption/stripping plant flowsheet

7.2 Operating parameters in the stripper

After the choice of the stripper configuration, before the design it was necessary to define several operating parameters that affect the performance of the process. These parameters are discussed separately in the next Subsections.

7.2.1 Stripper pressure

In general, the stripper operates at a pressure higher than the atmospheric one. As reported by Freguia [52], the heat of absorption of CO_2 in MEA is almost two times the heat of vaporization of the water. Then, according to the Clausius-Clapeyron equation, the CO_2 vapor pressure increases more rapidly compared to the H_2O vapor pressure. For this reason, the stripper must work at higher pressures compared to the absorber, in order to reach higher temperatures and favor the transfer of CO_2 over water. However, there is a limit on the pressure value which is imposed by the degradation temperature of MEA that, according to Alie et al. [14], is 121°C. Then, the column pressure must be set at the highest value that guarantees a boiling temperature of the solvent lower than the solvent degradation temperature. For a 30%wt MEA aqueous solution, this pressure corresponds to 1.8 bar, which was fixed in the stripper.

7.2.2 Condenser temperature

From the top of the stripper a gaseous mixture containing mainly CO_2 and water exits. This stream is sent to the condenser, of which the aim is to concentrate the CO_2 in the gas phase while water is recovered in the liquid phase. Remembering that the stripping reactions are endothermic, no reflux was sent back to the stripper top, as this would have penalized the process performance. Assuming the availability of cooling water at 25°C, the condenser temperature was set to 40°C. With this specification, a concentration of CO_2 in the gas of 96%mol was ensured before the compressor.

7.2.3 Rich solvent temperature

In order to favor the stripping process and to reduce the duty required at the reboiler, the temperature of the rich solvent entering the column must be the highest possible. However, the value of this temperature is limited by two factors: the first is represented by the solvent degradation temperature, while the latter, which is more tightening, is dictated by the minimum temperature approach in the heat-exchanger. In particular, the maximum temperature allowed is the highest one that ensures the respect of the minimum temperature driving force, fixed to 10°C in this thesis. The effect of the solvent temperature is analyzed in detail in Section 7.3.3.

7.2.4 Stripper performance

The stripper should be designed to remove the amount of CO_2 captured in the absorber. Removing a higher quantity would lead to higher energy consumptions, while removing a lower amount would lead to a dirtier solvent and, consequently, a higher lean solvent flow rate in the absorber to ensure the 90% CO_2 removal.

7.3 Stripper analysis and design implications

7.3.1 Rich solvent characterization

As already mentioned in Chapter 6, the three simulations corresponding to $L_0^{eff} = 1.2\ L_0^{min}$ were considered for the design of the stripper. Table 7.1 reports the characterization of the rich solvent for the three cases before the pump.

	Lean solvent loading mol CO_2/mol MEA		
	0.3	0.25	0.2
$\boldsymbol{L_0^{eff} = 1.2\ L_0^{min}}$			
Mass flow [kg/s]	604.1	484	412.7
Temperature [K]	320	317	315.4
Pressure [bar]	1	1	1
Apparent composition			
CO_2 [mol frac]	0.0614	0.062	0.0619
MEA [mol frac]	0.1171	0.1172	0.1171
H_2O [mol frac]	0.8214	0.8206	0.8171
Loading [mol CO_2/mol MEA]	0.525	0.53	0.529

Table 7.1: Rich solvent characterization for the three values of the lean solvent loading corresponding to $L_0^{eff} = 1.2\ L_0^{min}$

Before entering the stripping column, the pressure of the rich solvent was increased to 1.8 bar in the pump (PUMP 1 in Figure 7.1), while for what concerns the temperature, it was decided to fix it initially to the boiling point, since it is typical for the stripper to send the feed as a saturated liquid [68, 69].

7.3.2 Effect of the packing height

The stripper was simulated varying the packing height in order to investigate the effect of this parameter on the process. Since for the three cases different packing heights were involved, a model with 70 segments was used when the lean solvent loading is set to 0.3, while 90 and 120 segments models were used for the cases of lean solvent loading equal to 0.25 and 0.2, respectively. Figures 7.2(a)-7.2(c) report the liquid temperature profiles for different values of the packing heights for the three lean loading values, while Figures 7.2(d)-7.2(f) report the corresponding liquid temperature gradient profiles. Similarly to the case of the absorber, due to the different packing

heights considered, the relative distance from the bottom is reported in the x-axis.

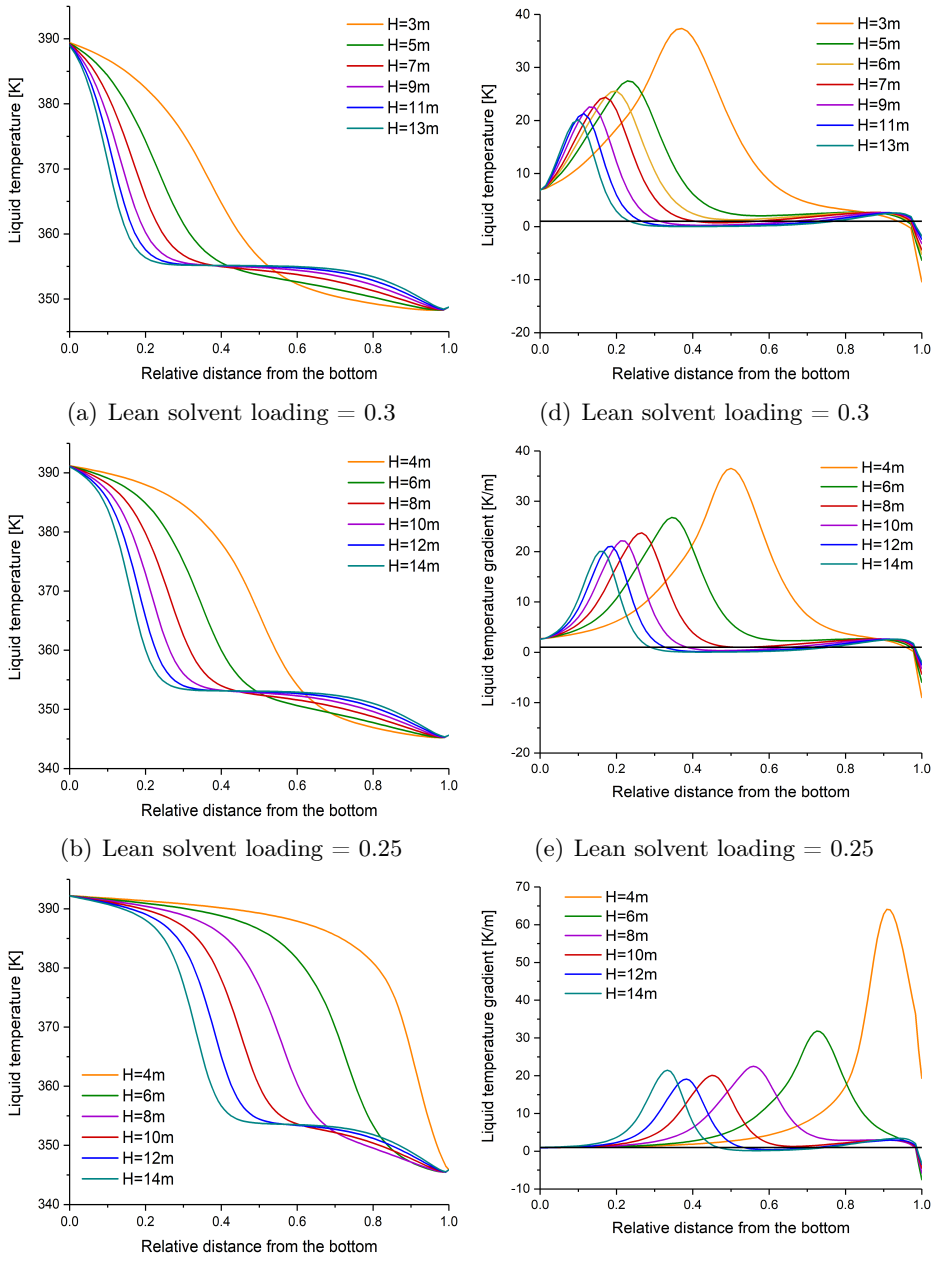

(a) Lean solvent loading = 0.3

(d) Lean solvent loading = 0.3

(b) Lean solvent loading = 0.25

(e) Lean solvent loading = 0.25

(c) Lean solvent loading = 0.2

(f) Lean solvent loading = 0.2

Figure 7.2: Variation of the liquid temperature profile for different lean solvent loading and packing height values

Table 7.2 reports the variation of the reboiler duty and column diameter for the three lean solvent loading cases and for different values of the packing height.

Packing height [m]	**Reboiler duty [MW]**			**Column diameter [m]**		
	Lean solvent loading mol CO_2/mol MEA			**Lean solvent loading mol CO_2/mol MEA**		
	0.3	0.25	0.2	0.3	0.25	0.2
3	145.7	135.7	148.3	6.93	6.59	6.64
4	145.7	135.4	133.5	6.92	6.59	6.43
5	145.7	135.4	127.7	6.91	6.58	6.34
6	145.8	135.4	126.7	6.91	6.58	6.33
7	145.8	135.4	126.7	6.9	6.58	6.32
8	145.8	135.4	126.7	6.89	6.58	6.32
9	145.8	135.4	126.7	6.89	6.57	6.32
10	145.8	135.5	126.7	6.88	6.57	6.32
11	145.8	135.5	126.7	6.88	6.57	6.32
12	145.8	135.5	126.7	6.87	6.57	6.32
13	145.8	135.5	126.7	6.87	6.57	6.32
14	145.8	135.5	126.7	6.86	6.57	6.32

Table 7.2: Variation of the reboiler duty and column diameter for the three values of the lean solvent loading and the packing height

From these results different conclusions can be made:

- the packing height has a low influence on both the reboiler duty and the column diameter values. Then, for the design of the stripper, it was not possible to make reference to the effective stripping agent for the evaluation of the packing height, like it was done in Chapter 6 for the absorber using the effective solvent flow rate. The only case where the packing height seems to have an effect on the reboiler duty and the diameter is the one related to the lean solvent loading fixed to 0.2. The initial variation of both the parameters can be explained by the fact that, when the packing height is low, the minimum required contact surface is not reached yet. For this reason, a higher duty is needed to guarantee the target removal. Once the minimum contact surface is achieved (in this case with 5 m of packing), then the reboiler duty and the column diameter remain practically constant with the variation of the packing height.

- from the analysis of the liquid temperature gradients in Figures 7.2(d)-7.2(f) it is possible to notice that from a certain value of the packing height an extended zone where the temperature gradient is less than 1 K/m appears. This means that in that portion the stripper can be considered isothermal. Then, it was decided to choose the maximum packing height at which the temperature gradient is always higher than 1 K/m [119]. This criterion, in analogy with the absorber cases previously analyzed in Chapter 6, leads to columns where the whole packing height is used, avoiding isothermal zones. In the specific case, values of the packing height of 7 m, 8 m and 10 m were found for lean solvent loading values of 0.3, 0.25 and 0.2, respectively. It must be highlighted that in the case of lean solvent loading equal to 0.3, the packing height selected according to this criterion should have been 6 m, but this would have been in contrast with the imposed constraint on the packing height/diameter ratio which must be at least 1 or higher, as reported in Chapter 6. The differences in the packing height values are due to the fact that the driving force between the two phases decreases with the loading decrease. Then, to ensure the same CO_2 removal, a higher exchange area is needed;
- for what concerns the reboiler duty, a decrease of the energy consumption is observed with the decrease of the lean solvent loading, although the amount of CO_2 to be removed is the same. This fact is a consequence of the different forms (free-CO_2, CO_3^{--}, HCO_3^-, $MEACOO^-$) in which carbon dioxide can be found in the solution for the different lean solvent loading cases.

7.3.3 Effect of the rich solvent temperature

As already mentioned in Subsection 7.2.3, the temperature of the rich solvent entering the stripper has a fundamental role in the process. As a matter of fact, when the stripper feed is sent to a high temperature the stripping process is favored for two main reasons:

- in the equilibrium reaction involving the CO_2:

$$CO_2 + 2H_2O \rightleftarrows H_3O^+ + HCO_3^- \tag{7.1}$$

  the formation of free-CO_2 is favored, increasing the amount of free carbon dioxide in the liquid phase. Moreover the material transfer from the liquid to the gaseous phase starts before the feed enters the stripper. This makes the separation easier and less vapor is needed in the process.

- since the stripping reactions, opposite to the absorption ones, are endothermic, a higher feed temperature increases the temperature in the column and, again, the amount of energy needed in the process is reduced.

Anyway, as reported in Subsection 7.2.3, the maximum temperature of the inlet rich solvent is the highest allowed by the minimum temperature approach in the heat-exchanger.
In the previous Subsection, the inlet feed temperature was set to the boiling point for the determination of the minimum packing height. From the process point of view, as it can be observed from Figures 7.3(a)-7.3(c), where the interphase CO_2 molar flow rate is reported, when the feed is sent at the boiling point, the first part of the column is characterized by the absorption process (it must be remembered that a "positive" interphase flow rate indicates a transfer from the vapor to the liquid phase), due to the low temperature in the top of the column. On the other hand, in the part close to the bottom of the stripper, where the temperature is higher, the desorption process prevails. From this result, it could be concluded that the column was not working correctly. For this reason, and with the purpose of quantify the possible reboiler duty reduction, the stripper was simulated for all the three lean solvent loading cases for two higher different feed temperatures:

- T_1=370.15 K: this temperature was chosen because it was found to be the first at which only the desorption process takes place all along the column;

- T_2=373.15 K: this temperature was found to be the maximum allowed by the minimum temperature approach cross heat-exchanger.

The results for the interphase CO_2 molar flow rate and the liquid temperature profiles are reported in Figures 7.3.

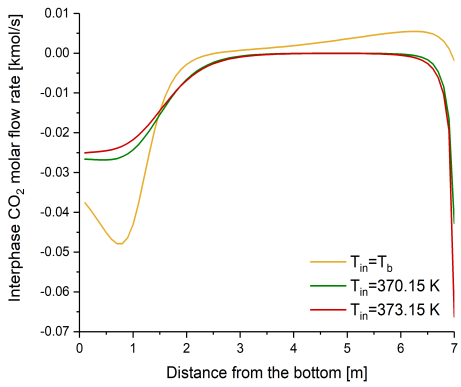

(a) Lean solvent loading = 0.3

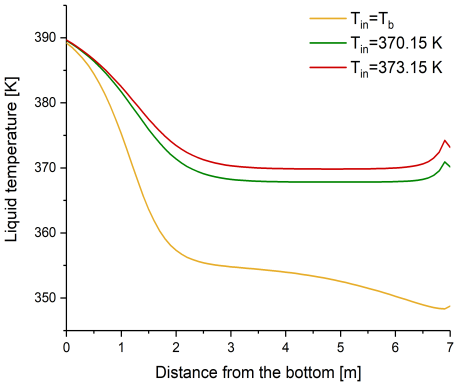

(d) Lean solvent loading = 0.3

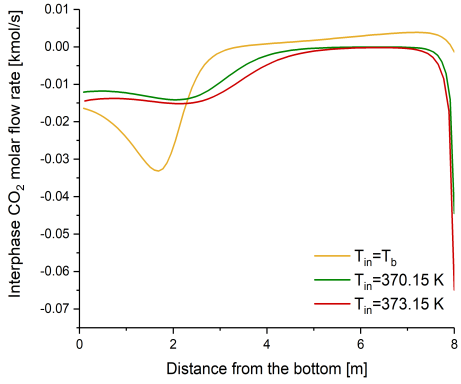

(b) Lean solvent loading = 0.25

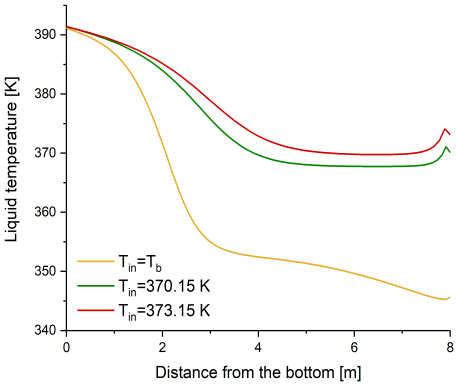

(e) Lean solvent loading = 0.25

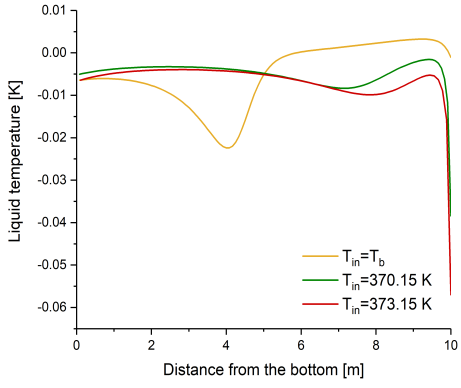

(c) Lean solvent loading = 0.2

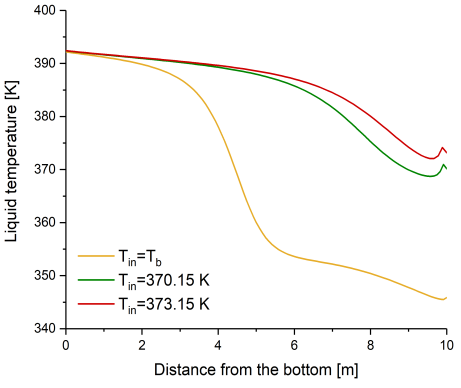

(f) Lean solvent loading = 0.2

Figure 7.3: Variation of the interphase CO_2 molar flow rate profile ((a)-(c)) and the liquid temperature profile ((d)-(f)) for different lean solvent loading and rich solvent temperature values

From the analysis of Figures 7.3(d)-7.3(f) it can be observed that the increase of the rich solvent temperature leads to have a large part of packing isothermal, indicating the possibility to have smaller columns. This is particularly evident when the loading in the lean solvent was fixed to 0.3 (Figure 7.3(d)) and 0.25 (Figure 7.3(e)), where a neat flat zone appears in the middle of the column. On the other hand, when the lean solvent loading was fixed to 0.2, the flat zone is less clear and appears in the bottom of the stripper.
For what concerns the variation of the reboiler duty and the column diameter with the rich solvent temperature, the results are reported in Table 7.3.

Rich solvent T [K]	**Reboiler duty [MW]**			**Column diameter [m]**		
	Lean solvent loading mol CO_2/mol MEA			**Lean solvent loading mol CO_2/mol MEA**		
	0.3	0.25	0.2	0.3	0.25	0.2
Boiling T	145.8	135.4	126.7	6.9	6.57	6.32
370.15	112.4	106.6	105.2	6.38	6.1	5.93
373.15	107	102.5	103.4	6.29	6.02	5.88

Table 7.3: Variation of the reboiler duty and column diameter for the three values of the lean solvent loading and the rich solvent temperature

From the value of the reboiler duty it is evident the positive effect derived from the increase of the rich solvent temperature at the maximum allowed value. Moving from the boiling point temperature to the maximum value allowed by the minimum temperature approach in the heat-exchanger, there is always an effective reduction of the reboiler duty . In particular, the reboiler duty is reduced, compared to the case when the feed was sent at the boiling point, by 27%, 24% and 18% for lean solvent loading values of 0.3, 0.25 and 0.2, respectively. For what concerns the column diameter, a reduction of about 0.5 m is observed for all the cases.
Comparing the different lean solvent loading cases, the results highlight that, once the solvent is sent at the highest allowed temperature, there is not significant change in the value of the reboiler duty. This fact leads to the conclusion that the reboiler duty is practically independent from the lean solvent loading once the best conditions from an energy consumption standpoint are achieved. The further conclusion is that the reboiler duty depends on the target removal only [119].

7.4 Chapter 7 Summary

In this chapter, the analysis and the design of the stripper were considered using the results previously obtained in Chapter 6 for the absorption section. Initially it was proposed an alternative plant configuration without reflux, differently from the classic stripper configuration. This choice was made in order to avoid the unneccesary heat of the cold water coming from the condenser. Then the influence of the stripper packing height was analyzed, founding that this parameter has no influence on the reboiler duty and, consequently, leading to the need of an alternative approach that differs from the typical approach using the minimum stripping agent. This is due to the fact that in the case of the CO_2-MEA stripping system the reboiler duty is needed only to reverse the absorption reaction. The criterion proposed for the choice of the packing height was to make reference to the maximum packing height at which the liquid temperature gradient is always higher than 1 K/m.
After the definition of the packing height, it was studied the effect of the rich solvent temperature on the stripping process. From the results obtained it was found that the rich solvent temperature represents the most crucial parameter for the reduction of the energy consumption. In particular, it was found that the minimum energy consumption is obtained when the stripper feed is sent to the highest possible value, which is defined as the maximum temperature that allows the respect of the minimum temperature approach in the cross heat-exchanger. Moreover, when the stripper is sent at the maximum allowed temperature the lean solvent loading has a low influence on the reboiler duty value. Then, the reboiler duty is dependent on the CO_2 removal target only.

Chapter 8

Conclusions

This thesis dealt with the modeling and the analysis of the CO_2 capture by means of reactive absorption-stripping process using MEA as solvent.
In the first part a rigorous rate-based model, considered the state of art for this kind of process, was developed using the *RadFrac*^{TM} model - Rate-Based mode on Aspen Plus®. Moreover it was introduced a new approach to the process modeling based on the analysis of the system fluid dynamics. In particular, the analysis consists in the evaluation of the dimensionless Peclet number to examine the possible effect of the axial dispersion followed by the definition of a proper number of segments to obtain the correct solution of the resulting system of algebraic equations from a numerical point of view. Once the correct solution is found, it is possible to investigate the possible effect of the backmixing generated by the countercurrent.
The developed model was firstly applied to the absorption section of two pilot-plant facilities with different packing and operating conditions. After the analysis of the system fluid dynamics and the obtainment of the correct numerical solution of the system, the kinetic parameters of the reaction between CO_2 and MEA were calibrated with the purpose of minimizing the standard error between the model results and the experimental data. In particular, a mean reduction of about 0.7 K and $1.1 \cdot 10^{-3}$ mol frac was observed for what concerns the liquid temperature and CO_2 vapor composition, respectively. The obtained model was able to describe correctly each set of experimental data, particularly for what concerns the typical absorber temperature bulge, independently on its position and magnitude.
After the model validation for the absorber, the stripping section was taken into account. Again, two different pilot-plant facilities were considered. In this case two sets of degrees of freedom were defined for the columns in order to test the model with respect to the evaluation of the temperature and composition profiles and the reboiler duty. With regards to the reboiler duty, it

was found that using a correct model of the process it was possible to reduce the error between the experimental value and the model result from 21.4% (10 segments) to 0.6% (90 segments). Even in the case of the stripper, the obtained model was validated for every set of experimental data considered. The developed model was then used with the aim to analyze the design of an industrial-scale plant. Initially the design of the absorber was considered for three different values of the lean solvent loading. A two-step procedure was proposed, which consisted in the evaluation of the minimum number of absorption units and minimum solvent flow rate with an infinite packing height column followed by the evaluation of the effective solvent flow rate and effective column dimensions. Furthermore, the operating conditions for which the absorber did not show any isothermal zones were defined on the basis of the liquid temperature profiles analysis. It was found that working with low lean solvent loading values led to the best results either in terms of amount of circulating solvent and column dimensions.
Finally, the results from the absorber design were used for the design of the stripping section, for which it was highlighted that the reboiler duty is needed to reverse the absorption reactions only. For this reason, an alternative plant configuration without reflux was adopted in order to avoid an unnecessary energy consumption to heat the water coming from the condenser. Futhermore, an alternative approach was proposed for the evaluation of the stripper packing height making reference to the maximum packing height at which the temperature gradient is always higher that 1 K/m. Then, the attention was moved to the rich solvent temperature, which was observed to be the most crucial parameter for what concerns the reduction of the energy consumption. In particular, it was found that the rich solvent must be sent at the maximum temperature, which is the highest allowed to respect the minimum temperature approach in the cross heat-exchanger, to obtain the minimum reboiler duty. In the end, the small changes in the value of the reboiler duty with the variation of the lean solvent loading led to the conclusion that the reboiler duty depends on the target removal only.
The model developed in this thesis is suitable for the extension to a dynamic analysis of the process and the subsequent implementation of a model-based control system.

Nomenclature

This section contains the list of the symbols used in this thesis. For each term, the units and the description are reported.

Roman symbols

Symbol	Units	Description
a	$[-]$	Activity
a_{dry}	$\left[\frac{m^2}{m^3}\right]$	Dry surface area
a_w	$\left[\frac{m^2}{m^3}\right]$	Wet surface area
C	$\left[\frac{kmol}{m^3}\right]$	Molar concentration
c_P	$\left[\frac{kJ}{kmol\ K}\right]$	Specific heat at constant pressure
$\mathfrak{D}$	$\left[\frac{m^2}{s}\right]$	Maxwell-Stefan binary diffusion coefficient
$\mathfrak{D}^o$	$\left[\frac{m^2}{s}\right]$	Maxwell-Stefan binary diffusion coefficient at infinite dilution
$\mathscr{D}$	$\left[\frac{m^2}{s}\right]$	Binary diffusion coefficient
dz	$[m]$	Stage or segment height
d_{eq}	$[m]$	Packing equivalent diameter
E	$\left[\frac{kJ}{m^2\ s}\right]$	Interphase energy flux
$\dot{E}$	$\left[\frac{kJ}{s}\right]$	Interphase energy flow rate
E_a	$\left[\frac{cal}{mol}\right]$	Activation energy
EF	$[-]$	Enhancement factor
F	$\left[\frac{kmol}{s}\right]$	Molar flow rate

Symbol	Units	Description
F_T	$[-]$	Correction factor for total hold-up due to effective wetted area
$\mathfrak{F}$	$[C]$	Faraday constant
FDR	$[-]$	Film discretization ratio
Fr	$[-]$	Freud number
g	$\left[\frac{m}{s^2}\right]$	Diffusive molar flux
H	$[m]$	Packing height
He	$[bar]$	Henry constant
h	$\left[\frac{kJ}{kmol}\right]$	Specific enthalpy
h_T	$\left[\frac{W}{m^2\ K}\right]$	Heat transfer coefficient
J	$\left[\frac{kmol}{m^2\ s}\right]$	Diffusive molar flux
K_{eq}	$[-]$	Equilibrium constant
k	$\left[\frac{m^3}{kmol\ s}\right]$	Kinetic constant
k_M	$\left[\frac{m}{s}\right]$	Material transfer coefficient
k_T	$\left[\frac{W}{m\ K}\right]$	Thermal conductivity
k^0	$\left[\frac{m^3}{kmol\ s}\right]$	Pre-exponential factor
L	$\left[\frac{kmol}{s}\right]$	Liquid molar flow rate
L_c	$[m]$	Characteristic length

Symbol	Units	Description
L_s	$\left[\frac{kg}{m^2\ s}\right]$	Superficial mass velocity of liquid
L_0	$\left[\frac{kmol}{s}\right]$	Solvent flow rate
M	$[kmol]$	Molar hold-up
MSE	$[-]$	Mean squared error
N	$\left[\frac{kmol}{m^2\ s}\right]$	Interphase molar flux
$\dot{N}$	$\left[\frac{kmol}{s}\right]$	Interphase molar flow rate
$\dot{N}^R$	$\left[\frac{kmol}{s}\right]$	Reaction molar flow rate
P	$[bar]$	Pressure
P^{sat}	$[bar]$	Vapor pressure
Pe	$[-]$	Peclet number
q	$\left[\frac{kW}{m^2}\right]$	Conductive flux
$\dot{Q}$	$\left[\frac{kJ}{s}\right]$	Heat flow rate input to a segment
$\dot{Q}^R$	$\left[\frac{kJ}{s}\right]$	Reaction energy flow rate
$\dot{Q}^{vap}$	$\left[\frac{kJ}{s}\right]$	Vaporization/Condensation energy flow rate
R	$\left[\frac{cal}{mol\ K}\right]$	Gas constant
$\underline{\underline{R}}$	$[-]$	Inverse of the material transfer coefficients matrix

Symbol	Units	Description
R_{mass}	$\left[\frac{kg}{kg}\right]$	Mass reflux ratio
RCF	$[-]$	Reaction condition factor
Re	$[-]$	Reynolds number
r	$\left[\frac{kmol}{m^3\ s}\right]$	Reaction rate
S	$\left[m^2\right]$	Column cross-sectional area
SE	$[-]$	Standard error
Sc	$[-]$	Schmidt number
T	$[K]$	Temperature
t	$[s]$	Time
U	$[kJ]$	Energy hold-up
u	$\left[\frac{m}{s}\right]$	Velocity
V	$\left[\frac{kmol}{s}\right]$	Gas/Vapor molar flow rate
V_s	$\left[\frac{kg}{m^2\ s}\right]$	Superficial mass velocity of gas/vapor
We	$[-]$	Weber number
x	$[mol\ frac]$	Liquid component molar fraction
y	$[mol\ frac]$	Gas/Vapor component molar fraction

Symbol	Units	Description
y^*	$[mol\ frac]$	Equilibrium gas/vapor component molar fraction
z	$[m]$	Axial coordinate
$\hat{z}$	$[-]$	Component electric charge number

Greek symbols

Symbol	Units	Description
$\underline{\underline{\Gamma}}$	$[-]$	Matrix of thermodynamic factors
γ	$[-]$	Activity coefficient
ΔG^0	$\left[\frac{cal}{mol}\right]$	Standard Gibbs free-energy change
ΔP	$[Pa]$	Pressure drop
$\Delta\Phi$	$\left[\frac{V}{m}\right]$	Chemical potential gradient
δ	$[m]$	Film thickness
δ^{CC}	$[-]$	Chilton-Colburn averaging parameter
ϵ	$\left[\frac{m^3}{m^3}\right]$	Void fraction
η	$[-]$	Murphree efficiency
θ	$[deg]$	Angle with horizontal for falling film or corrugation channel
μ	$[-]$	Chemical potential

Symbol	Units	Description
$\hat{\mu}$	$\left[\frac{kg}{m\ s}\right]$	Dynamic viscosity
ν	$[-]$	Stoichiometric coefficient
ξ	$[-]$	Film dimensionless coordinate
ρ	$\left[\frac{kg}{m^3}\right]$	Mass density
Φ	$[V]$	Electrical potential
ϕ	$[-]$	Fugacity coefficient
σ^L	$\left[\frac{N}{m}\right]$	Liquid surface tension
σ_C	$\left[\frac{N}{m}\right]$	Critical surface tension of packing material
ψ	$\left[\frac{m^3}{m^3}\right]$	Fractional hold-up

Subscripts

Symbol	Description
$cond$	Condenser
eff	Effective
f	Forward reaction
i	i-th Component
j	j-th Stage or segment
k	k-th Component
M	Material
m	m-th Component
min	Minimum

Symbol	Description
n	n-th Component
mix	Mixture
r	Reverse reaction
T	Thermal

Superscripts

Symbol	Description
app	Apparent
avg	Average
f	Film
int	Interface
L	Liquid phase
p	Phase
SS	Steady-state
V	Gas/Vapor phase

Indexes extremes

Symbol	Description
n_c^f	Number of reactants involved in the forward reaction
n_c^L	Number of components in the liquid phase
n_c^r	Number of reactants involved in the reverse reaction
n_c^V	Number of components in the gas/vapor phase

Bibliography

[1] "Scripps Institution of Oceanography - The Keeling Curve," *https://scripps.ucsd.edu/programs/keelingcurve/*, November 2017.

[2] M. Errico, C. Madeddu, D. Pinna, and R. Baratti, "Model calibration for the carbon dioxide-amine absorption system," *Appl. Energy*, vol. 183, p. 958, 2016.

[3] D. G. Victor, D. Zhou, E. H.M. Ahmed, P. K. Dadhich, J. G.J. Olivier, H. H. Rogner, K. Sheikho, and M. Yamaguchi, "Introductory chapter in: Climate change 2014: Mitigation of climate change," tech. rep., Contribution of Working Group III to the Fifth Assessment Report of the Intergovernmental Panel on Climate Change Cambridge University Press, Cambridge, United Kingdom and New York, NY, USA, 2014.

[4] IPCC, "Intergovernmental Panel on Climate Change, Special Report on Carbon Dioxide Capture and Storage," tech. rep., Cambridge University Press, Cambridge, United Kingdom, 2005.

[5] M. Wang, A. Lawal, P. Stephenson, J. Sidders, and C. Ramshaw, "Post-combustion CO_2 capture with chemical absorption: A state-of-the-art-review," *Chem. Eng. Res. Des.*, vol. 89, p. 1609, 2011.

[6] G. S. Krishna Priya, S. Bandyopadhyay, and R. R. Tan, "Power system planning with emission constraints: Effects of CCS retrofitting," *Process Saf. Environ.*, vol. 92, p. 447, 2014.

[7] U. E. Aronu, H. F. Svendsen, K. A. Hoff, and O. Juliussen, "Solvent selection for carbon dioxide absorption," *Energy Procedia*, vol. 1, p. 1051, 2009.

[8] S. Ma'mun, H. F. Svendsen, K. A. Hoff, and O. Juliussen, "Selection of new absorbents for carbon dioxide capture," *Energy Convers. Manage.*, vol. 48, p. 251, 2007.

[9] P. M.M. Blauwhoff, G. F. Versteeg, and W. P.M. Van Swaaij, "A study on the reaction between CO_2 and alkanolamines in aqueous solutions," *Chem. Eng. Sci.*, vol. 39, p. 207, 1984.

[10] P. V. Danckwerts, "The reaction of CO_2 with ethanolamines," *Chem. Eng. Sci.*, vol. 34, p. 443, 1979.

[11] J. Jung, Y. S. Jeong, U. Lee, Y. Lim, and C. Han, "New configuration of the CO_2 capture process using aqueous monoethanolamine for coal-fired power plants," *Ind. Eng. Chem. Res.*, vol. 54, p. 3865, 2015.

[12] G. Cau, V. Tola, and P. Deiana, "Comparative performance assessment of USC and IGCC power plants integrated with CO_2 capture systems," *Fuel*, vol. 116, p. 820, 2014.

[13] G. Cau, V. Tola, and P. Deiana, "Performance evaluation of high-sulphur coal-fired USC plant integrated with SNOX and CO_2 capture sections," *Appl. Therm. Eng.*, vol. 74, p. 136, 2015.

[14] C. Alie, L. Backham, E. Croiset, and P. L. Douglas, "Simulation of CO_2 capture using MEA scrubbing: a flowsheet decomposition method," *Energy Convers. Manage*, vol. 46, no. 3, p. 475, 2005.

[15] A. Aboudheir, P. Tontiwachwuthikul, and R. Idem, "Rigorous Model for Predicting the Behavior of CO_2 Absorption into AMP in Packed-Bed Absorption Columns," *Ind. Eng. Chem. Res.*, vol. 45, no. 8, p. 2553, 2006.

[16] F. A. Tobiesen and H. F. Svendsen, "Experimental Validation of a Rigorous Absorber Model for CO_2 Postcombustion Capture," *AIChE J.*, vol. 53, no. 4, p. 846, 2007.

[17] M. R.M. Abu-Zahra, L. H.J. Schneiders, J. P.M. Niedered, P. H.M. Feron, and G. F. Versteeg, "CO_2 capture from power plants - Part i. A parametric study of the technical performance based on monoethanolamine," *Int. J. Greenhouse Gas Control*, vol. 1, no. 1, p. 37, 2007.

[18] M. R.M. Abu-Zahra, J. P.M. Niedered, P. H.M. Feron, and G. F. Versteeg, "CO_2 capture from power plants - Part ii. A parametric study of the economical perfromance base on monoethanolamine," *Int. J. Greenhouse Gas Control*, vol. 1, p. 135, 2007.

[19] C. Biliyok, A. Lawal, M. Wang, and F. Seibert, "Dynamical modelling, validation and analysis of post-combustion chemical absorption CO_2 capture plant," *Int. J. Greenhouse Gas Control*, vol. 9, p. 428, 2012.

[20] J. Gáspár and A.-M. Cormoş, "Dynamic modeling and validation of absorber and desorber columns for post-combustion CO_2 capture," *Comput. Chem. Eng.*, vol. 35, no. 10, p. 2044, 2011.

[21] H. M. Kvamsdal, J. P. Jakobsen, and K. A. Hoff, "Dynamic modeling and simulation of a CO_2 absorber column for post-combustion CO_2 capture," *Chem. Eng. Process. Intensif.*, vol. 49, no. 1, p. 135, 2009.

[22] S. Ziaii, G. T. Rochelle, and T. F. Edgar, "Dynamic Modeling to Minimize Energy Use for CO_2 Capture in Power Plants by Aqueous Monoethanolamine," *Ind. Eng. Chem. Res.*, vol. 48, no. 13, p. 6105, 2009.

[23] D. M. Austgen, G. T. Rochelle, X. Peng, and C. Chen, "Model of Vapor-Liquid Equilibria for Aqueous Acid Gas-Alkanolamine Systems Using the Electrolyte-NRTL Equation," *Ind. Eng. Chem. Res.*, vol. 28, no. 7, p. 1060, 1989.

[24] M. D. Hilliard, *A Predictive Thermodynamic Model for an Aqueous Blend of Potassium Carbonate, Piperazine, and Monoethanolamine for Carbon Dioxide Capture from Flue Gas.* PhD thesis, The University of Texas at Austin, 2008.

[25] L. E. Øi, "Aspen HYSYS Simulation of CO_2 Removal by Amine Absorption from a Gas Based Power Plant Removal by Amine Absorption from a Gas Based Power Plant," *SIMS2007 Conference, Gøteborg, October 30-31st 2007*, 2007.

[26] P. Mores, N. Scenna, and S. Mussati, "Post-combustion CO_2 capture process: Equilibrium stage mathematical model of the chemical absorption of CO_2 into monoethanolamine (MEA) aqueous solution," *Chem. Eng. Res. Des.*, vol. 89, no. 9, p. 1587, 2011.

[27] P. Mores, N. Scenna, and S. Mussati, "A rate based model of a packed column for CO_2 absorption using aqueous monoethanolamine solution," *Int. J. Greenhouse Gas Control*, vol. 6, p. 21, 2012.

[28] S. A. Jayarathna, B. Lie, and M. C. Melaaen, "Dynamic modelling of the absorber of a post-combustion CO_2 capture plant: Modelling and simulations," *Comput. Chem. Eng.*, vol. 53, p. 178, 2013.

[29] S. A. Jayarathna, B. Lie, and M. C. Melaaen, "Amine based CO_2 capture plant: Dynamic modeling and simulations," *Int. J. Greenhouse Gas Control*, vol. 14, p. 282, 2013.

[30] R. D. Deshmukh and A. E. Mather, "A Mathematical Model for Equilibrium Solubility of Hydrogen Sulfide and Carbon Dioxide in Aqueous Alkanolamine Solutions," *Chem. Eng. Sci.*, vol. 36, p. 355, 1981.

[31] C.-C. Chen and L. B. Evans, "A Local Composition Model for the Excess Gibbs Energy of Aqueous Electrolyte Systems," *AIChE J.*, vol. 32, no. 3, p. 444, 1986.

[32] A. Benamor and M. K. Aroua, "Modeling of CO_2 solubility and carbamate concentration in DEA, MDEA and their mixtures using the Deshmukh-Mather model," *Fluid Phase Equilibr.*, vol. 231, p. 150, 2005.

[33] R. H. Weiland, T. Chakravarty, and A. E. Mather, "Solubility of Carbon Dioxide and Hydrogen Sulfide in Aqueous Alkanolamines," *Ind. Eng. Chem. Res.*, vol. 32, no. 7, p. 1419, 1993.

[34] F.-Y. Jou, A. E. Mather, and F. D. Otto, "The Solubility of CO_2 in a 30 Mass Percent Monoethanolamine Solution," *Can. J. Chem. Eng.*, vol. 73, no. 1, p. 140, 1995.

[35] E. A. Guggenheim and R. H. Stokes, "Activity Coefficients of 2:1 and 1:2 Electrolytes in Aqueous Solution from Isopiestic Data," *Trans. Faraday Soc.*, vol. 54, p. 1646, 1958.

[36] A. Lawal, M. Wang, P. Stephenson, and H. Yeung, "Dynamic modelling of CO_2 absorption for post combustion capture in coal-fired power plants," *Fuel*, vol. 88, no. 12, p. 2455, 2009.

[37] J. M. Plaza, D. V. Wagener, and G. T. Rochelle, "Modeling CO_2 Capture with Aqueous Monoethanolamine," *Energy Procedia*, vol. 1, no. 1, p. 1171, 2009.

[38] Y. Zhang, C.-C. C. H. Chen, J. M. Plaza, R. Dugas, and G. T. Rochelle, "Rate-Based Process Modeling Study of CO_2 Capture with Aqueous Monoethanolamine Solution," *Ind. Eng. Chem. Res.*, vol. 48, no. 20, p. 9233, 2009.

[39] H. M. Kvamsdal and G. T. Rochelle, "Effects of the Temperature Bulge in CO_2 Absorption from Flue Gas by Aqueous Monoethanolamine," *Ind. Eng. Chem. Res.*, vol. 47, no. 3, p. 867, 2008.

[40] J. Oexmann and A. Kather, "Post-combustion CO_2 capture in coal-fired power plants: comparison of integrated chemical absorption processes with piperazine promoted potassium carbonate and MEA," *Energy Procedia*, vol. 1, no. 1, p. 799, 2009.

[41] D. H. Van Wagener and G. T. Rochelle, "Stripper configurations for CO_2 capture by aqueous monoethanolamine," *Chem. Eng. Res. Des.*, vol. v89, no. 9, p. 1639, 2011.

[42] R. Strube and G. Manfrida, "CO_2 capture in coal-fired power plants - Impact on plant performance," *Int. J. Greenhouse Gas Control*, vol. 5, no. 4, p. 710, 2011.

[43] S. Moioli, L. A. Pellegrini, and S. Gamba, "Simulation of CO_2 capture by MEA scrubbing with a rate-based model," *Procedia Eng.*, vol. 42, p. 1651, 2012.

[44] N. Razi, H. F. Svendsen, and O. Bolland, "Validation of mass transfer correlations for CO_2 absorption with MEA using pilot data," *Int. J. Greenhouse Gas Control*, vol. 19, p. 478, 2013.

[45] S. Posch and M. Haider, "Dynamic modeling of CO_2 absorption from coal-fired power plant into an aqueous monoethanolamine solution," *Chem. Eng. Res. Des.*, vol. 91, no. 6, p. 977, 2013.

[46] C. Madeddu, M. Errico, and R. Baratti, "Rigorous Modeling of a CO_2-MEA Stripping System," *Chem. Eng. Trans.*, vol. 57, p. 451, 2017.

[47] X. Luo and M. Wang, "Improving Prediction Accuracy of a Rate-Based Model of an MEA-Based Carbon Capture Process for Large-Scale Commercial Deployment," *Engineering*, vol. 3, p. 232, 2017.

[48] K. A. Hoff, O. Juliussen, O. Falk-Pedersen, and H. F. Svendsen, "Modeling and Experimental Study of Carbon Dioxide Absorption in Aqueous Alkanolamine Solutions Using a Membrane Contactor," *Ind. Eng. Chem. Res.*, vol. 43, p. 4908, 2004.

[49] F. A. Tobiesen, O. Juliussen, and H. F. Svendsen, "Experimental validation of a rigorous desorber model for CO_2 post-combustion capture," *Chem. Eng. Sci.*, vol. 63, no. 10, p. 2641, 2008.

[50] N. Harun, T. Nittaya, P. L. Douglas, E. Croiset, and L. A. Ricardez-Sandoval, "Dynamic simulation of MEA absorption process for CO_2 capture from power plants," *Int. J. Greenhouse Gas Control*, vol. 10, p. 295, 2012.

[51] W. V. K. D., P. J. Hoftijzer, and F. J. Huntjens, "Composition and Vapour Pressures of Aqueous Solutions of Ammonia, Carbon Dioxide and Hydrogen Sulphide," *Rec. Trav. Chim.*, vol. 68, p. 191, 1949.

[52] S. Freguia, "Modeling of CO_2 Removal from Flue Gases with Monoethanolamine," Master's thesis, The University of Texas at Austin, 2002.

[53] T. Neveux, Y. L. Moullec, J.-P. Corriou, and E. Favre, "Modeling CO_2 Capture in Amine Solvents: Prediction of Performance and Insights on Limiting Phenomena," *Ind. Eng. Chem. Res.*, vol. 52, no. 11, p. 4266, 2013.

[54] A. Lawal, M. Wang, P. Stephenson, G. Koumpouras, and H. Yeung, "Dynamic modelling and analysis of post-combustion CO_2 chemical absorption process for coal-fired power plants," *Fuel*, vol. 89, no. 10, p. 2791, 2010.

[55] Y. Lin, T.-H. Pan, D. Shan-Hill Wong, S.-S. Jang, Y.-W. Chi, and C.-H. Yeh, "Plantwide Control of CO_2 Capture by Absorption and Stripping Using Monoethanolamine Solution," *Ind. Eng. Chem. Res.*, vol. 50, no. 3, p. 1338, 2011.

[56] P. Tontiwachwuthikul, A. Meisen, and C. Jim Lim, "CO_2 Absorption by NaOH, Monoethanolamine and 2-Amino-2-Methyl-1-Propanol Solutions in a Packed Column," *Chem. Eng. Sci.*, vol. 47, no. 2, p. 381, 1992.

[57] F. M. Khan, V. Krishnamoorti, and T. Mahmud, "Modelling reactive absorption of CO_2 in packed columns for post-combustion carbon capture applications," *Chem. Eng. Res. Des.*, vol. 89, no. 9, p. 1600, 2011.

[58] S. A. Jayarathna, B. Lie, and M. C. Melaaen, "NEQ Rate Based Modeling of an Absorption Column for Post Combustion CO_2 Capturing," *Energy Procedia*, vol. 4, p. 1797, 2011.

[59] P. Mores, N. Scenna, and S. Mussati, "CO_2 capture using monoethanolamine MEA aqueous solution: Modeling and optimization of the solven regeneration and CO_2 desorption process," *Energy*, vol. 45, p. 1042, 2012.

[60] B. R. W. Pinsent, L. Pearson, and F. J. W. Roughton, "The Kinetics of Combination of Carbon Dioxide with Hydroxide Ions," *Trans. Faraday Soc.*, 1956.

[61] A. Aboudheir, P. Tontiwachwuthikul, A. Chakma, and R. Idem, "Kinetics of the reactive absorption of carbon dioxide in high CO_2-loaded, concentrated aqueous monoethanolamine solutions," *Chem. Eng. Sci.*, 2003.

[62] L. Faramarzi, G. M. Kontogeorgis, M. L. Michelsen, K. Thomsen, and E. H. Stenby, "Absorber Model for CO_2 Capture by Monoethanolamine," *Ind. Eng. Chem. Res.*, vol. 49, no. 8, p. 3751, 2010.

[63] J. H. Meldon and J. A. Morales-Cabrera, "Analysis of carbon dioxide absorption in and stripping from aqueous monoethanolamine," *Chem. Eng. Journ.*, 2011.

[64] J. K. A. Clarke, "Kinetics of Absorption of Carbon Dioxide in Monoethanolamine Solutions at Short Contact Times," *Ind. Eng. Chem. Fundament.*, vol. 313, p. 239, 1964.

[65] G. Astarita, D. W. Savage, and A. Bisio, *Gas treating with chemical solvents*. John Wiley & Sons, 1983.

[66] H. Hikita, S. Asai, H. Ishikawa, and M. Honda, "The Kinetics of Reactions of Carbon Dioxide with Monoethanolamine, Diethanolamine and Triethanolamine by a Rapid Mixing Method," *Chem. Eng. Journ.*, 1977.

[67] Y. Liu, L. Zhang, and S. Watanasiri, "Representing Vapor-Liquid Equilibrium for an Aqueous MEA-CO_2 System Using the Electrolyte Nonrandom-Two-Liquid Model," *Ind. Eng. Chem. Res.*, 1999.

[68] J. D. Seader, E. J. Henley, and D. K. Roper, *Separation Process Principles: Chemical and Biochemical Operations (3rd Ed.)*. John Wiley & Sons, 2010.

[69] R. K. Sinnot, *Coulson & Richardson's Chemical Engineering Volume 6 (4th Ed.) - Chemical Engineering Design*. Elsevier Butterworth-Heinemann, 2005.

[70] E. V. Murphree, "Rectifying Column Calculations with Particular Reference to N Component Mixtures," *Ind. Eng. Chem.*, vol. 17, no. 7, p. 747, 1925.

[71] J. F. Walter and T. K. Sherwood, "Gas Absorption in Bubble-Cap Columns," *Ind. Eng. Chem.*, vol. 33, no. 4, p. 493, 1941.

[72] M. Afkhamipour and M. Mofarahi, "Comparison of rate-based and equilibrium-stage models of a packed column for post-combustion CO_2 capture using 2-amino-2-methyl-1-propanol (AMP) solution," *Int. J. Greenhouse Gas Control*, vol. 15, p. 186, 2013.

[73] L. E. Øi, "Comparison of Aspen HYSYS and Aspen Plus simulation of CO_2 absorption into MEA from atmospheric gas," *Energy Procedia*, vol. 23, p. 360, 2012.

[74] W. K. Lewis and W. G. Whitman, "Principles of Gas Absorption," *Ind. Eng. Chem.*, vol. 16, no. 12, p. 1215, 1924.

[75] R. Higbie, "The rate of absorption of a pure gas into a still liquid during short periods of exposure," *Trans. Am. Inst. Chem. Engrs.*, vol. 31, p. 365, 1935.

[76] P. V. Danckwerts, "Significance of Liquid-Film Coefficients in Gas Absorption," *Ind. Eng. Chem.*, vol. 43, no. 6, p. 1460, 1951.

[77] F. Leder, "The absorption of CO_2 into chemically reactive solutions at high temperatures," *Chem. Eng. Sci.*, vol. 26, p. 1381, 1971.

[78] M. A. Pacheco and G. T. Rochelle, "Rate-Based Modeling of Reactive Absorption of CO_2 and H_2S into Aqueous Methyldiethanolamine," *Ind. Eng. Chem. Res.*, vol. 37, no. 10, p. 4107, 1998.

[79] L. Kucka, I. Müller, E. Y. Kenig, and A. Górak, "On the modelling and simulation of sour gas absorption by aqueous amine solutions," *Chem. Eng. Sci.*, vol. 58, p. 3571, 2003.

[80] A.-M. Cormos and J. Gaspar, "Assessment of mass transfer and hydraulic aspects of CO_2 absorption in packed columns," *Int. J. Greenhouse Gas Control*, vol. 6, no. 201, 2012.

[81] J. Gaspar and A.-M. Cormos, "Dynamic modeling and absorption capacity assessment of CO_2 capture process," *Int. J. Greenhouse Gas Control*, vol. 8, p. 45, 2012.

[82] H. M. Kvamsdal and M. Hillestad, "Selection of model parameter correlations in a rate-based CO_2 absorber model aimed for process simulation," *Int. J. Greenhouse Gas Control*, vol. 11, p. 11, 2012.

[83] N. Mac Dowell, N. J. Samsatli, and N. Shah, "Dynamic modelling and analysis of an amine-based post-combustion CO_2 capture absorption column," *Int. J. Greenhouse Gas Control*, vol. 12, p. 247, 2013.

[84] T. Nittaya, P. L. Douglas, E. Croiset, and L. A. Ricardez-Sandoval, "Dynamic Modeling and Evaluation of an Industrial-Scale CO_2 Capture Plant Using Monoethanolamine Absorption Processes," *Ind. Eng. Chem. Res.*, vol. 53, no. 28, p. 11411, 2014.

[85] C. Noeres, E. Y. Kenig, and A. Górak, "Modelling of reactive separation processes: reactive absorption and reactive distillation," *Chem. Eng. Process. Intensif.*, vol. 42, no. 3, p. 157, 2003.

[86] S. M. P. Ooi, *Development and Demonstration of a New Non-Equilibrium Rate-Based Process Model for the Hot Potassium Carbonate Process*. PhD thesis, The University of Adelaide, 2008.

[87] R. Taylor and R. Krishna, *Multicomponent Mass Transfer*. John Wiley & Sons, 1993.

[88] W. V. K. D. and P. J. Hoftijzer, "Kinetics of Gas-Liquid Reactions Part i. General Theory," *Rec. Trav. Chim.*, vol. 67, no. 7, p. 563, 1948.

[89] G. F. Froment, K. B. Bischoff, and J. De Wilde, *Chemical Reactor Analysis and Design (2nd Ed.)*. Wiley, 1990.

[90] Y. Zhang and C.-C. Chen, "Modeling CO_2 absorption and desorption by aqueous monoethanolamine solution with Aspen rate-based model," *Energy Procedia*, vol. 37, p. 1584, 2013.

[91] K. Onda, H. Takeuchi, and Y. Okumoto, "Mass Transfer Coefficients Between Gas and Liquid Phases in Packed Columns," *J. Chem. Eng. Jpn.*, vol. 1, no. 1, p. 56, 1968.

[92] J. L. Bravo, J. A. Rocha, and J. R. Fair, "Mass Transfer in Gauze Packings," *Hydrocarb. Processes*, vol. 64, no. 1, p. 91, 1985.

[93] J. L. Bravo, J. A. Rocha, and J. R. Fair, "Comprehensive model for the performance of columns containing structured packings," in *Inst. Chem. Eng. Symp. Ser.*, vol. 128, p. A489, 1992.

[94] M. Henriques de Brito, U. von Stockar, A. Menendez Bangerter, P. Bomio, and M. Laso, "Effective Mass-Transfer Area in a Pilot Plant Column Equipped with Structured Packings and with Ceramic Rings," *Ind. Eng. Chem. Res.*, vol. 33, no. 3, p. 647, 1994.

[95] R. E. Tsai, A. F. Seibert, R. B. Eldridge, and G. T. Rochelle, "Influence of viscosity and surface tension on the effective mass transfer area of structured packing," *Energy Procedia*, vol. 1, p. 1197, 2009.

[96] R. E. Tsai, A. F. Seibert, R. B. Eldridge, and G. T. Rochelle, "A Dimensionless Model for Predicting the Mass-Transfer Area of Structured Packing," *AIChE J.*, vol. 57, no. 5, p. 1173, 2011.

[97] R. Billet and M. Schultes, "Predicting Mass Transfer in Packed Columns," *Chem. Eng. Technol.*, vol. 16, no. 1, p. 1, 1993.

[98] B. Hanley and C.-C. Chen, "New Mass-Transfer Correlations for Packed Towers," *AIChE J.*, vol. 58, no. 1, p. 132, 2012.

[99] J. A. Rocha, J. L. Bravo, and J. R. Fair, "Distillation Columns Containing Structured Packings: A Comprehensive Model for Their Performance. 2. Mass Transfer Model," *Ind. Eng. Chem. Res.*, vol. 35, no. 5, p. 1660, 1996.

[100] T. H. Chilton and A. P. Colburn, "Mass Transfer (Absorption) Coefficients. Prediction from Data on Heat Transfer and Fluid Friction," *Ind. Eng. Chem.*, vol. 26, no. 11, p. 1183, 1934.

[101] P. Suess and L. Spiegel, "Hold-up of Mellapak structured packing," *Chem. Eng. Process. Intensif.*, vol. 31, no. 2, p. 119, 1992.

[102] J. A. Rocha, J. L. Bravo, and J. R. Fair, "Distillation Columns Containing Structured Packings: A Comprehensive Model for Their Performance. 1. Hydraulic Models," *Ind. Eng. Chem. Res.*, vol. 32, no. 4, p. 641, 1993.

[103] J. Stichlmair, J. L. Bravo, and J. R. Fair, "General model for prediction of pressure drop and capacity of countercurrent gas/liquid packed columns," *Gas Sep. Purif.*, vol. 3, no. 1, p. 19, 1989.

[104] R. Billet and M. Schultes, "Influence of Phase Ratio on Packing Efficiency in Columns for Mass Transfer Processes," *Chin. J. Chem. Eng.*, vol. 5, no. 2, p. 117, 1997.

[105] R. Billet and M. Schultes, "Predicition of Mass Transfer Columns with Dumped and Arranged Packings: Updated Summary of the Calculation Method of Billet and Schultes," *Chem. Eng. Res. Des.*, vol. 77, no. 6, p. 498, 1999.

[106] R. E. Dugas, "Pilot Plant Study of Carbon Dioxide Capture by Aqueous Monoethanolamine," Master's thesis, The University of Texas at Austin, 2006.

[107] M. E. Davis, *Numerical methods and modelling for chemical engineers.* New York: John Wiley & Sons, 1984.

[108] E. Y. Kenig, R. Schneider, and A. Górak, "Rigorous dynamic modelling of complex reactive absorption processes," *Chem. Eng. Sci.*, vol. 54, no. 21, p. 5195, 1999.

[109] R. Schneider, E. Y. Kenig, and A. Górak, "Complex reactive absorption processes: model optimisation and dynamic column simulation," *Comput. Aided Chem. Eng.*, vol. 9, p. 285, 2001.

[110] P. Tontiwachwuthikul, A. Meisen, and C. J. Lim, "Novel Pilot Plant Technique for Sizing Gas Absorbers with Chemical Reactions," *Can. J. Chem. Eng.*, vol. 67, no. 4, p. 602, 1989.

[111] T. F. Edgar, D. M. Himmelblau, and L. S. Lasdon, *Optimization of chemical processes*. McGraw Hill, 2001.

[112] L. J. Rodríguez-Aragón and J. López-Fidalgo, "Optimal designs for the Arrhenius equation," *Chemometr. Intell. Lab.*, vol. 77, no. 1, p. 131, 2005.

[113] M. van der Spek, A. Ramirez, and A. Faaij, "Improving uncertainty evaluation of process models by using pedigree analysis. a case study on CO_2 capture with monoethanolamine," *Comput. Chem. Eng.*, vol. 85, p. 1, 2016.

[114] T. Nagy, E. Valkó, I. Sedyó, I. Gy. Zsély, M. J. Pilling, and T. Turányi, "Uncertainty of the rate parameters of several important elementary reactions of the H_2 and syngas combustion systems," *Combust. Flame*, vol. 162, no. 5, p. 2059, 2015.

[115] M. Schwaab and J. C. Pinto, "Optimum reference temperature for reparameterization of the Arrhenius equation. Part 1: Problems involving one kinetic constant," *Chem. Eng. Sci.*, vol. 10, no. 2750, 62.

[116] T. Pintola, P. Tontiwachwuthikul, and A. Meisen, "Simulation of pilot-plant and industrial CO_2-MEA absorbers," *Gas Sep. Purif.*, vol. 7, no. 1, p. 47, 1993.

[117] D. Singh, E. Croiset, P. L. Douglas, and M. A. Douglas, "Techno-economic study of CO_2 capture from an existing coal-fired power plant: MEA scrubbing vs. O_2/CO_2 recycle combustion," *Energy Convers. Manage.*, vol. 44, p. 3073, 2003.

[118] A. Lawal, M. Wang, P. Stephenson, and O. Obi, "Demonstrating full-scale post-combustion CO_2 capture for coal-fired power plant through dynamic modelling and simulation," *Fuel*, vol. 101, p. 115, 2012.

[119] C. Madeddu, M. Errico, and R. Baratti, "Process analysis for the carbon dioxide chemical absorption-regeneration system," *Appl. Energy*, vol. 215, p. 532, 2018.

[120] L. S. Tan, A. M. Shariff, K. K. Lau, and M. A. Bustam, "Factors affecting CO_2 absorption efficiency in packed column: A review," *J. Ind. Eng. Chem.*, vol. 18, no. 6, p. 1874, 2012.

[121] M. Bui, I. Gunawan, V. Verheyen, P. Feron, E. Meuleman, and S. Adeloju, "Dynamic modelling and optimisation of flexible operation in post-combustion CO_2 capture plants - A review," *Comput. Chem. Eng.*, vol. 61, p. 245, 2014.

[122] F. de Miguel Mercader, G. Magneschi, E. S. Fernander, G. J. Stienstra, and E. L. V. Goetheer, "Integration between a demo size post-combustion CO_2 capture and full size power plant. An integral approach on energy penalty for different process options," *Int. J. Greenhouse Gas Control*, vol. 11S, p. S102, 2012.

[123] Y.-J. Lin, D. S.-H. Wong, and S.-S. Jang, "Control Strategies for Flexible Operation of Power Plant with CO_2 Capture Plant," *AIChE J.*, vol. 58, no. 9, p. 2697, 2012.

[124] C. A. Kang, A. R. Brandt, L. J. Durlofsky, and I. Jayaweera, "Assessment of advanced solvent-based post-combustion CO_2 capture processes using a bi-objective optimization technique," *Appl. Energy*, vol. 179, p. 1209, 2016.